INTEGRATED GEOPHYSICAL METHODS IN MAPPING SANDFILLED CHANNEL AT

MTU CAMPUS, SOUTHWESTERN NIGERIA

By

OGIRRI GODFREY EMMANUEL

19010401011

A PROJECT SUBMITTED TO THE DEPARTMENT OF GEOSCIENCES

COLLEGE OF BASIC AND APPLIED SCIENCES, IN PARTIAL FULFILMENT OF THE REQUIREMENT FOR THE AWARD OF DEGREE OF BACHELOR OF SCIENCE (B.SC.) IN GEOPHYSICS.

AUGUST, 2022

DECLARATION

I hereby declare that this project has been written by me and is a record of my own research work. It has not been presented in any previous application for a higher degree of this or any other University. All citations and sources of information are clearly acknowledged by means of reference

……..

OGIRRI, GODFREY EMMANUEL

……..……

DATE

CERTIFICATION

This is to hereby certify that project work entitled as **Integrated Geophysical Methods (GPR and 2D-ERT) In Mapping Sandfilled Channel at MTU Campus, Southwestern Nigeria** was prepared and submitted by **OGIRRI GODFREY EMMANUEL** in partial fulfilment of the requirements for the degree of **BACHELOR OF SCIENCE IN APPLIED GEOPHYSICS.**

The original research work was carried out by him under my supervision and is hereby accepted

MR R.P. AKINWALE _____

Supervisor *(Signature and Date)*

DR. O.B. BALOGUN _____

Head of Department *(Signature and Date)*

DEDICATION

This project is dedicated to God Almighty for giving the strength and grace to carry out this research successfully.

ACKNOWLEDGEMENT

My sincere and profound gratitude goes to God Almighty, the Beginning and the end who has been so kind and merciful to me throughout my sojourn in this institution and given the strength and guidance to carry out my project work successfully.

My thanks also go to the Head of the Department (HOD) and lecturers of the department of Geosciences for their full support in the completion of this project work.

I would also like to send my heartfelt appreciation to my able supervisor Mr. R. P. Akinwale for his effortless and relentless support in the completion of this project even in his tight schedule. I pray that God would honour and increase his grace upon your life and your family.

Finally, I would like to deeply appreciate my mother and father Mrs. Stella Ogirri Dupe and Mr Joseph Ogirri for their love, support and un- ending prayers towards the completion of this project. I pray humbly pray that God will reward your hard work with success.

TABLE OF CONTENTS

LIST OF TABLES

LIST OF FIGURES

LIST OF ABBREVIATIONS

GPR: Ground Penetrating Radar,

2D-ERT: Two-Dimensional Electrical Resistivity Topography

3D ERT: Three-Dimensional Electrical Resistivity Tomography

ns: Nanoseconds

ABSTRACT

Integrated geophysical survey has been used in mapping a sandfilled channel within Mountain Top University. The width of the sandfilled region has been mapped with the aid of historical satellite images but the thickness and depth are unknown. Therefore, Ground Penetrating Radar (GPR), and Electrical Resistivity Tomography (ERT) methods were integrated to delineate the thickness and depth of the sandfilled/river channel, characterise the infill materials and deduce its engineering implications.

Nine traverses each about 60 m long were established at inter-traverse spacing of 10 m across the strike of the river channel. 2D ERT data were acquired with ABEM LS and 1m electrode spacing using dipole-dipole array. The resistivity data were inverted using smooth-model inversion with 2D EarthImager. The parallel 2D ERT lines were further combined and inverted with 3D EarthImager to generate an 3D inverted resistivity cube of the subsurface. The GPR data were acquired with Mala ProEx and 160MHz antenna to obtain high resolution and good depth of penetration. Several processing steps including time-zero correction, energy decay, background removal and normalisation were applied on the radargram.

The results of 2D ERT have characterised the subsurface into two main geoelectric units within the depth of 13.8m. The first region is represented by varying resistivity (5 to 1576 Ωm) and thickness range of 3 to 8m. At lateral distances of about 16 to 48 m, low resistivity anomalies (5 to 49 Ωm) were observed at a depth range of about 1.5 to 3.8m. The configuration of this low resistivity anomaly is analogous to the configuration of an incised channel against the background/country rock (relatively high resistivity range of 30 to 1576 Ωm). This region is therefore associated with the main course of the sandfill/river channel region. The augmented 3D view of the parallel 2D ERT lines and inverted 3D ERT have shown that the regions proximal to the river channel are infilled with relatively highly conductive materials compared to distal regions. This may indicate varying infill materials (such as peat/clay against sand/clayey sand) or water saturation levels and therefore calls for adequate engineering precautions in foundation designs if the region will be considered for future development.

The GPR method has provided a high-resolution image of the subsurface and has been able to identify two main anomalous plane continuous reflectors interpreted as the sandfilled and channel fill boundaries at respective depth range of about 0.5 to 1.3 m and 1.5 to 3.5m.

Keywords: GPR, 2D ERT, 3D ERT, buried channel, sandfill

CHAPTER ONE

INTRODUCTION

1.0 Background of Study

Backfilling is the process of putting soil sand into a trench or foundation once evacuation, and the related work has been completed. A river channel can be sandfilled with soil by natural occurrence (which could either be erosion, weathering) or by human activities during reclamation, landscaping or other engineering purposes. Sand Filling is the process of filling a depression or trench with sand.

Geophysical methods can be deployed to investigate and obtain more information about the sandfilled region (Van Dam, 2012 and Nimnante et al, 2017). Geophysical methods are of preference because they are faster, cost-effective, and non-destructive compared to the conventional ways such as boring and drilling which is expensive, invasive, and provide information in discrete areas, they also cover the flaws of conventional engineering (Van Dam, 2012). Geophysical investigations provide a wider picture of the subsurface that aid in the evaluation of ground fitness for construction purposes.

The following geophysical methods which are The Ground Penetrating Radar (GPR) and ERT (Electrical Resistivity Tomography) have been used in the past for describing lithological and sedimentology of the subsurface. ERT (Electrical Resistivity Tomography) is a geophysical technique that produces tomographic images of the subsurface based subsurface electrical resistivity distribution. Two-dimensional (2-D) resistivity tomography has been a vital tool in depicting subsurface layers due to its continuous lateral and vertical imaging along a traverse (Ayolabi et al., 2009). For defining the lithological and sedimentological properties of Quaternary deposits, the Electrical Resistivity Tomography (ERT) technique and Ground Penetrating Radar (GPR) approaches have been frequently employed in the past. (Nimante, 2017).

The Ground Penetrating Radar (GPR) method has been used of recent times for engineering and environmental purposes. It maps shallow geological subsurface of a site by measuring the contrast of different electrical properties (conductivity and the dielectric constant) of the soil (Pantelis and Eleni, 2016).

The importance of the 2D-ERT technique in engineering investigations cannot be over emphasised, its images at high resolution the lateral and depth of the subsurface, with respect to the electrical resistivity of the soil at shallow and deep surveys (Ayolabi et al., 2009).

The integration of the aforementioned geophysical methods (Electrical Resistivity ad GPR methods) is used because a particular geophysical method may give partial information. Different geophysical methods are therefore combined in order to reduce uncertainty, avoid misinterpretations and provide highly accurate and reliable results of the site which is then used to determine the engineering suitability of the soil against future use.

Therefore, in this study, 2D ERT and GPR are employed for investigating a suspected sandfilled river channel region in MTU campus during land reclamation and use. This study attempts to characterise and delineate the sandfilled region and the channel fill by delineating the thickness and depth of these regions which will serve as a guide in future use of the land.

1.1 Statement of Problem

Study of previous satellite imagery within the Mountain Top University Mini mart and previous history information revelated that a channel was sand filled (Figs 1.1a and 1.1b), and this could have engineering implications if the region is proposed for construction. The width of the sand filled region can be mapped with the aid of previous satellite images (Fig 1.1a and 1.1b), but the thickness and depth are unknown. Therefore, integration of Ground Penetrating Radar (GPR), and Electrical Resistivity Tomography (ERT) methods are used to delineate the depth of the sand filled channel, thickness of the sandfilled channels in order to deduce its engineering implications. This method is of preference compared to geotechnical methods such as boring, pitting, and trenching which are soil disturbing, discrete, expensive, and more time-consuming in sample acquiring and laboratory analysis.

1.2 Aim of the Study

This research aims to integrate GPR method and 2D-ERT technique in mapping sandfilled river channels to delineate the thickness of the sandfill and depth of the channel to deduce its engineering implications.

1.3 Objectives of the Study

The objectives of this study include to

i. characterize the sandfilled region based on the response from the integrated geophysical methods;

ii. delineate sandfilled regions and determine its thickness;
iii. delineate the depth of the sandfilled river channel;
iv. deduce the engineering implications of the sandfilled region.

1.4 Location and Accessibility

The study area is located at the Mountain Top University within Mountain of Fire and Miracle Ministries (MFM) Prayer City, at KM 12, Lagos – Ibadan express way, Ibafo, Ogun State Nigeria with geographic coordinates of Latitude 6°43’39.9’’N to 6°43’44.3’’N and Longitudes 3°24’41.04’’E to 3°24’44.9’’E (WGS, 1984) within Mountain top university campus, behind the mini mart. It is an extension of the branches of MTU lake that was later sandfilled (Fig 1a and 1b). The campus is accessible through the Lagos-Ibadan expressway.

1.5 Significance of the Study

The importance of this study is the engineering implications of the study area as it will guide future land use of the area.

1.6. Definition of terms

i. Channel fill: The sediment infill of a channel, produced either by the accretion of sediment transported by water flowing through the channel, or by the infilling of an abandoned channel.
ii. River channel: A type of landform consisting of the outline of a path of relatively shallow and narrow or other fluids, most commonly the confine of a river.
iii. Infill: material that fills or is used to fill a space or hole.
iv. Back filled: to refill (something, such as an excavation) usually with excavated material sandfill a trench.
v. Sand Filled: is the process of filling a depression or trench with sand.

Figure 1.1a. Satellite Imagery showing the study area as an abandoned river channel (yellow dashed line) in January 2015 prior to sandfilling

Figure 1.1b Satellite Imagery showing a recent state of the study area (yellow dashed line) after sandfilling

CHAPTER TWO

LITERATURE REVIEW

2.0 Review of Previous Works Done

In order to map the lithology and geometry of channel belts and valley fills, Daves et al. (2002) showed how electrical resistivity imaging (ERI) can be used. Comparisons were made between ERI profiles and lithostratigraphic profiles derived from drill logs, sediment cores, wireline logs, and GPR. Even when covered by 1–20 m of silt/clay, the ERI profiles can accurately detect and outline the depth, breadth, and lithology of sand and gravel channel-fills and neighbouring sediments.

Electrical resistivity imaging was used by Abayomi et al. (2016) to conduct a geophysical investigation on a section of an abandoned railway line covered with sand at Oke-Ibadan Estate, Ibadan. The study's goal was to identify the cause or causes of settlement that contributed to the demise of a building's foundation. The least-squares inversion approach was used to plot the apparent resistivity values acquired from the traverse versus the midpoint of electrode separation after five profile lines were produced throughout the study. With resistivity values ranging from 77 -m to 400 -m, pockets of low resistivity zone were found in the inverted sections. Clay and clayey sand were the alleged components of the sand-filled soil materials. The results showed that the materials utilized to sandfill the disused rail track were not properly compacted. In light of this, the structural breakdown of structures along the abandoned route was attributed to the varied clay and clayey sand towns on which they were built.

In order to comprehend the evolution of the fluvial system and to discuss the benefits of two shallow geophysical methods for describing subsurface morphology of modern and paleo-channels, Nimnate et al. (2017) used geophysical data to image and locate paleo-channels from the meandering system of the Mun River, Khorat Plateau, North-eastern Thailand. The lateral, vertical morphological, and sedimentary structures of paleo-channels, floodplains, and recent point bars were characterized using electrical resistivity tomography (ERT) and ground penetrating radar (GPR). The physical characteristics of subsurface sediments were described using both techniques in conjunction with on-site boreholes. It was determined that four radar reflection patterns, including reflection free, shingled, inclined, and hummocky reflections, were appropriate to apply as criteria to characterize lateral accretion. The meandering rivers with a channel-filled sequence and floodplain were found from ERT profiles. The variations in

resistivity show a connection to ERT lithological classes and nicely match variations in particle size. The data on resistivity were used to categorize bedrock, clay, silt, sand, and loam. While GPR provides more in-depth subsurface facies for describing point bar sand deposit than ERT does, both the geometry of paleo-channel embayment and lithological differences can be detected using ERT.

In order to conduct pre-construction studies, Obare, (2020) used geophysical methods in the structural foundation investigation at Olkaria (V) field in the Kenyan rift valley. The investigation's goal was to ascertain the depth at which bedrock provides a solid base for construction. When evaluating the suitability of the ground for structural development, electrical resistivity and seismic methods were used. The ERT survey was carried out to evaluate the bedrock profile before the construction project for the power plant and to characterize the soil layers above the bedrock. Reliable information about the stability of the ground was obtained using inversion models from the acquired data. Layers of sediment are what are responsible for the resistivity zones in the profiles. High-resistivity zones (> 112 m) are believed to be composed of solid bedrock. The soil stiffness was evaluated using this seismic survey. Low shear wave velocity regions (100-160 m/s) are thought to be loose soft soil materials, whereas high velocity regions (above 220 m/s) are thought to be solid bedrock at depths below 25 m. The bed rock suggests stiff soils that are generally suitable for any type of construction development.

2.1 Geology of the study area

2.1.1 Regional geology of the Dahomey Basin

Inland, coastal, and offshore basins are combined in the Dahomey Basin, which stretches from southern Ghana through Togo and the Republic of Benin to southwestern Nigeria. I Fig 2.1. The Okitipupa Ridge, a subsurface basement high, separates it from the Niger Delta. How far offshore it goes is unknown. Sediment deposition follows an east-west trend. The Republic of Benin's geology is well known (Billman, 1976; De Klasz, 1977). The Cretaceous strata are about 200 meters thick onshore (Okosun, 1990). A non-fossiliferous basal sequence sits on top of the Precambrian basement. The cycles of clays, marls, and coal that contain fossiliferous horizons come next. Offshore, a sequence of sandstones with a top thickness of 1,000 meters and black fossiliferous shales has been found. A pre-Albian to Maastrichtian age was given to this by Billman (1976). The Cretaceous can be divided into two regions: north and south. The sequence in the northern zone consists of a basal sand that grades gradually into clay beds with intercalations of lignite and shales. The uppermost beds of the Maastrichtian are argillaceous

in almost all cases. Nigeria and Benin geologies are very similar to that of the Togo sector. A variety of formal and informal lithostratigraphic nomenclatures have been used by earlier researchers to describe the significant lithological changes that the Cretaceous succession displays. Multiple nomenclatures or nomenclature conflicts could result from this.

2.1.2 Stratigraphic setting of Benin (Dahomey) Basin

Both Cretaceous and Tertiary sediments were recognized in an early study on the basin stratigraphy by Jones & Hockey (1964). Later researchers identified three chronostratigraphic units:

a) Pre-lower Cretaceous folded sequence,

b) Cretaceous sequence and

c) Tertiary sequence (Table 2.0).

The Abeokuta Group is divided into three informal formational units, based on the Cretaceous stratigraphy compiled from outcrop and borehole records: Ise, Afowo, and Araromi, Omatsola, and Adegoke (1981). Olabode (2016) described the formations as follows: The Ise Formation, which is composed of coarse conglomeratic sediments, is inconformably deposited over the basement complex. The Afowo Formation's interbedded shales and siltstone are variable but thick in the transitional to marine sands and sandstone. With interbeds of limestone and sands, the uppermost formation, known as Araromi, is made up of shales and siltstone (Table 2.0). The Tertiary sediments include the formations known as the Ewekoro, Akinbo, Oshosun, Ilaro, and Benin (Coastal Plain Sands) (Table 2.0). The Ewekoro Formation is made up of fossiliferous well-bedded limestone, in contrast to the flaggy grey and black shales that make up the Akinbo and Oshosun Formations. Phosphatic beds and glauconitic rock bands distinguish the Ewekoro and Akinbo Formations from one another. The majority of the beds in the Ilaro and Benin Formations are estuarine, deltaic, and continental.

In the Nigerian sector of the basin, there is significant disagreement regarding the stratigraphy of the Cretaceous and Tertiary Formations. This is primarily due to the fact that different locations throughout the basin have given the same Formation different stratigraphic names (Billman, 1992 & Coker, 2002). This situation is largely attributable to the dearth of sufficient outcrops and complete borehole coverage for stratigraphic studies.

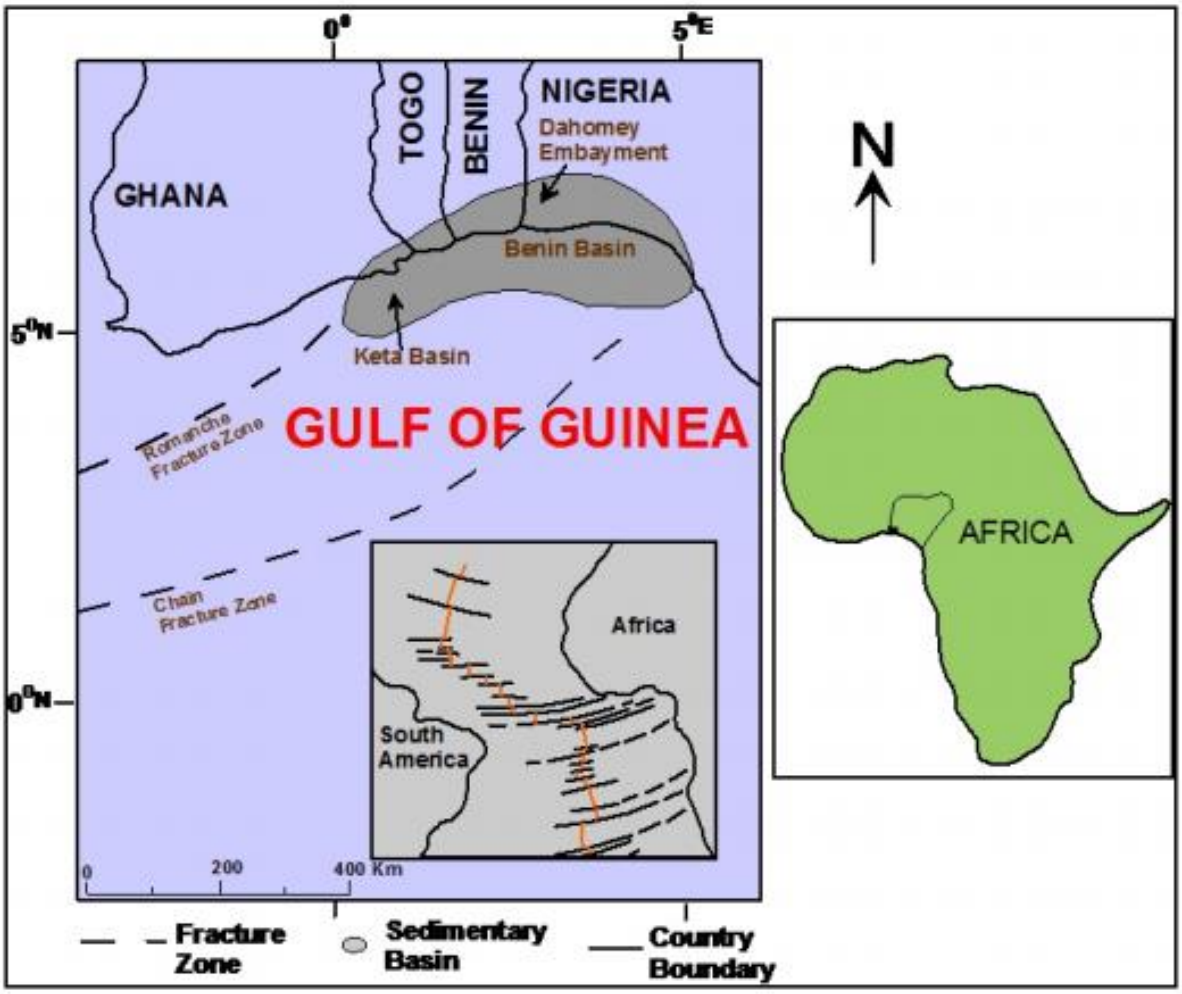

Figure 2.1 Regional map of the Gulf of Guinea showing the location of Benin (Dahomey) Basin in relation to other basins (Olabode *et al*, 2016).

Table 2.0: Generalized stratigraphic column showing age, lithology, and sequence of the formations and tectonic stage of basin development in the Nigerian sector of the Benin (Dahomey) Basin. (Olabode *et al*, 2016).

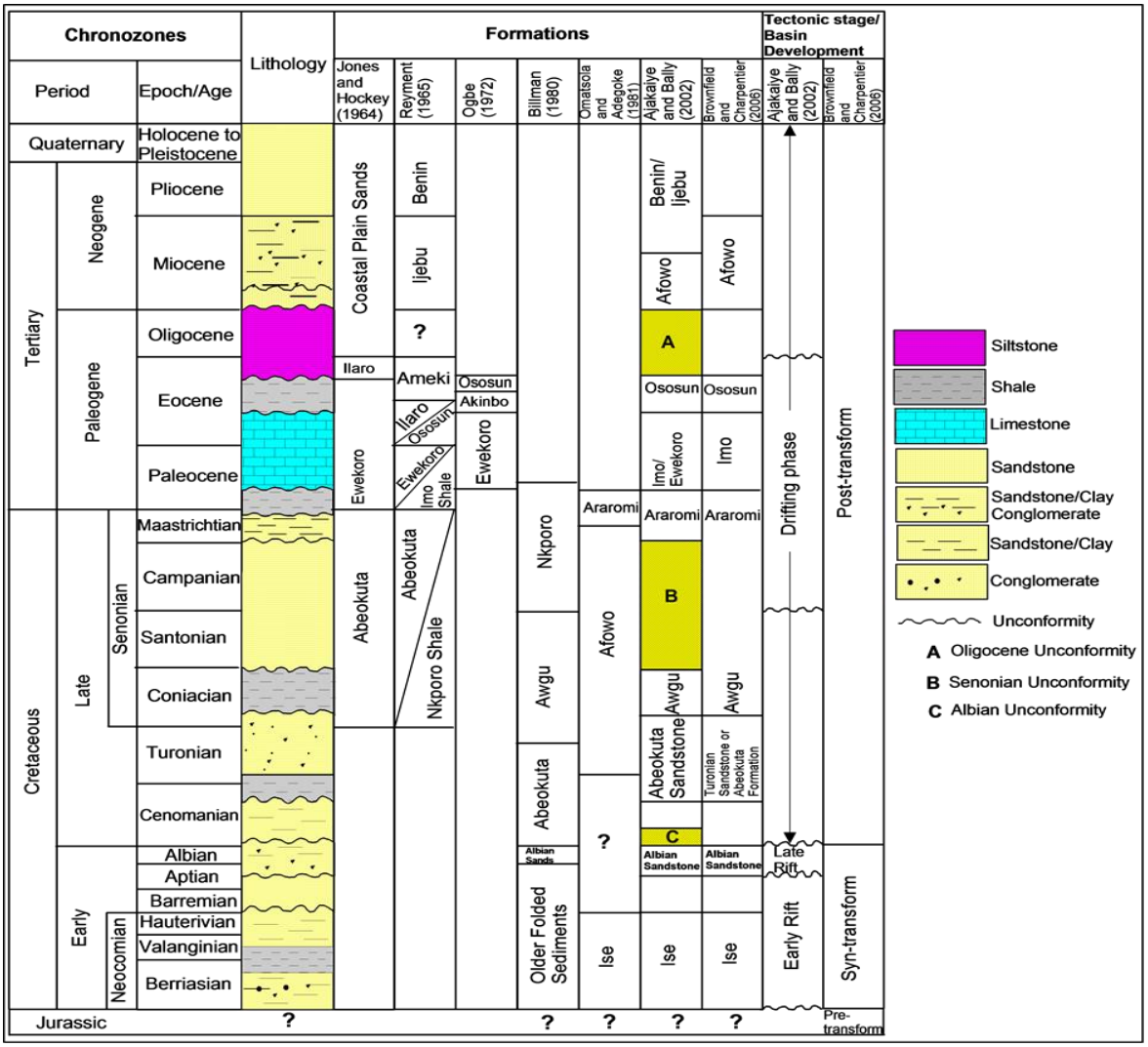

In 1964, Jones and Hockey gave the name "Abeokuta Formation" to the mudstone, silt, clay, and shale interbeds in the mainly arenaceous strata that crop out onshore. The Abeokuta Formation was divided into three lithostratigraphic units by Billman (1976): "Unnamed Older Folded Sediments," "Unnamed Albian Sands," and Abeokuta Formation. Based on their age equivalent, he referred the remaining Cretaceous strata to the Awgu and Nkporo Shales. Omatsola & Adegoke (1981) opposed this nomenclature on two main grounds. The first of these is that only one portion of the succession was given the same name when the Abeokuta Formation was divided, which is against a standard stratigraphic procedure.

The second is that if age were the only factor, the Nkporo and Awgu Shales, two well-known Anambra Basin names, would be ineligible. They consequently proposed the Ise, Afowo, and Araromi Formations as three new lithostratigraphic units and ascribed them to the Abeokuta Group. The Unnamed Older Folded Sediments and the Unnamed Albian Sands are equivalent to the Ise Formation, the Afowo Formation, the outcropping Abeokuta Formation, and the Araromi Formation. Okosun concurred that the Dahomey Basin shouldn't use Anambra Basin lithostratigraphic names solely based on age (1990).

Additionally, it is improper to use the same names for lithostratigraphic units found in various basins that are geographically distinct from one another and have experienced various geological eras. This holds true even if deep well cores, which are challenging to study, contain the only material for comparing complex lithologic sequences. The Nkporo Shale's previous name, Araromi Formation, was thus changed by Okosun (1990). Omatsola & Adegoke (1981) assert that the lithology of the Ise and Afowo formations is extremely similar. They are both primarily made of sand, but the sandstone has a sizable amount of shale interbeds.

To support the development of different lithostratigraphic units, the distinction is insufficient. The two forms were seen as one by Okosun (1990). It was found in that investigation that the Ise, Afowo, and Abeokuta formations had equivalent lithologic and electric log properties.

Okosun claims that the Abeokuta Formation's highest beds and the shallow boreholes at Itori, Wasimi, and Ishaga are predominantly made up of fine- to coarse-grained sand with interbeds of shale, mudstone, limestone, and silt (1990). According to Okosun's research, the top of the neostratotype in the Ojo-1 Borehole and these lithofacies are very similar (1990). Although the Afowo Formation features shale interbeds, Okosun (1990) stressed that its predominantly sandy nature qualifies it, along with the arenaceous Ise Formation, for inclusion in the Abeokuta Formation, which also has shale interbeds as shown in the neostratotype he described

and as seen in many surface outcrops. The Abeokuta Formation, which has primacy of publication and a wider acknowledged usage, has taken the place of the designations Ise and Afowo Formations as a result, and their use has been discontinued. The Abeokuta Formation, according to Jones and Hockey (1964), is composed of grits, loose sand, sandstone, kaolinitic clay, and shale. It was further explained as typically having a ferruginized basal sandstone or basal conglomerate (Obaje, 2009).

2.1.2 Local Geology

The study area lies within the Recent Alluvium region of the Nigerian sector of the Dahomey basin, southwestern Nigeria (Figure 2.2).

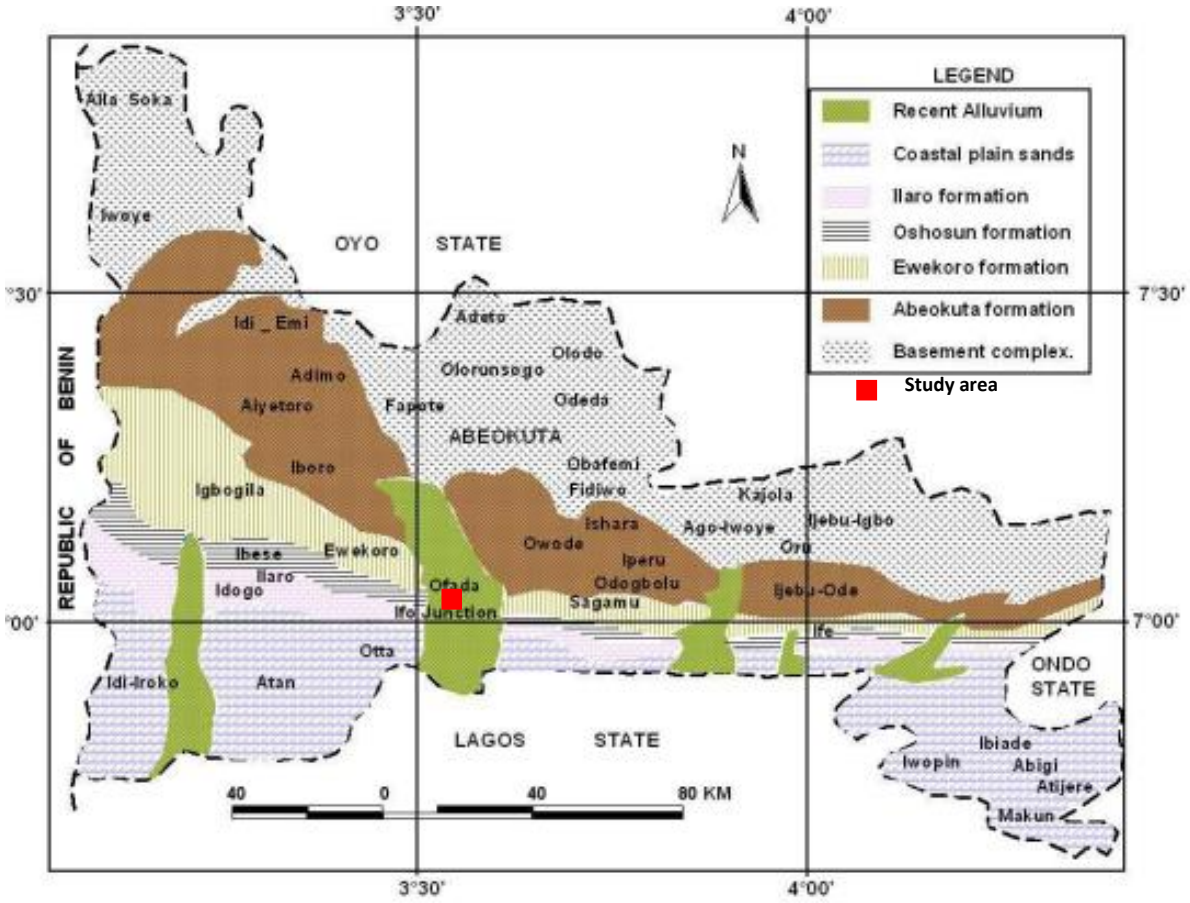

Figure 2.2. Geological map of Ogun State showing (modified after Petters, 1982)

2.2 Basic Theory of Methods Used

Different geophysical methods are applied to environmental and engineering field studies. These methods use different theories of physics and mathematics to model geological features and subsurface structures. Some methods rely on the injection of electrical current into the substrate in order to observe flow paths. Other methods use sound waves or transmit electromagnetic waves in the background. All methods create anomalies (strong responses above or below the background levels) based on the different ways the earth's materials respond to the propagation signal. Popular geophysical methods used for environmental monitoring include electrical resistivity (receiving electrical current), seismic reflection and resonance (receiving sound), ground-penetrating radar (receiving electrical signal), electromagnetic induction (receiving electrical signal), and gravity (measurement of weight changes in the background). The specific methods used in this study are discussed in more detail in the following sections.

2.2.1 Electrical Resistivity Method

Electrical resistivity methods are a form of geophysical surveying help visualize the subsurface. These techniques identify subsurface material by using variatio ns in electric potential.

2.2.1.2 Fundamentals

Ohm's Law, which measures resistance, is fundamentally related to resistivity. The value of a material's resistance depends on the resistivity of that substance and is described as the voltag e divided by the current (R = V/I).

Resistivity is the measure of a material's ability to obstruct the flow of a moving current, (Marshall, S. (n.d.)

Resistivity (ρ) values are related by the equation describing current refraction (Marshall, S. (n.d.)

$$\rho_1 \tan(\theta 1) = \rho_2 \tan(\theta 2) \qquad (2.0)$$

The current moving from a layer of lower resistivity to a layer of higher resistivity would move at a smaller refraction angle under this law, which operates in opposition to Snell's Law.

2.2.1.3 Configuration ad electrode spacing

Four electrodes and a resistivity meter make up the bare minimum setup for a resistivity survey shown in Fig 2.3.

The resistivity meter is an instrument that measures both voltage (V) and current (I) and logs resistance values (V/I).

Using the following formula, these resistance values are transformed into apparent resistivity values:

$$\rho a = \frac{kV}{I}[\Omega m] \quad (2.1)$$

where ρ_a = apparent resistivity and k = geometric factor. The geometric factor varies based on the geometry of each electrode spacing setup.

In typical field work, data is acquired as an apparent resistivity value and later interpreted to obtain true resistivity (Marshall, S. (n.d.).

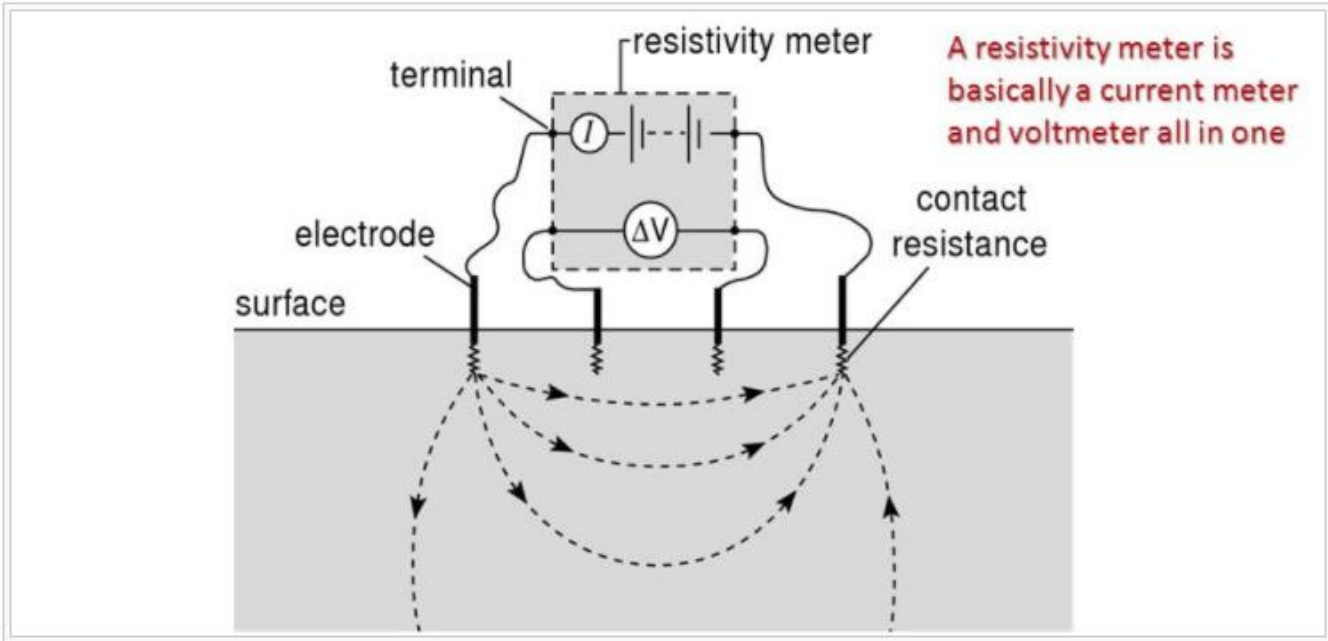

Fig 2.3: Showing the basic setup involving a resistivity meter and four electrodes. Provided by Appalachian State University.

Wenner Array

Two of the resistivity meter's four electrodes are used to conduct current, while the other two measure changes in potential.

The Wenner Array uses four electrodes with identical spacing between them. Depending on the survey's depth, the spacing can be altered. The depth that the survey can measure is typically inversely proportional to the distance between the outer electrodes. This array is among the most frequently used ones (Pomposiello et al., 2012 & EPA,2016)

Schlumberger Array

Only the outer two electrodes (the electrodes supplying and receiving the current) are moved in the Schlumberger array. The benefit of this is that it is significantly because only two electrodes, as opposed to four with the Wenner array, need to be moved, the process is quicker.

The outer electrodes would be continuously moved during fieldwork until the recorded potential reached a minimum value. The survey is then continued after the set-up has been established in a different location. (EPA,2016)

Dipole-dipole Array

The dipole-dipole array (figure 2.7c) is one member of a family of arrays using dipoles (closely spaced electrode pairs) to measure the curvature of the potential field. If the separation between both pairs of electrodes is the same *a*, and the separation between the centres of the dipoles is restricted to *a(n+1)*, the apparent resistivity is given by:

$$\rho_a = \pi an(n+1)(n+2)\frac{v}{I} \qquad \textbf{(2.2)}$$

This array is especially useful for measuring lateral resistivity changes and has been increasingly used in geotechnical applications.

3D Array

The most common way to build a 3D data set is by applying number of 2D survey parallel lines, and these lines then combined into 3D data set for 3D inversion. The ideal three-dimension 3D imaging measurements are collected by using multi electrodes in a rectangular grid and measuring the apparent resistivity along possible directions. Figure 2.5 shows one

possible arrangement of the electrodes for a 3D survey using a 25-electrode system. For convenience the electrodes are usually arranged in a square grid with the same unit electrode spacing in the x- and y-directions. In order to map slightly elongated bodies, a rectangular grid with different numbers of electrodes and spacings in the x- and 1-directions could be used. The pole- pole electrode configuration is commonly used for 3D surveys, such as the E-SCAN method (Li and Oldenbvg 1992). The maximum number of independent measurements n_{max} that can be made with n_e. electrodes (Xu and Noel 1993) is given by

$$n_{max} = n_e (n_e - 1)/2 \qquad (2.3)$$

The Gradient Array

The gradient array moves the two inner electrodes (the potential electrodes), while maintaining a constant spacing between the two outer electrodes. The inner electrodes are moved as a pair in the space between the outer electrodes while maintaining a constant distance between them, measuring the potential as they move.

Various array spacings

A resistivity survey can have other array spacings besides these. Others consist of the square array, the Lee-partition array, the pole pole array, and the dipole-dipole array. The electrode spacing and movement of either the current or potential electrodes vary between each of these different arrays. (Aziz, B. Q. (n.d.)

A few of the array spacings are shown in Fig2.4

Methods

Vertical electric sounding (VES), electric profiling, and electric imaging are the three primary techniques for conducting electric resistivity surveys. Each of these makes use of one of the aforementioned array configurations.

Vertical Electric Sounding

VES, or vertical electric sounding, is one of the more popular and economical resistivity survey techniques. From one current electrode to the next, current is moved through the subsurface, and the potential as the current moves is recorded. From this data, the resistivity values of various layers and layer thickness are obtained. The determined apparent resistivity values are plotted as a log function versus the log of the electrode distance. These plotted curves show the

layer thickness. The acquired data is compared to a master curve to determine layer thickness if there are multiple layers (more than 2).

With VES, there are some restrictions. The electrode spacing is the first restriction on the depth of the survey. Second, the resistivity of layers can differ horizontally. At this point, it would be preferable to employ an electric profiling technique. Finally, each layer needs to be the same thickness. The results for resistivity will be incorrect if the middle layer is significantly thinner than the layers above and below it. The reading will be impacted by the middle layer's thin layer's resistivity. Equivalence is the term for this. AGI. (n.d.)

Electric profiling

Electric profiling aims to identify resistivity variations on a horizontal scale, while VES concentrates on determining resistivity variations on a vertical scale. The same VES electrode spacing configurations can be used for profiling. The profiling method does not involve adjusting electrode spacing because doing so only alters the depth to which the survey can penetrate. Instead, to measure horizontal changes in resistivity, the electrode spacing is maintained while the entire survey is moved along a line or a "profile." (EPA,2016 & Aziz, B. Q. (n.d.)

Electric Imaging

In many instances, as depth and horizontal distance increase, resistivity can change. Electric profiling and VES can only survey in one direction. Resistivity changes can occur both vertically and horizontally, which is possible with electric imaging. The other two methods are essentially combined in this method. The survey is moved along a profile and electrode spacing is increased to measure both vertical and horizontal resistivity. The pseudo section is then made using these values.

One can create an image of the subsurface using the pseudo section. (Loke et al., 2012).

Imaging can be done in two dimensions or three.

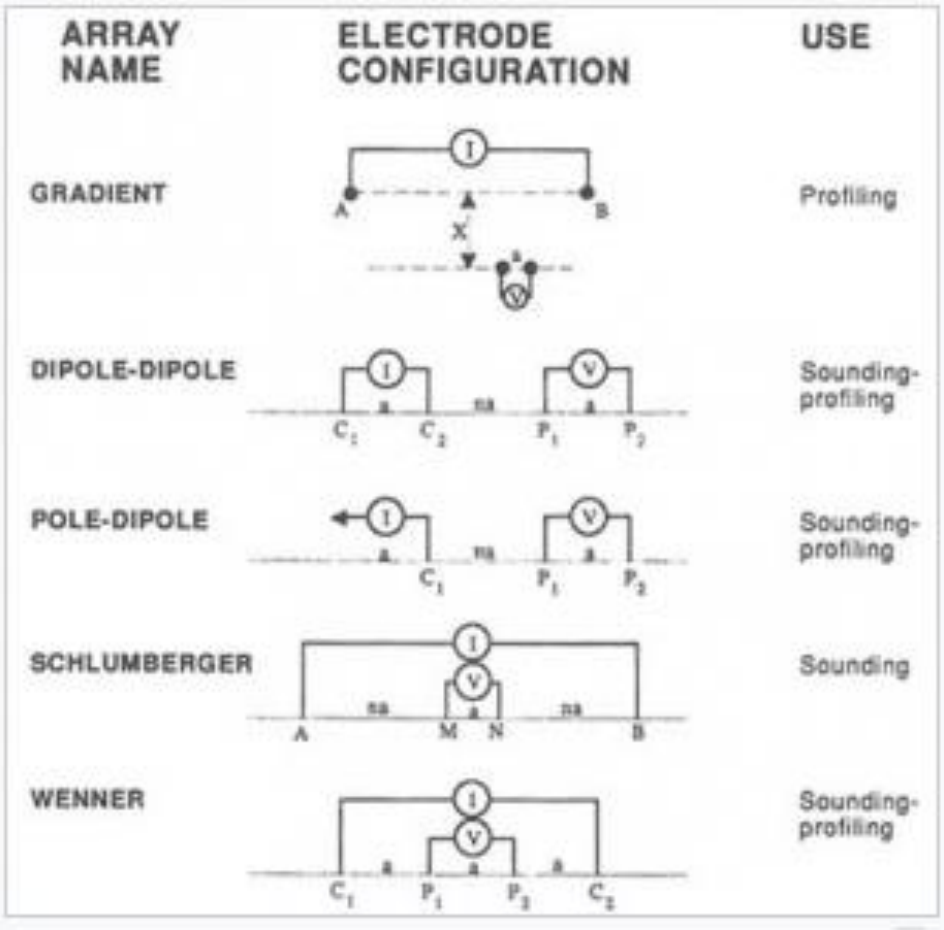

Fig 2.4: Showing various electrode spacings. Provided by National Research Council

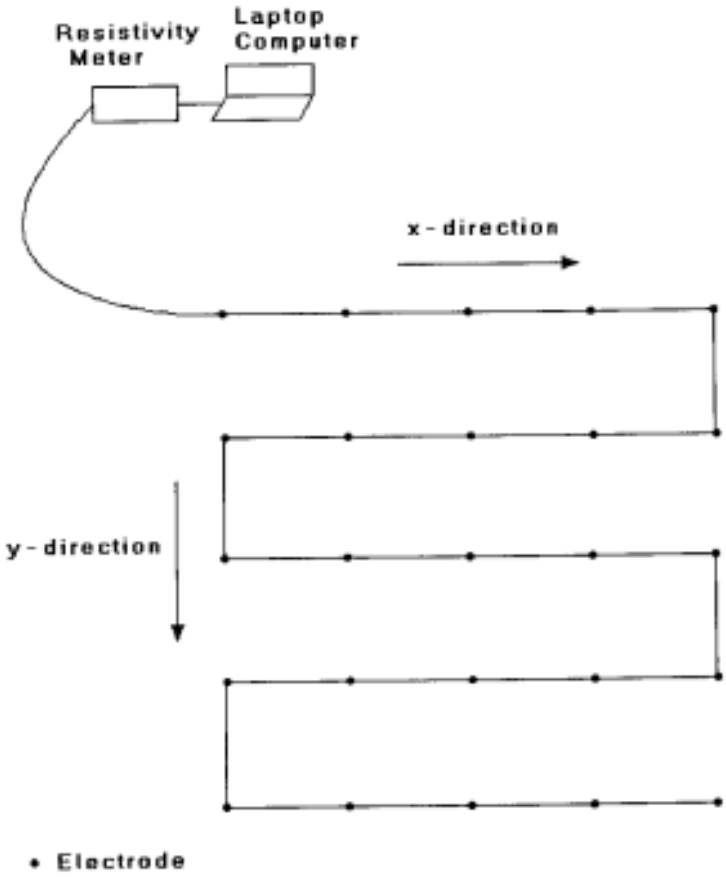

Arrangement of electrodes along a multicore cable for a 3D resistivity survey.

Figure 2.5: Arrangement of electrodes along a multicore cable for a 3D resistivity survey

Limitations

An alternative imaging method that is effective at locating subsurface material is resistivity surveys. There are some restrictions, just like with other geophysical techniques, though. For instance,

i. The detectable depth of VES surveys has a maximum depth. The greatest possible separation between the current electrodes is crucial in this.
ii. Additionally, because VES typically works with horizontal layers, a steep topographic variation will make the survey challenging.
iii. The surveys take a lot of time and effort to complete. The electrodes must constantly be moved along a specific profile, as with electric profiling.

2.2.2 Ground Penetrating Radar

2.2.2.1 Theory

The primary purpose of ground penetrating radar (GPR), a high-resolution electromagnetic technique, is to explore the earth's subsurface at depths of up to a few meters. Roads, bridges, and building supplies. Over the past thirty years, GPR has been developed for shallow, high-resolution subsurface investigations. GPR is a subsurface geophysical method that depends on time. GPR can deliver accurate information about buried objects under the right circumstances. This method can be used to determine an object's depth. utilizing easy formulas. GPR uses electromagnetic wave scattering to find objects that are buried. Electrical engineering and seismic exploration have shaped the fundamental concepts and theory of operation for GPR, and most GPR experts have electrical engineering or geophysical exploration backgrounds. Antennas TX and RX are used by the GPR to transmit and receive electromagnetic waves. As a result, field operational principles similar to the seismic reflection method are now being used. For shallow environmental, engineering, archaeological, and other investigations, GPR is a method that is frequently used. to investigate interesting subsurface features. A time-domain system is the fundamental form of GPR. It consists of a transmitter that produces pulsed signals and a receiver that samples the signal that is returned over time. A frequency-domain system is another typical type in which sinusoidal waves are sent and received while sweeping a specific frequency. One can figure out the time-domain response by performing an inverse Fourier transform of the. response in the frequency domain. The following two principles,

which form the basis of the electromagnetic theory that underlies this technique, can be used to understand its fundamentals:

The propagation velocity v of the electromagnetic wave in soil is characterized by the dielectric permittivity and magnetic permeability of the medium:

$$v = \frac{1}{\sqrt{\varepsilon}\mu} = \frac{1}{\sqrt{\varepsilon_0 \varepsilon_r \mu_0 \mu_r}} \quad \textit{(2.4)}$$

$$\boldsymbol{\lambda = \frac{v}{f} = \frac{2n}{\omega\sqrt{\varepsilon}\mu}} \quad \textit{(2.5)}$$

The same goes for the wave velocity inside the medium:

$$v = \frac{C}{\sqrt{\varepsilon_r}} \quad \textit{(2.6)}$$

Each wave from the antenna takes a different trajectory depending on the characteristics of the media. In the next graphic the image is an insight about how a GPR Survey array should works and the different kinds of waves involved.

2.2.2.2 Wave Propagation

Electromagnetic waves are propagated in a vacuum, in dielectrics and conductors. The propagation of radiated waves of periodic type that are characterized by a wavelength and defined by a wave velocity which depends on the permittivity and permeability of the crossed medium are very interested. Thus, plane wave, as represented in Figure 2.6, propagating in direction x of an orthogonal reference system (x, y, z) while transporting the electric field E polarized in the direction y and the magnetic induction B in the direction z. The properties of such a wave can be deduced from Maxwell's equations, which link together the electric field E, the magnetic induction B, and the current density J (Barué, 2008).

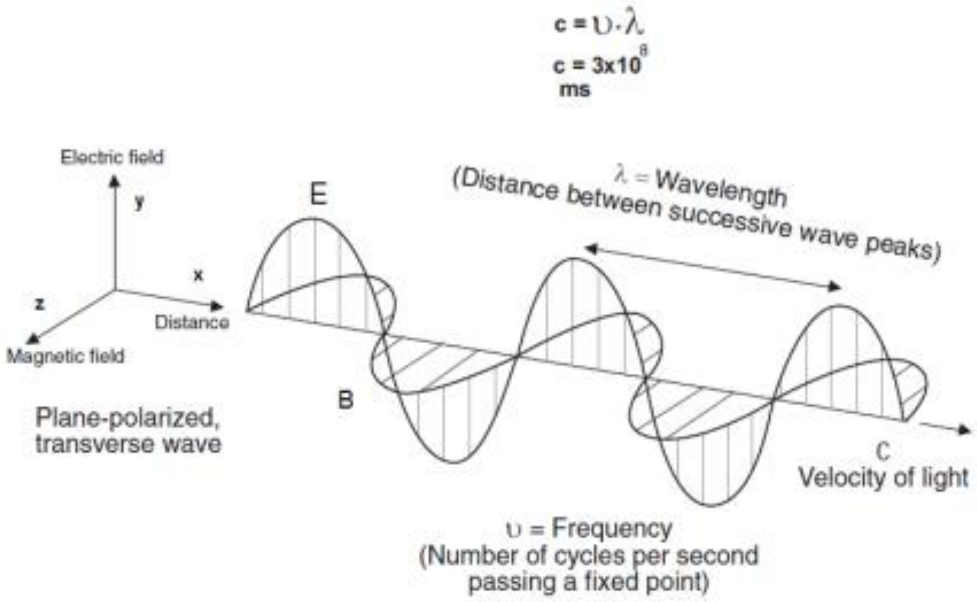

Figure 2.6. Generation and Propagation of Electromagnetic Wave (Lusch,1999)

2.2.2.3 Maxwell Equations

In 1864, J.C. Maxwell established, and synthesized preceding results obtained by M. Faraday, and A. Ampere and K.F. Gauss (Qian and Chen, 1996) about the interaction between the electric field, the magnetic field and currents, generalizing them to variable regimes in time. The Maxwell equations represent the starting point to solve electromagnetic problems 69 as they govern the generation and propagation of electromagnetic waves, as well as the interaction of these waves with the matter. For electromagnetic sources in non-conducting lossless, isotropic media, the Maxwell equations can be written as; (Khuut, 2009).

$$\nabla \mathbf{X}\, \mathbf{E} = -\frac{\partial B}{\partial t} \qquad (2.7)$$

$$\nabla \mathbf{X}\, \mathbf{H} = \mathbf{J} + \frac{\partial D}{\partial t} \qquad (2.8)$$

$$\nabla \mathbf{X}\, \mathbf{B} = \mathbf{0} \qquad (2.9)$$

$$\nabla \mathbf{X}\, \mathbf{D} = \rho_v \qquad (2.10)$$

$$D = \varepsilon \cdot E \qquad (2.11)$$

$$J = \sigma \cdot E \qquad (2.12)$$

$$B = \mu \cdot H \qquad (2.13)$$

Where E -The electric field intensity vector in Volt/meter.

B -The magnetic flux density vector in Tesla.

H -The magnetic field intensity vector in Ampere/meter.

D -The current displacement vector in Coulomb/meter^2

J - The electric current density vector in Ampere/meter^2

ρ -The electric charge density in Coulomb/meter^2

ε -The dielectric permittivity. μ -The magnetic permeability.

σ -The electric conductivity.

2.2.2.4 Principles of Ground-Penetrating Radar:

Operation and Modes of Data Acquisition

GPR measurements are based on the transmission and reflection of an electromagnetic wave in the studied medium (Chanzy et al., 1996). The radar system causes the transmitter antenna (x T) to generate a wave train of radiowaves which propagates away in a broad beam (Reynolds, 1997). Variation in the electrical properties of the subsurface cause part of the transmitted signal to be reflected and this reflected signal is detected by the receiver (Davis and Annan, 1989). As indicated in Figure 2.7, several waves may reach the receiver antenna (Du and Rummel, 1994): the ground wave is that propagating directly from the transmitter to the receiver through the ground, the air wave is that which travels directly between the transmitter and receiver antennas, the reflected waves represent energy returned directly at a boundary while refracted waves occur when a change in electrical property is encountered and the wave travels along the interface and consequently arrives later than its corresponding reflected wave.(Charlton, 2006).

The depth of penetration of radio waves depends on their frequency and the nature of the material being surveyed. Figure 2.8 shows how the penetration varies in different materials over the frequency range 1–500 MHz. The permittivity of water is high compared to dry materials, so the water content and porosity are important controls on penetration. (Kearey et al, 2002). GPR is normally used in reflection profiling mode which produces a section Figure 2.9 showing the travel time to the reflectors versus horizontal position (Davis and Annan, 1989).

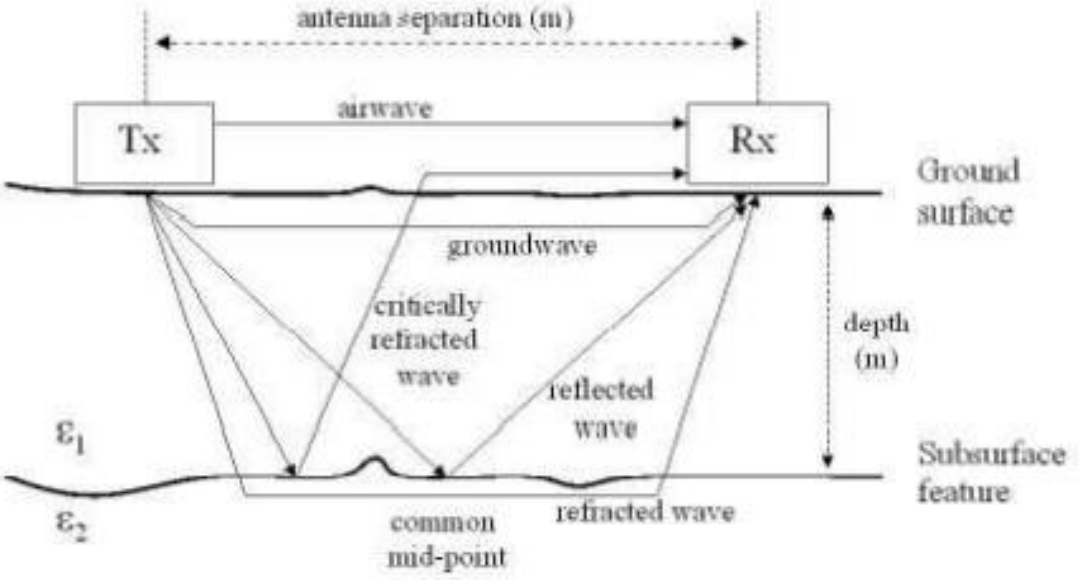

Figure 2.7: Waves reaching the receiver antenna. (Du and Rummel, 1994).

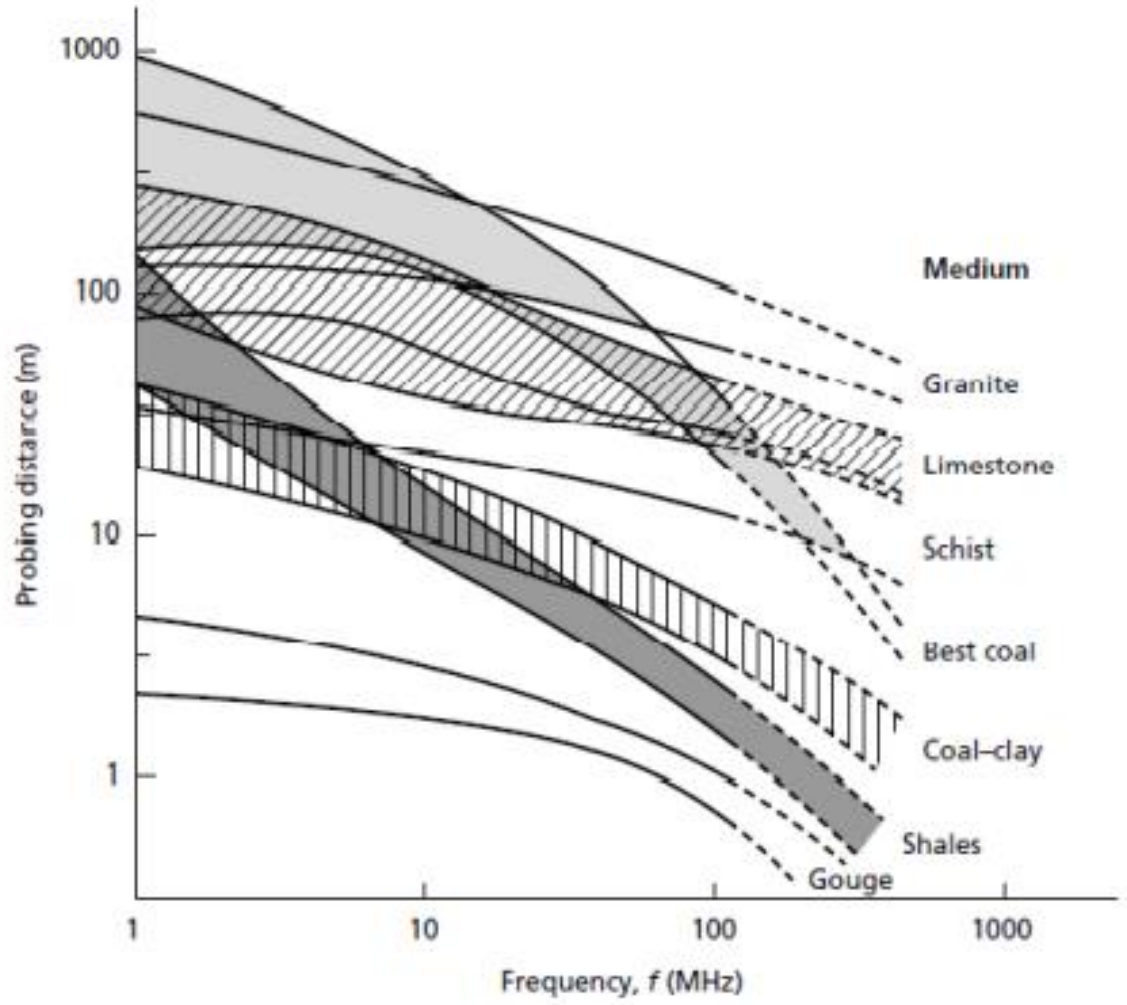

Figure 2.8: The relationship between probing distance and frequency for different materials. (Cook,1975).

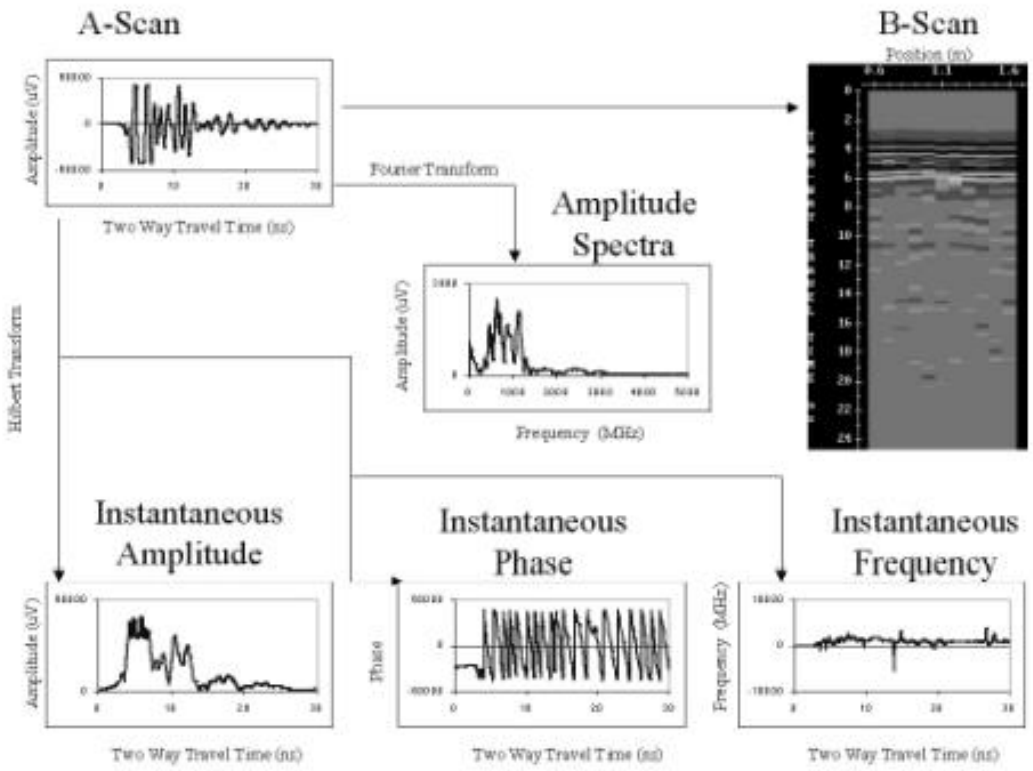

Figure 2.9: Schematic of GPR measurement and analysis domains. Time domain traces (A-scan) can be arranged by sample position (B-scan) and processed into frequency domain (amplitude spectra (Fourier Transform)), and time-frequency representations (instantaneous amplitude, phase and frequency (Hilbert Transform)). (Charlton 2006).

There are three basic modes of deployment in GPR surveys, as explained in Figure 2.10:

1. Reflection profiling (Figure 2.10 (a)), in which the transmitter and receiver antenna are kept at a small, fixed separation; this is often achieved by using the same antenna for transmission and reception. (Kearey and et al, 2002) One or more radar antennae are moved over the ground surface simultaneously, with the measured travel time to radar reflectors being displayed on vertical axis while the distance the antenna has travelled is shown on horizontal axis. This mode of surveying is analogous to continuous seismic reflection profiling (Reynolds 1997).
2. Velocity sounding (Figure 2.10 (b)), in which transmitter and receiver antenna are moved apart about a fixed central point (the common depth point (CDP) method), or one kept stationary while the other is progressively moved away (the wide-angle reflection and refraction (WARR) method). The methods are designed to show how the radar velocity changes with depth. Without this information, velocities might be determined by correlating the radargram with a borehole section or with signals reflected from a body at known depth. In many cases, however, the velocities are guessed. (Kearey et al, 2002).
3. Transillumination (Figure 2.10 (c)), in which the transmitter and receiver antenna are mounted on either side of the object of interest (e.g. a pillar in a mine). If it is arranged that there are many different configurations of transmitter and antenna, radar tomography can be carried out in a similar fashion to seismic. (Kearey et al, 2002) These surveys examine signals transmitted through a volume and use tomographic reconstruction techniques to image the volume between measurement points. These types of measurements have been conducted sporadically to look at rock stability between boreholes. Extensive work has been done in boreholes for nuclear waste disposal assessment. (Annan and Davis 1997)

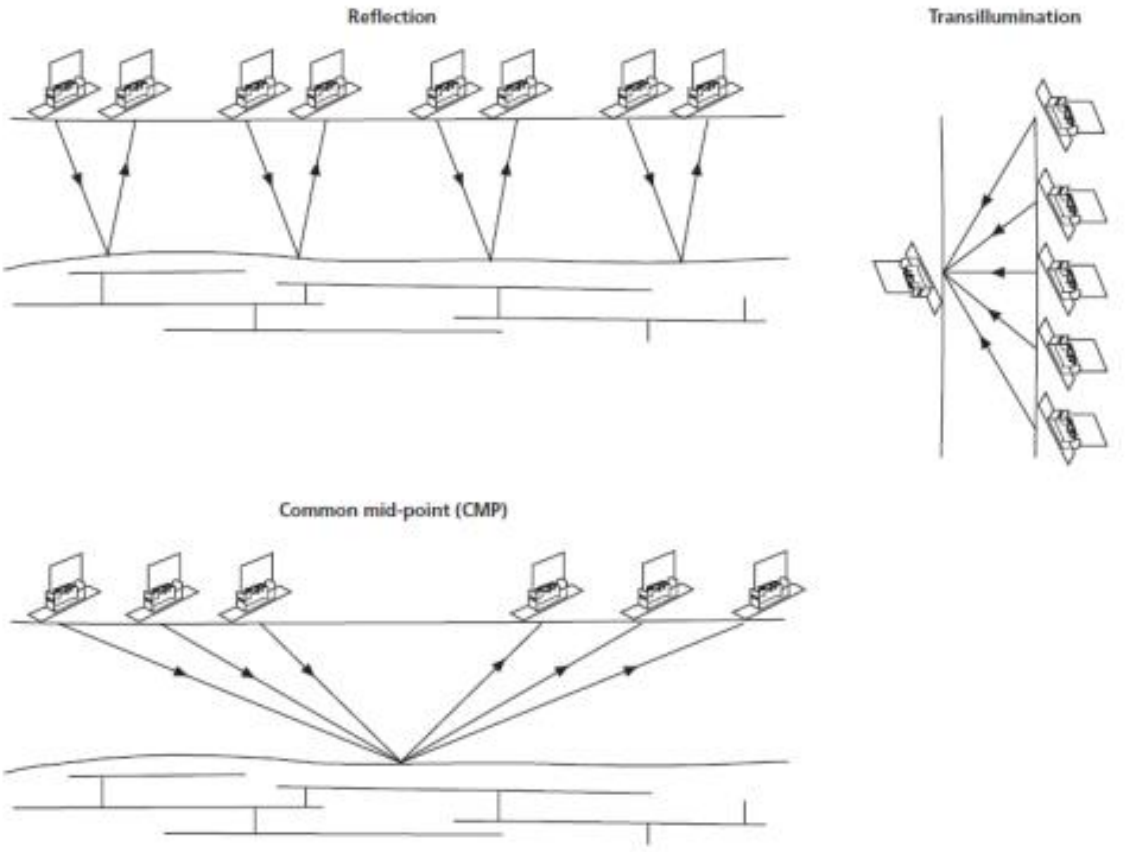

Figure 2.10. The three basic modes of ground-penetrating radar. (Annan, 2001)

CHAPTER THREE

METHODOLOGY

The two geophysical methods integrated for the study of the sand filled region are 2D electrical resistivity and Ground Penetrating Radar. These methods are selected based on their ability give different responses from the sand filled region and two-dimensional images across the strike of the buried channel. The selected geophysical techniques have proven effect in engineering and environmental purposes and providing reliable, accurate and high-resolution images of the subsurface. The combination of more than one geophysical technique helps in reducing the uncertainty of each method due to ambiguity and non-uniqueness. The GPR method has shown its proficiency in engineering and environmental purposes, it measures Radar reflections result from contrasts in dielectric properties between adjacent layers, which can be induced by, amongst others, changes in textural characteristics, water content and state (i.e., liquid, frozen), and fluid conductivity.

3.1 Data Acquisition

3.1.1 GPR Method

The GPR Mala Ground Explorer was used to acquire data for this investigation as shown in (Figure 3.1). The GPR system is composed of a shielded antenna, a control unit, and a MALA rough terrain cart. Due to the depth of investigation, 3 antennas were deployed (80 MHz, 160 MHz, and 450 MHz). Low frequency antennas tend to propagate deeper into the earth's interior but produce low resolution data, while high frequency antenna's get absorbed faster in the earth's interior therefore cannot propagate deep but produce high resolution data. The equipment comes with an inbuilt DGPS (differential GPS) that accurately measures the path of the GPR.

A total of nine traverses of about 60m long were mapped perpendicular to the strike of the river channel as shown in (Fig 3.2), with traverse spacing of 10m. The 450 and 160 MHz antennas were fixed in the rough terrain cart and pushed manually through the 9 traverses. The 80 MHz, due to its size was placed in a rugged plastic cover and pulled on the ground. The data was automatically saved in the equipment and the file number for each of the traverses was recorded.

3.1.2 Instrumentation

i. MALA Ground Explorer.

ii. MALA rough terrain cart.

iii. Control Unit.

iv. A Shielded antenna.

3.1.3 Precautions

i. I ensured to avoid the rough terrain where possible and move the equipment gently.

ii. I ensured the location surface was dry as possible, as any wet surface would be conducive and give false readings.

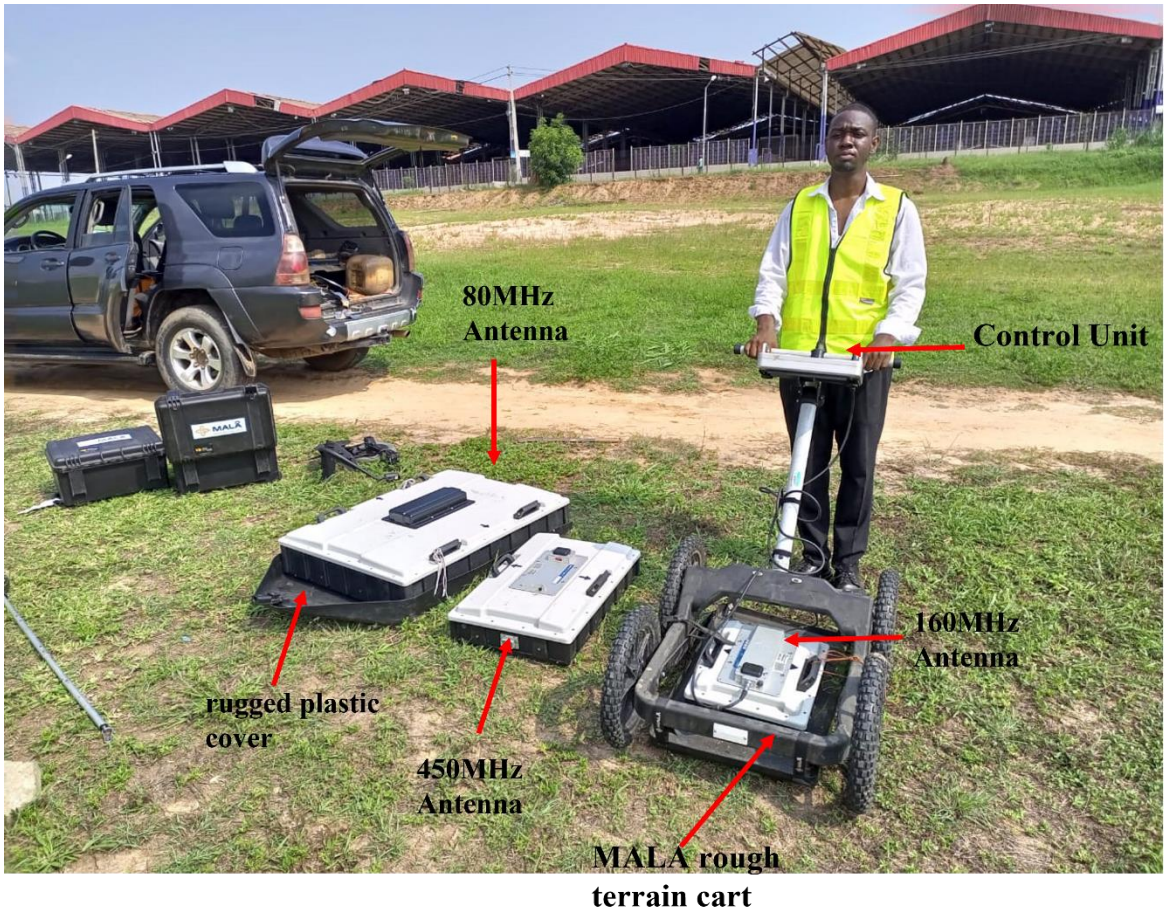

Figure 3.1. Mala GPR Explorer with all three antennas

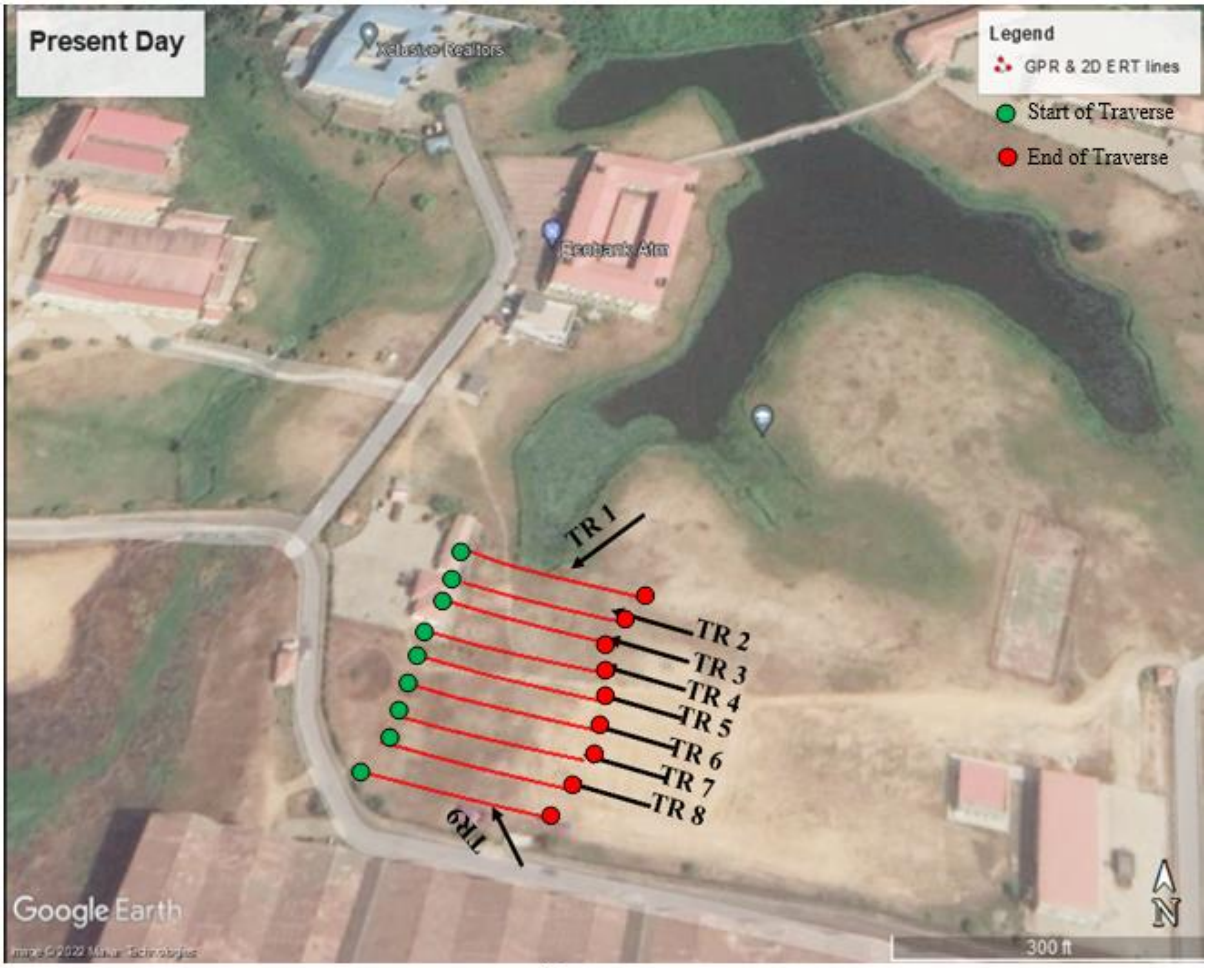

Figure 3.2. Satellite imagery showing the GPR lines

3.1.4 Electrical Resistivity Dipole-Dipole ERT.

The ABEM Terrameter LS was used to obtain data for the 2D Electrical Resistivity Survey. The ABEM LS is made up of Resistivity and IP surveying system, with 64 electrodes that connected via cable and a power source that powers up the Resistivity/IP system. The system setup for the data acquisition is seen in (Figure 3.3). Data were collected along nine traverses using Dipole – Dipole array because of its lateral resolution, depth of penetration and ability to resolve vertical structures. 1m electrode spacing was used to ensure high subsurface resolution and a length of 63m was covered.

The 2D-ERT is a prominent in engineering investigations. Two-dimensional (2-D) resistivity tomography is a vital tool in measuring the subsurface layers due to its continuous lateral and vertical imaging along a traverse. (Figure 3.4) shows nine traverses mapped out in the survey area. The readings took about an hour per traverse. The total resistivity data points acquired on each traverse is about 1,980. The data was automatically saved in the equipment and the file number for each of the traverses was recorded.

3.1.5 Instrumentation

2D Electrical Resistivity method requires the following equipment:

i. ABEM LS
ii. 63 steel electrodes and clips
iii. Multicore Cable.
iv. GPS Device.
v. Metre Rule.

3.1.6 Precautions

i. Good ground contact was ensured for the electrodes
ii. Clips on each electrode was properly connected to the cables

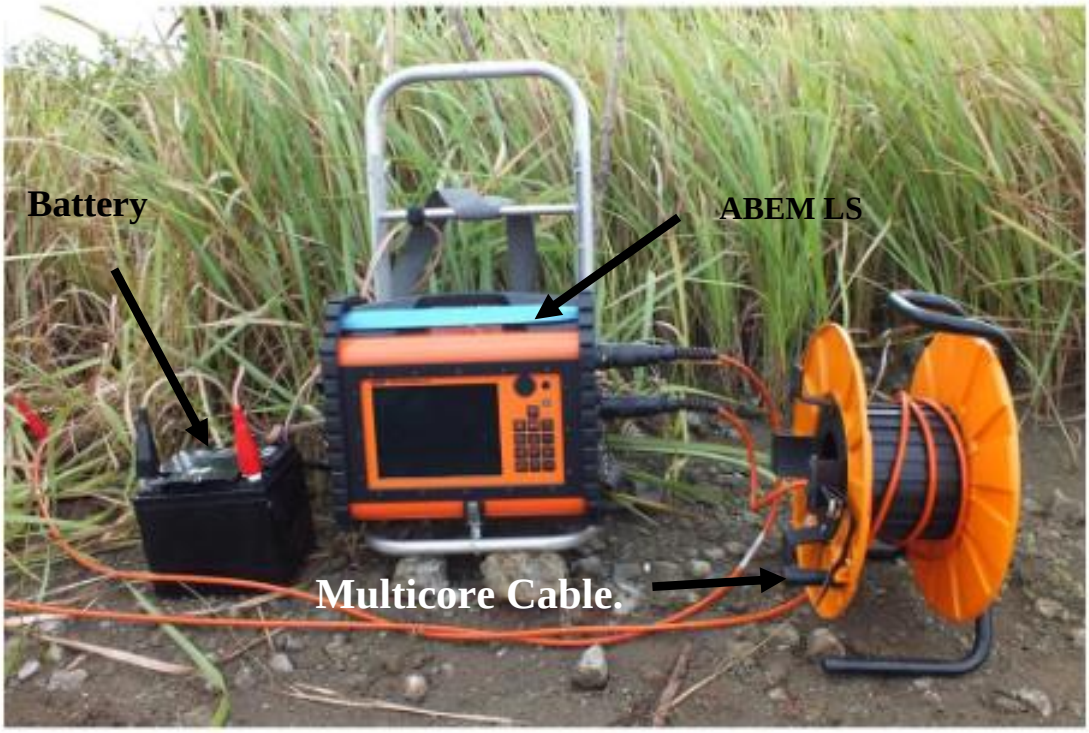

Figure 3.3. ABEM Terrameter LS

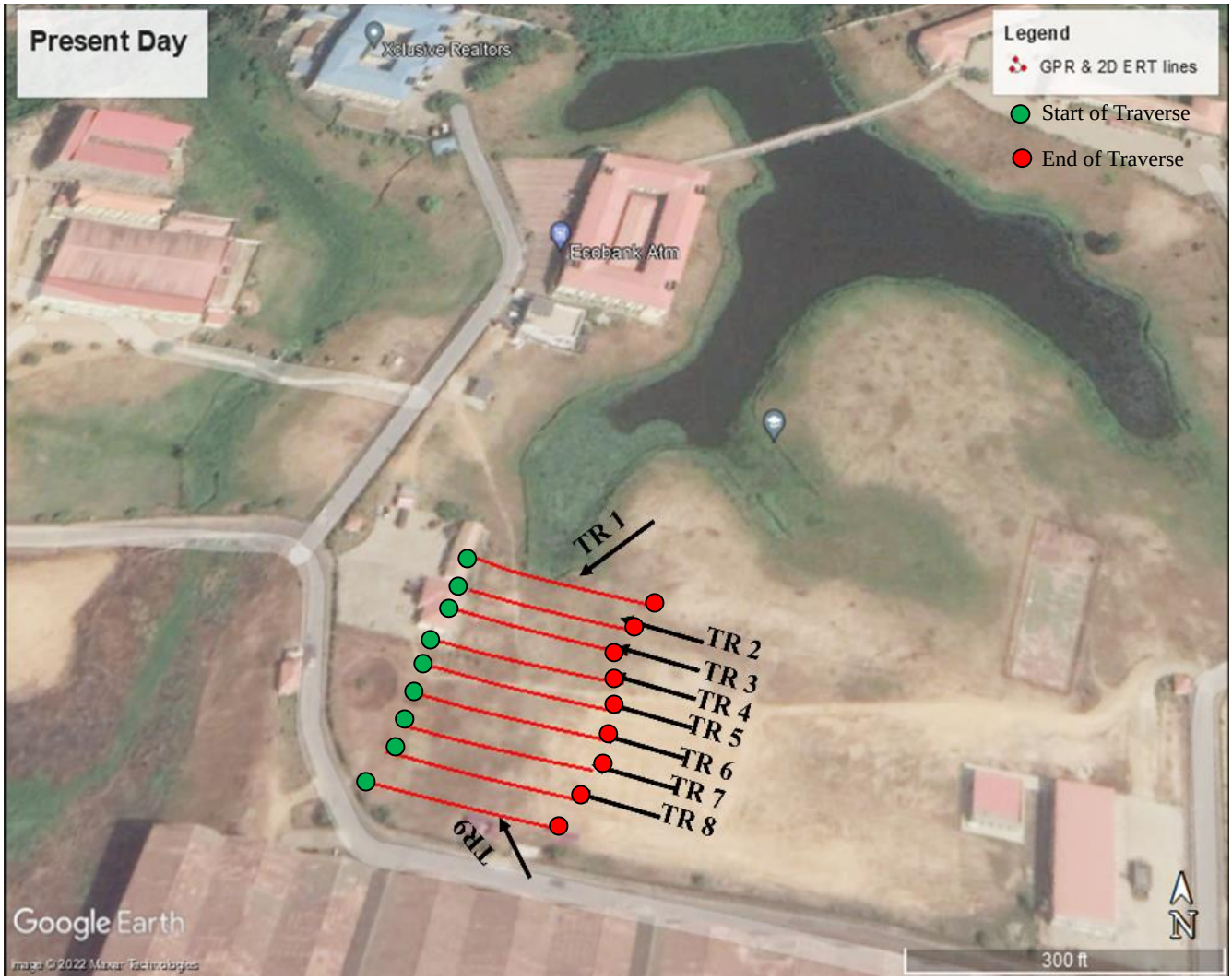

``

Figure 3.4. Satellite imagery showing the 2D ERT lines

3.2 DATA PROCESSING AND INTERPRETATION

Prior to data processing, the field data were downloaded from each of the equipment. The Mala GPR data comprises of different files that stores both measurement parameters and field data. The. rd3 is the file format that stores the GPR data while .cor files stores the coordinate data of each traces acquired. The .mrk file stores the antenna frequency and other acquisition parameters such as number of traces, length of profile and type of antenna.
The 2D ERT data was downloaded in .dat format.

Ground Penetrating Radar

The data were processed and analysed with Geolitix Software which is a cloud-based processing software at https://www.geolitix.com/. Apart from data processing, the software has the capability of mapping point events such as hyperbola arising from utilities (pipes, cables etc.) and horizon events such as horizontal reflector from contrast in physical boundaries (change in lithology, unconformity, water table etc.).

Different processing was carried out on the GPR field data to enhance the subsurface information. The major aim of GPR data processing was to improve the reflected signals from buried utilities and attenuate the noise signals. The processes are basically gain and time filters. Time zero adjustment was used to eliminate air waves and bring the first event to the surface for proper depth measurements. Energy decay was used to supress signal attenuation with depth. Background removal was used to remove instrumental and electrical noise while normalisation was used to suppress high amplitudes and enhance low amplitude events for enhanced visualisation/balancing. Velocity of 0.1m/ns was adopted for depth estimation as this is an average velocity for soils (Reynolds, 2002).

Events related to the sandfill and channel fill appears as continuous reflectors with abrupt termination at the flanks that are expressive of incised channels configurations. These events were mapped on each GPR line and the arrival time and estimated depths were exported as csv (comma separated version) files. The data across all the traverses were compiled in excel and saved as a single file prior to gridding in Surfer software.

Surfer Software was used to grid the arrival time and depth against the coordinates of the mapped events. This was used to generate time and depth map of the events interpreted as the sandfill and channel fill in the study area.

2D (and 3D ERT) Method

The field apparent resistivity data (in .dat format) was uploaded into the Earth Imager Software (AGI, 2009) for processing and inversion. Smooth model inversion was selected and the software generated a calculated model and after several iterations an inverted 2D resistivity section was generated. The rms error of the inverted resistivity section are generally within 10 to 20%. The result of the inversion is presented as a color-coded 2D inverted electrical resistivity section. The resistivity (range) of each color is presented as a logarithmic color scale bar on the section, while the lateral and depth investigated are represented as the horizontal and vertical scale in meters, respectively.

The parallel 2D lines/traverse were combined with EarthImager 3D to generate a 3D resistivity file (Fig 3.4a) which was inverted to generate a 3D inverted resistivity model of the investigated area. The RMS of the 3D inversion is as presented in Fig 3.4b. The 3D inverted resistivity model is presented as a 3D resistivity cube that was sliced in different directions along the X, Y and Z axis. For enhanced visualization, the 3D cube was sliced dynamically. Expected low resistivity anomaly response associated with channel or buried channel against the lateritic soil background was also isolated in the 3D resistivity cube to form a 3D iso-resistivity contour surface for visual rendering of the sandfill/channel fill.

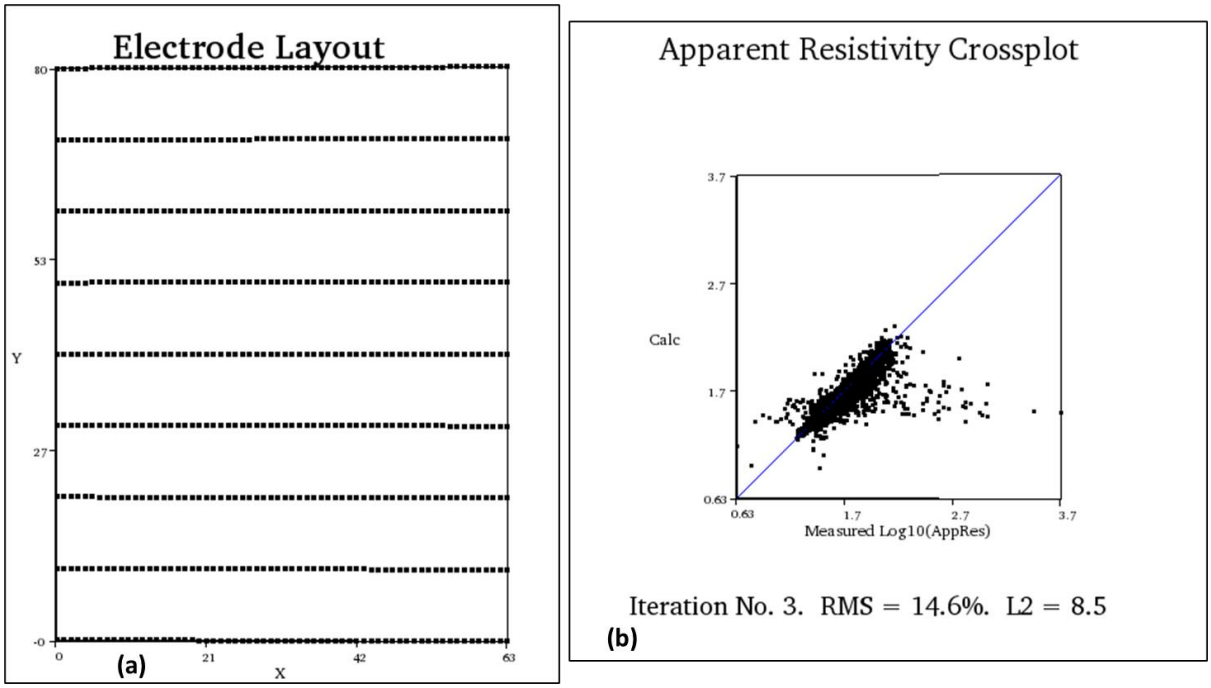

Fig 3.4 (a) Layout of 3D ERT from the combined parallel 2D Lines (b) Cross plot showing the RMS after 3D resistivity inversion of the parallel 2D lines

CHAPTER FOUR

RESULTS AND DISCUSSION

4.1 RESULTS

The result of the Electrical Resistivity method is presented as 2D inverted resistivity sections in Figs 4.1 to 4.9. The result of the inverted 3D resistivity data from the joined parallel 2D lines is presented as 3D inverted resistivity cube in Fig 4.10, X and Y slices in Fig 4.11a and 4.11b, Dynamic slices in Fig 4.12a and 4.12b and 3D iso-resistivity surfaces (Fig 4.13).

The result of the processed GPR data is presented as GPR sections in Appendix A and Figs 4.14 to 4.22 of which the vertical section is in depth as converted by an average velocity of 0.1m/ns while the horizontal axis is the trace number.

4.2 DISCUSSION OF RESULTS

4.2.1 2D Electrical Resistivity Imaging (ERI)

Traverse 1

Figure 4.1 is the interpreted 2D inverted electrical resistivity section along Traverse 1. The resistivity along this section ranges from 9Ωm to about 214 Ωm and a depth of about 13.8m was investigated.

The 2D electrical resistivity section can be characterized into two main geoelectric layers based on its vertical and lateral variation in electrical resistivity values. The first region is represented by varying resistivity range of 9 to 214 Ωm and thickness range of 5 to 7.5m. Within the lateral distance of about 24 to 46m a low resistivity anomaly (9 to 43 Ωm) can be observed at a depth range of about 3 to 3.4m. The configuration of this low resistivity anomaly is analogous to the configuration of an incised channel against the background/country rock. This region is therefore associated to the main course of the sandfill/river channel region. Other regions within the first geoelectric layer are with relatively high electrical resistivity value range of 44 to 214 Ωm expressive of the topsoil/lateritic soil.

The second geoelectric layer is with relatively low resistivity range of 19 to 43 Ωm expressive of clay/sandy clay layer and delineated to an average depth of about 13.8m.

Traverse 2

Figure 4.2 is the interpreted 2D electrical resistivity section along Traverse 2. The resistivity along this section ranges from 14.4 Ωm to about 430 Ωm and a depth of about 13.8m was investigated.

The 2D electrical resistivity section can be characterized into two main geoelectric layers based on its vertical and lateral variation in electrical resistivity values. The first region is represented by varying resistivity range of 14 to 430 Ωm and thickness range of 3 to 6m. Within the lateral distance of about 20 to 48m a low resistivity anomaly (14 to 33 Ωm) can be observed at a depth range of about 1.5 to 3.4m. The configuration of this low resistivity anomaly is analogous to the configuration of an incised channel against the background/country rock. This region is therefore associated to the main course of the sandfill/channel region.

The second geoelectric layer is with relatively low resistivity range of 14 to 54 Ωm expressive of clay/sandy clay layer and delineated to an average depth of about 13.8m.

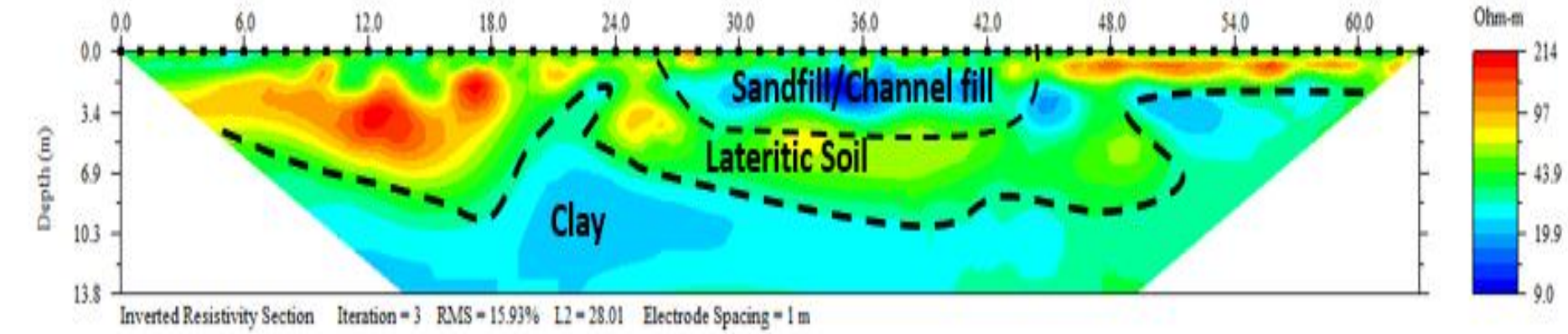

Figure 4.1. Inverted Resistivity Section for traverse 1

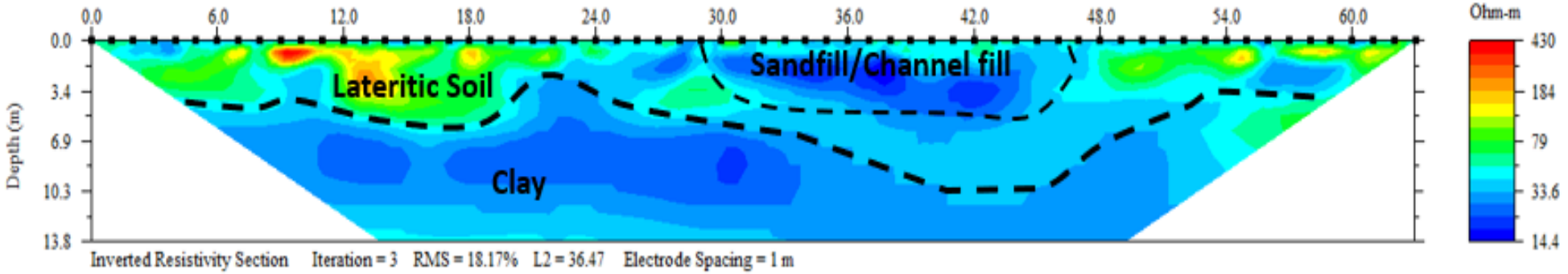

Figure 4. 2 Inverted Resistivity Section for traverse 2.

Traverse 3

Figure 4.3 is the interpreted 2D inverted electrical resistivity section along Traverse 3. The resistivity along this section ranges from 8.1 Ωm to about 1576 Ωm and a depth of about 13.8m was investigated.

Similarly, the 2D electrical resistivity section can be characterized into two main geoelectric layers based on its vertical and lateral variation in electrical resistivity values. The first region is represented by varying resistivity range of 8 to 1576 Ωm and varying thickness range of 3 to 7m. Within the lateral distance of about 22 to 48m a low resistivity anomaly of 8 to 30 Ωm can be observed at a depth range of about 1.5 to 3.8m. The configuration of this low resistivity anomaly is analogous to the configuration of an incised channel against the background/country rock. This region is therefore associated to the main course of the sandfilled river channel region. Other regions within the first geoelectric layer are with varying electrical resistivity value range of 30 to 1576 Ωm expressive of the topsoil/lateritic soil.

The second geoelectric layer is with relatively low resistivity range of 8 to 58 Ωm expressive of clay/sandy clay/Sand layer and delineated to an average depth of about 13.8m.

Traverse 4

Figure 4.4 is the interpreted 2D inverted electrical resistivity section along Traverse 4. The resistivity along this section ranges from 10.9 Ωm to about 221 Ωm and a depth of about 13.8m was investigated.

The 2D electrical resistivity section can be characterized into two main geoelectric layers based on its vertical and lateral variation in electrical resistivity values. The first region is represented by varying resistivity range of 10 to 221 Ωm and thickness range of 4.5 to 8m. Within the lateral distance of about 20 to 46m a low resistivity anomaly (10 to 23 Ωm) can be observed at a depth range of about 1.5 to 2.4m. The configuration of this low resistivity anomaly is analogous to that of an incised channel against the background/country rock. This region is therefore suggestive of the main course of the sandfilled region/river channel. Other regions within the first geoelectric layer are with relatively high electrical resistivity value range of 49 to 221 Ωm which can be associated to the topsoil/lateritic soil.

The second geoelectric layer is with relatively low resistivity range of 10 to 23 Ωm expressive of clay/sandy clay layer and delineated to an average depth of about 13.8m.

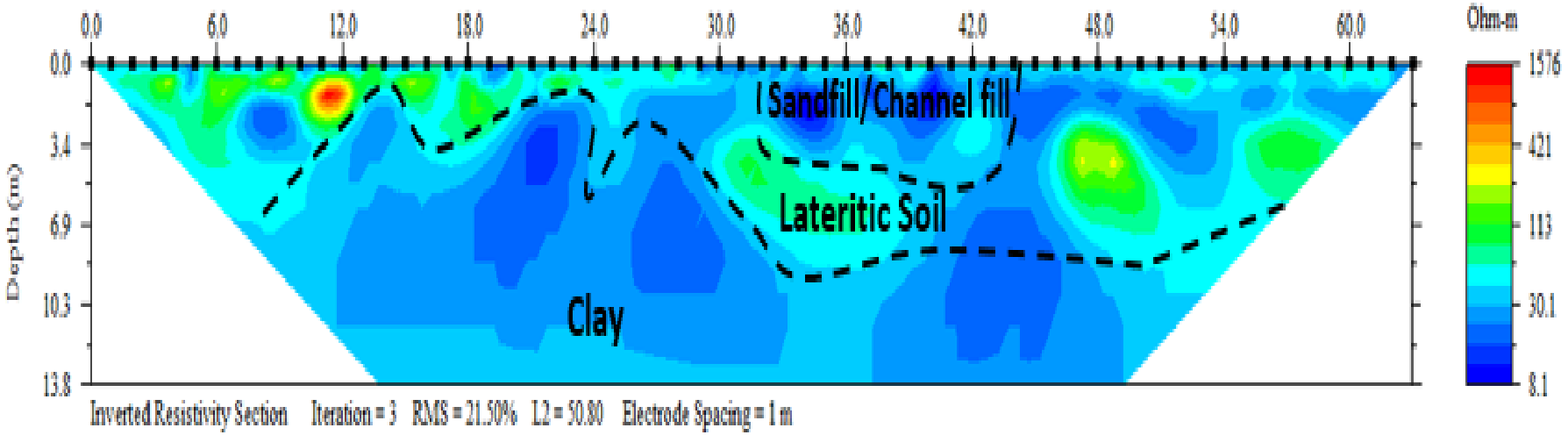

Figure 4.3. Inverted Resistivity Section for traverse 3.

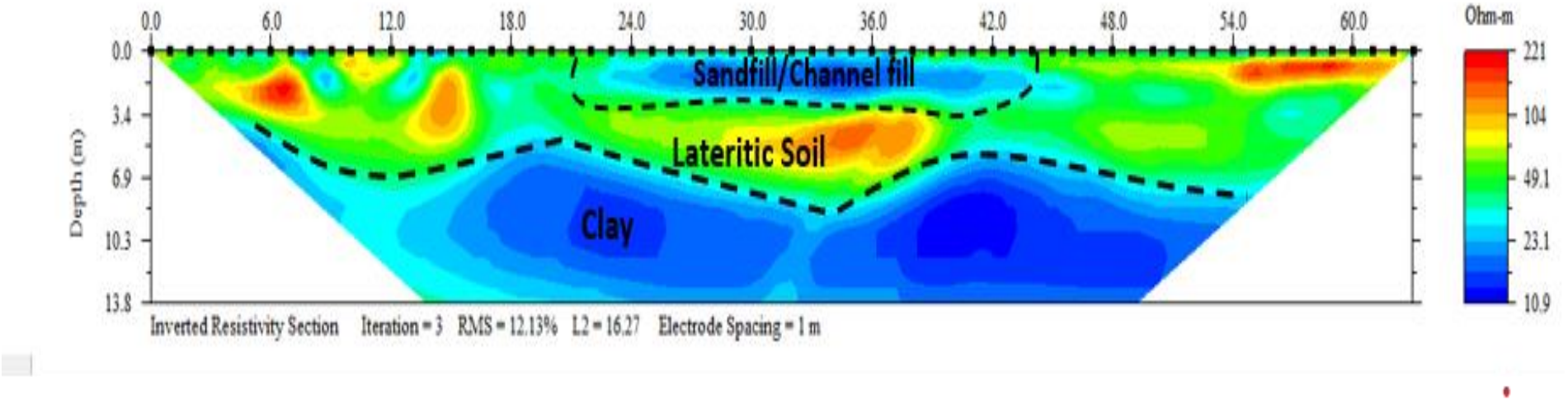

Figure 4.4. Inverted Resistivity Section for traverse 4

Traverse 5

Figure 4.5 is the interpreted 2D inverted electrical resistivity section along Traverse 5. The resistivity along this section ranges from 7.2 Ωm to about 341 Ωm and a depth of about 13.8m was investigated.

Similarly, the 2D electrical resistivity section can be characterized into two main geoelectric layers. The first region is represented by varying resistivity range of 7 to 341 Ωm and thickness range of 4 to 7.2 m. At a lateral distance of about 18 to 36 m a low resistivity anomaly of 7 to 49 Ωm can be observed at a depth range of about 2 to 2.5m. The configuration of this low resistivity anomaly is analogous to that of an incised channel against the background/country rock. This region is therefore indicative of the main course of the sandfilled region/river channel. Other regions within the first geoelectric layer are with relatively high electrical resistivity value range of 49 to 341 Ωm which can be associated to the topsoil/lateritic soil.

The second geoelectric layer is with relatively low resistivity range of 7 to 19 Ωm indicative of clay/sandy clay layer and delineated to an average depth of about 13.8m.

Traverse 6

Figure 4.6 is the interpreted 2D inverted electrical resistivity section along Traverse 6. The resistivity along this section ranges from 4.9 Ωm to about 935 Ωm and a depth of about 13.8m was investigated.

This 2D ERT can be characterized into two main geoelectric layers. The first region is represented by varying resistivity range of 5 to 935 Ωm and thickness range of 5 to 7 m. At a lateral distance of about 18 to 37 m, a low resistivity anomaly of 5 to 35 Ωm can be observed at a depth range of about 1.5 to 2.5m. The configuration of this low resistivity anomaly is similar to that of an incised channel against the background/country rock. This region is therefore indicative of the main course of the sandfilled region/river channel. Other regions within the first geoelectric layer are with relatively high electrical resistivity value range of 67 to 935 Ωm which can be associated to the topsoil/lateritic soil.

The second geoelectric layer is with relatively low resistivity range of 5 to 18 Ωm indicative of clay/sandy clay layer and delineated to an average depth of about 13.8m.

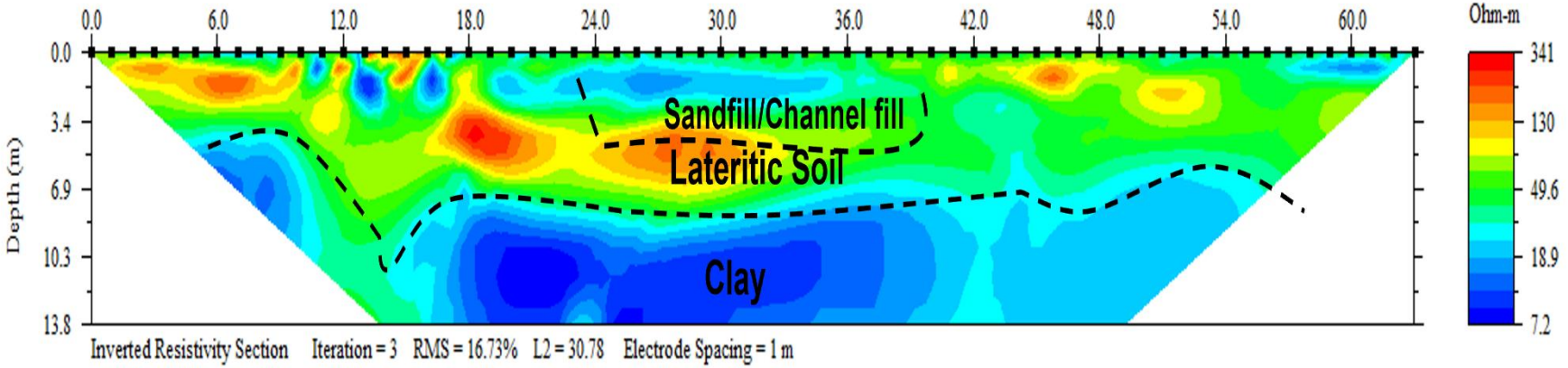

Figure 4.5. Inverted Resistivity Section for traverse 5

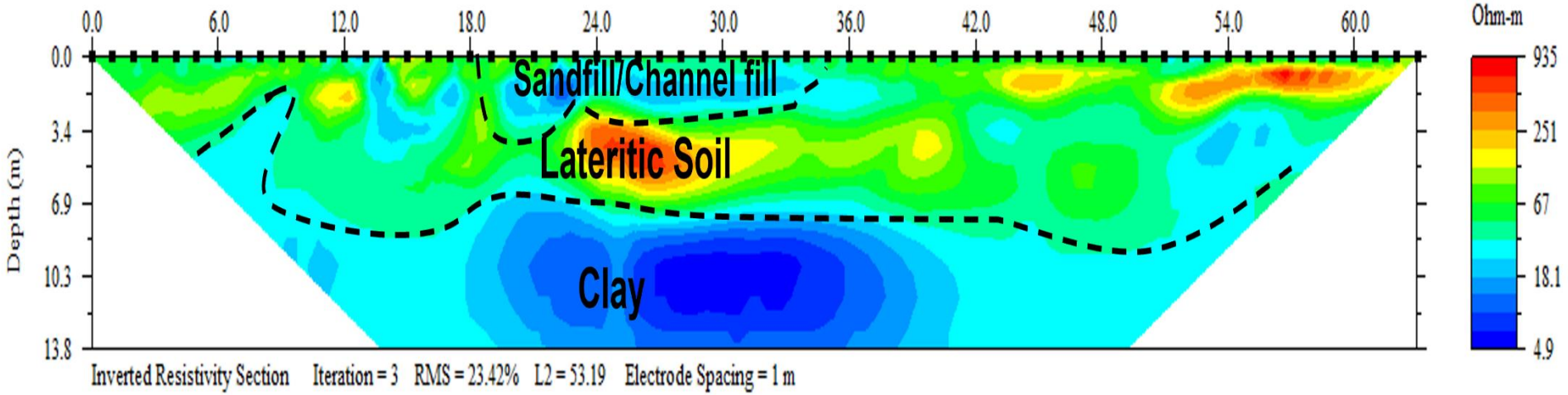

Figure 4.6 Inverted Resistivity Section for traverse 6

Traverse 7

Figure 4.7 is the interpreted inverted 2D electrical resistivity section along Traverse 7. The resistivity along this section ranges from 7.2 Ωm to about 281 Ωm and a depth of about 13.8m was delineated.

This 2D ERT can be characterized into two main geoelectric layers. The first region is represented by resistivity range of 45 to 281 Ωm and thickness range of 5 to 7 m. At a lateral distance of about 16 to 36 m, region of relatively low resistivity anomaly of about 45 Ωm can be observed within the first geoelectric layer at a depth range of about 1.5 to 2m. The shape of this relatively low resistivity region is analogous to the shape of an incised channel against the background/country rock. This region is therefore indicative of the region occupied by the main course of the sandfilled region/river channel. Other regions within the first geoelectric layer are with relatively high electrical resistivity value range of 67 to 935 Ωm which can be associated to the topsoil/lateritic soil.

The second geoelectric layer is with relatively low resistivity range of 7 to 18 Ωm indicative of clay/sandy clay layer and delineated to an average depth of about 13.8m.

Traverse 8

Figure 4.8 is the interpreted inverted 2D electrical resistivity section along Traverse 8. The resistivity along this section ranges from 8.5 Ωm to about 240 Ωm and a depth of about 13.8m was investigated.

This 2D ERT can be characterized into two main geoelectric layers. The first region is represented by resistivity range of 45 to 240 Ωm and thickness range of 4 to 6.5 m. At a lateral distance of about 18 to 34 m, region of relatively low resistivity anomaly of about 45 to 68 Ωm can be observed within the first geoelectric layer at a depth range of about 1.5 to 2m. The shape of this relatively low resistivity region is analogous to the shape of an incised channel against the background/country rock. This region is therefore indicative of the region occupied by the main course of the sandfilled region/river channel. Other regions within the first geoelectric layer are with relatively high electrical resistivity value range of 68 to 240 Ωm which is descriptive of the topsoil/lateritic soil.

The second geoelectric layer is with relatively low resistivity range of 8 to 45 Ωm suggestive of clay/sandy clay layer and delineated to an average depth of about 13.8m.

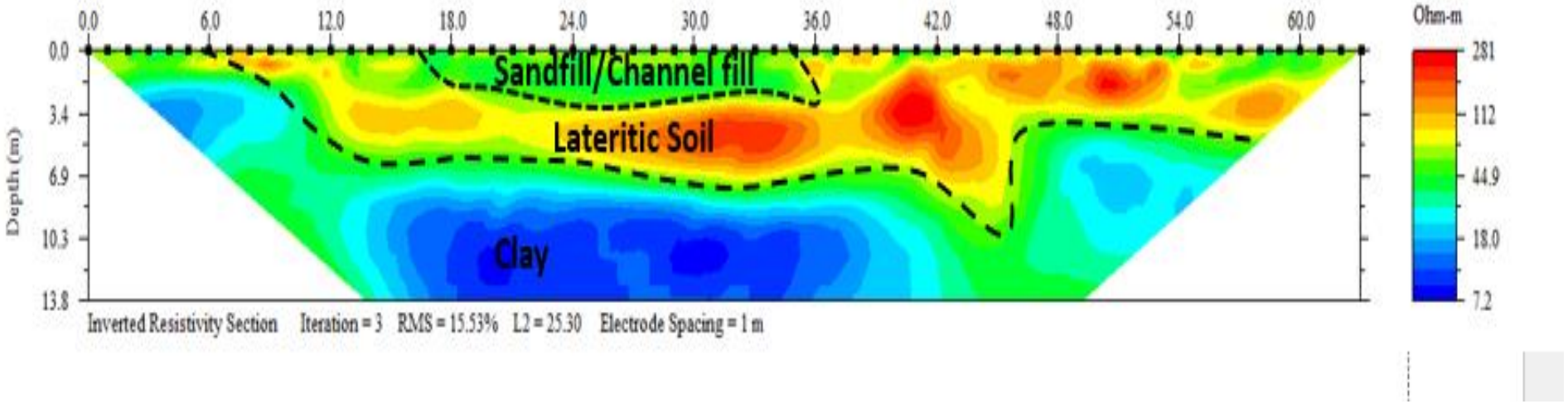

Figure 4.7. Inverted Resistivity Section for traverse 7

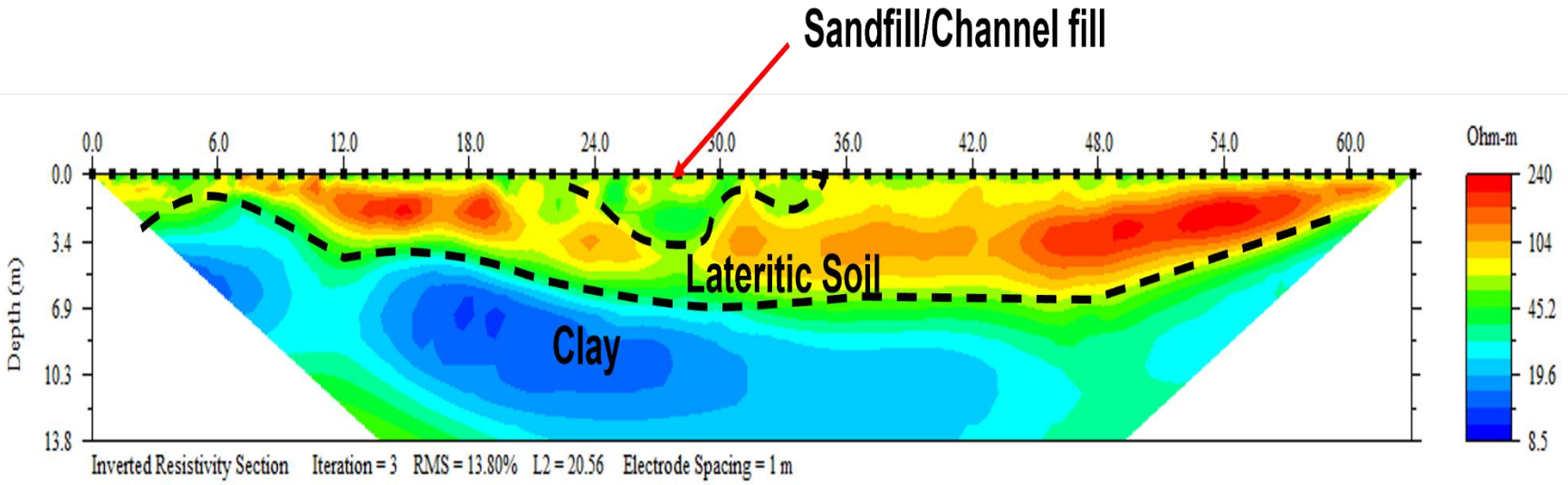

Figure 4.8. Inverted Resistivity Section for traverse 8

Traverse 9

Figure 4.9 is the interpreted inverted 2D electrical resistivity section along Traverse 9. The resistivity along this section ranges from 12.8 Ωm to about 190 Ωm and a depth of about 13.8m was investigated.

This 2D ERT can be characterized into two main geoelectric layers. The first region is represented by resistivity range of 49 to 190 Ωm and thickness range of 4 to 5.5 m. At a lateral distance of about 18 to 26 m, subtle relatively low resistivity anomalies of about 49 to 60 Ωm can be observed within the first geoelectric layer at a depth range of about 1.5 to 2.5m. The shape of this relatively low resistivity region is analogous to the shape of an incised channel against the background/country rock and therefore indicative of the region occupied by the main course of the sandfilled region/river channel. Other regions within the first geoelectric layer are with relatively high electrical resistivity value range of 68 to 190 Ωm which is descriptive of the topsoil/lateritic soil.

The second geoelectric layer is with relatively low resistivity range of 12 to 25 Ωm suggestive of clay/sandy clay layer and delineated to an average depth of about 13.8m.

3D augmented view of parallel 2D ERT Lines

The parallel 2D ERT lines have been correlated and presented as a 3D augmented view in Fig 4.10. The existing lake/river is at the Northern region of the parallel lines. The near surface anomalously low resistivity region can be observed across all the 2D ERT lines which depicts the region occupied by the buried/sandfilled part of the river channel. Resistivity variation can also be observed from the proximal end (northern part) to distal end (southern part) of the buried river channel. The proximal end is represented by relatively lower resistivity compared to the distal end which can be indicative of varying materials such as clay/peat at the proximal part and sandy material at the distal end. This calls for adequate engineering precautions in the foundation design such as pile foundation if the region will be considered for future engineering development. This could also be as a result of higher water saturation at the proximal end compared to the distal end of the buried/sandfilled river channel.

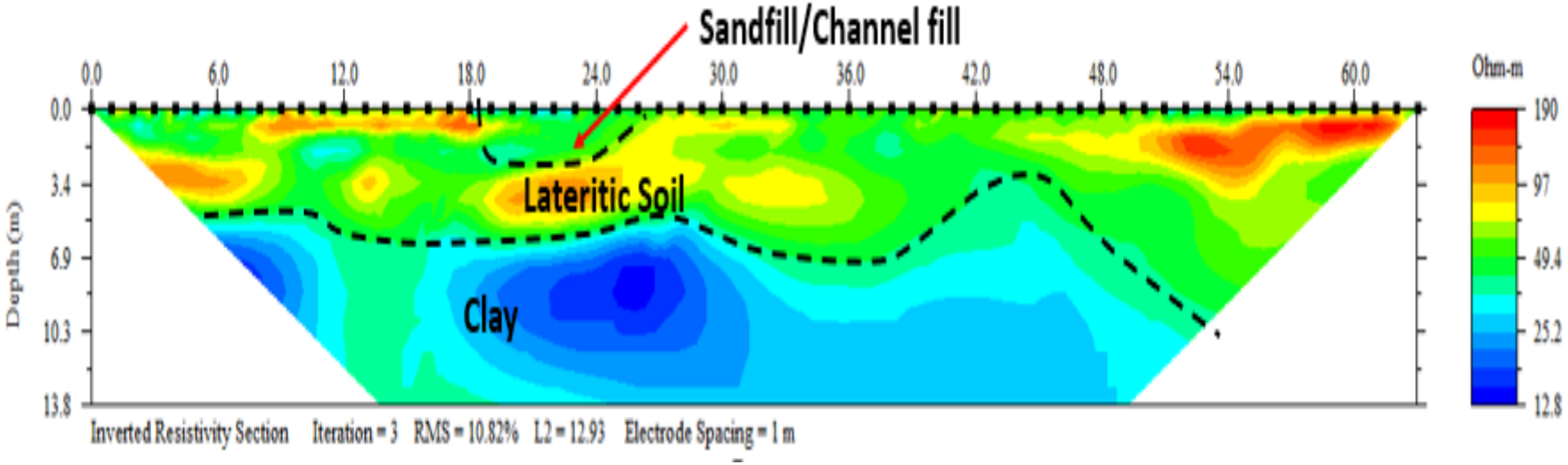

Figure 4.9. Inverted Resistivity Section for traverse 9.

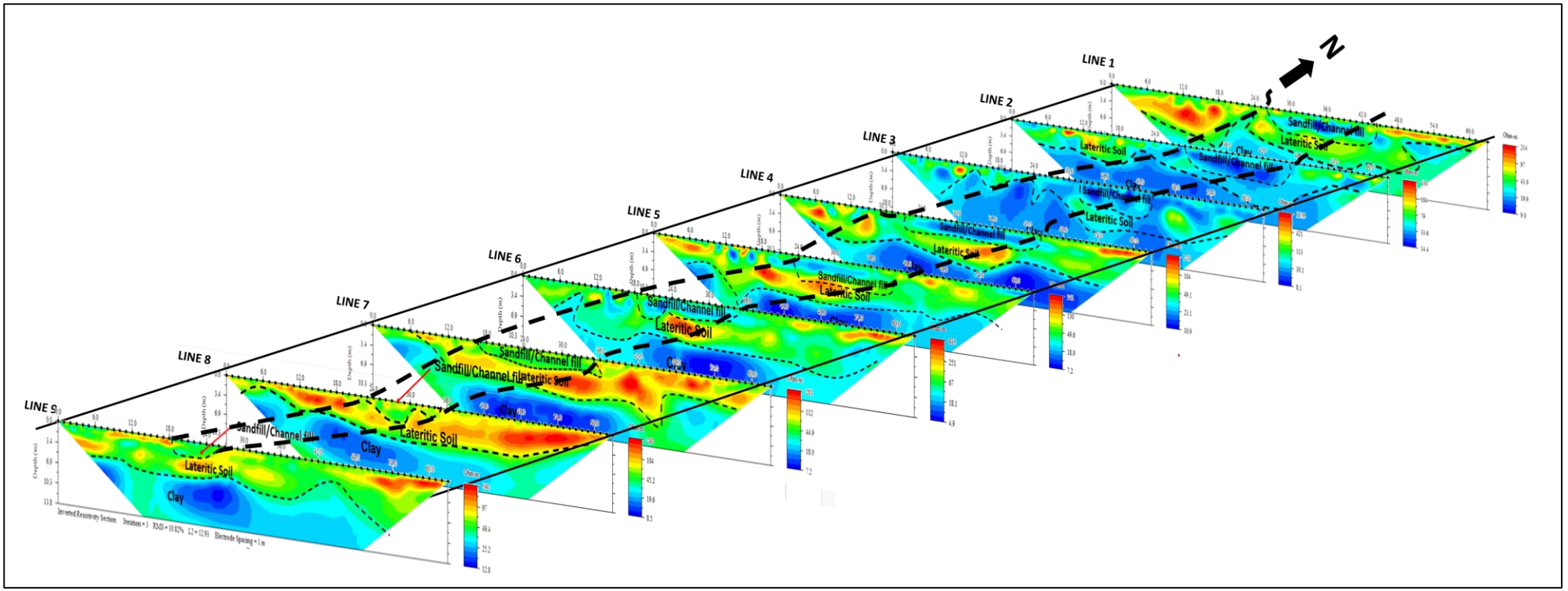

Fig 4.10 Correlation of parallel 2D lines in 3D view showing the region depicting the sandfill/buried river channel region on the 2D lines. Note the variation in resistivity of the channel fill from proximal (North) to distal (South) of the existing river/lake.

4.2.2 3D Electrical Resistivity Tomography

3D Inverted Resistivity Image

The interpreted 3D inverted resistivity image derived from combining the parallel 2D ERT lines is presented in Fig 4.11. Low resistivity anomalies can be observed at the central part of the 3D ERT cube which is expressive of the region with the buried/sandfilled river channel. The low resistivity at the central part is analogous to an incised channel fill while the high resistivity regions are analogous to the non-incised country rocks.

X and Y slices of 3D Inverted Resistivity Image

The interpreted X and Y slices of the 3D inverted Resistivity Image is presented in Fig 4.12a and 4.12b. The path of occupied by the buried/sandfilled river channel is represented by low resistivity anomalies parallel to the X slices and perpendicular to the Y slices.

3D Dynamic Slices of Inverted Resistivity Image

Fig 4.13a is the 3D dynamic slice of the 3D inverted resistivity cube at depth of about 1.5m. The low resistivity region observed is that associated to the buried/sandfilled river channel. On the other hand, the low resistivity observed on the 3D dynamic slice of the 3D inverted resistivity cube at depth of about 9.7m (Fig 4.13b) is associated to the underlying clay layer.

3D Resistivity Contour Plot

The low resistivity signatures attributed to buried/sandfilled channel fill have been isolated and presented as 3D Iso-Resistivity contour plot map in Fig 4.14. The near surface isolated low resistivity values have been interpreted as the buried/sandfilled river channel while the deeper isolated low resistivity anomalies are the subsurface clay layers.

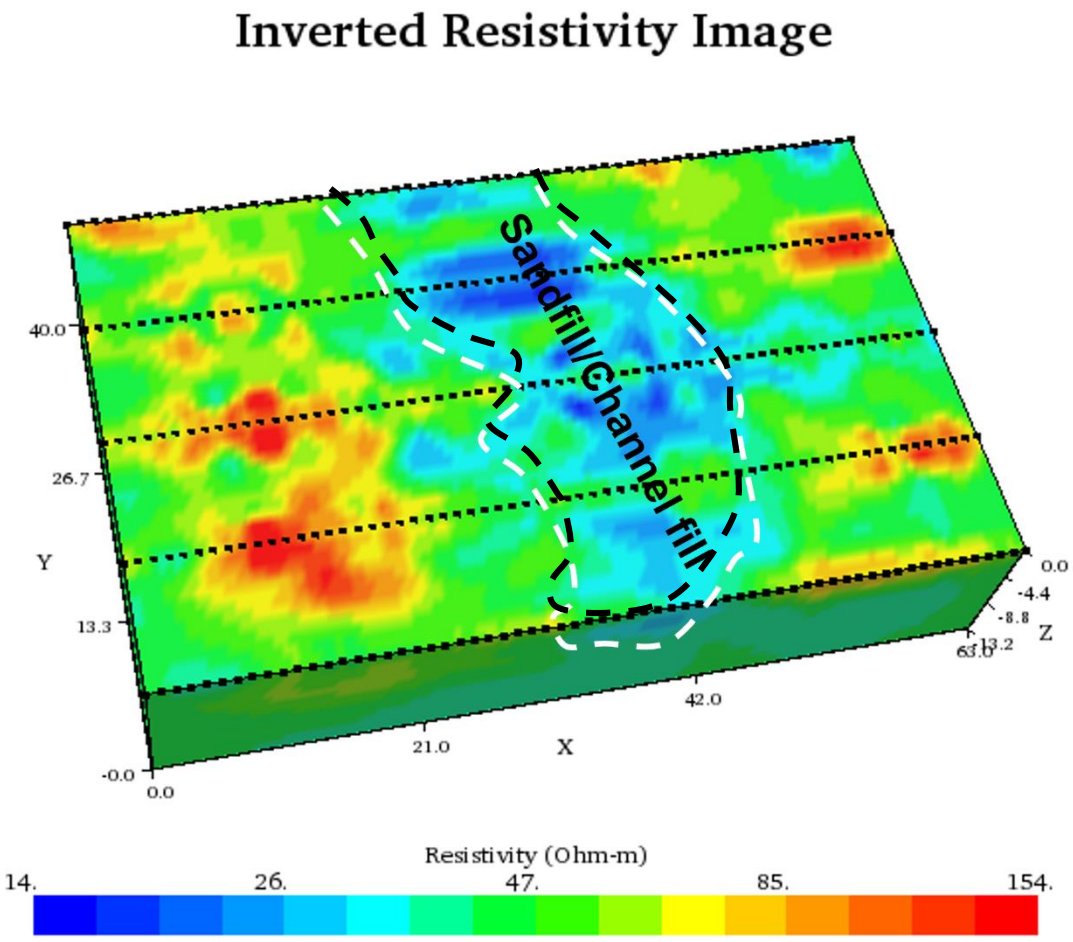

Figure 4.11: Interpreted 3D Inverted Resistivity Image for traverses 1-9.

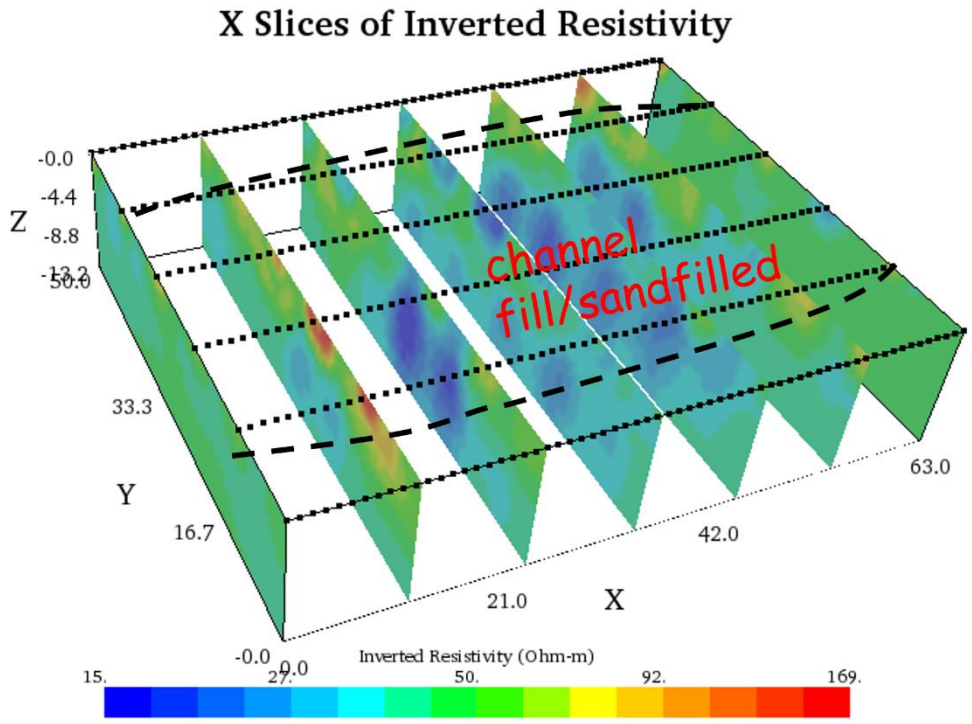

Fig 4.12a Interpreted X slices of 3D inverted resistivity

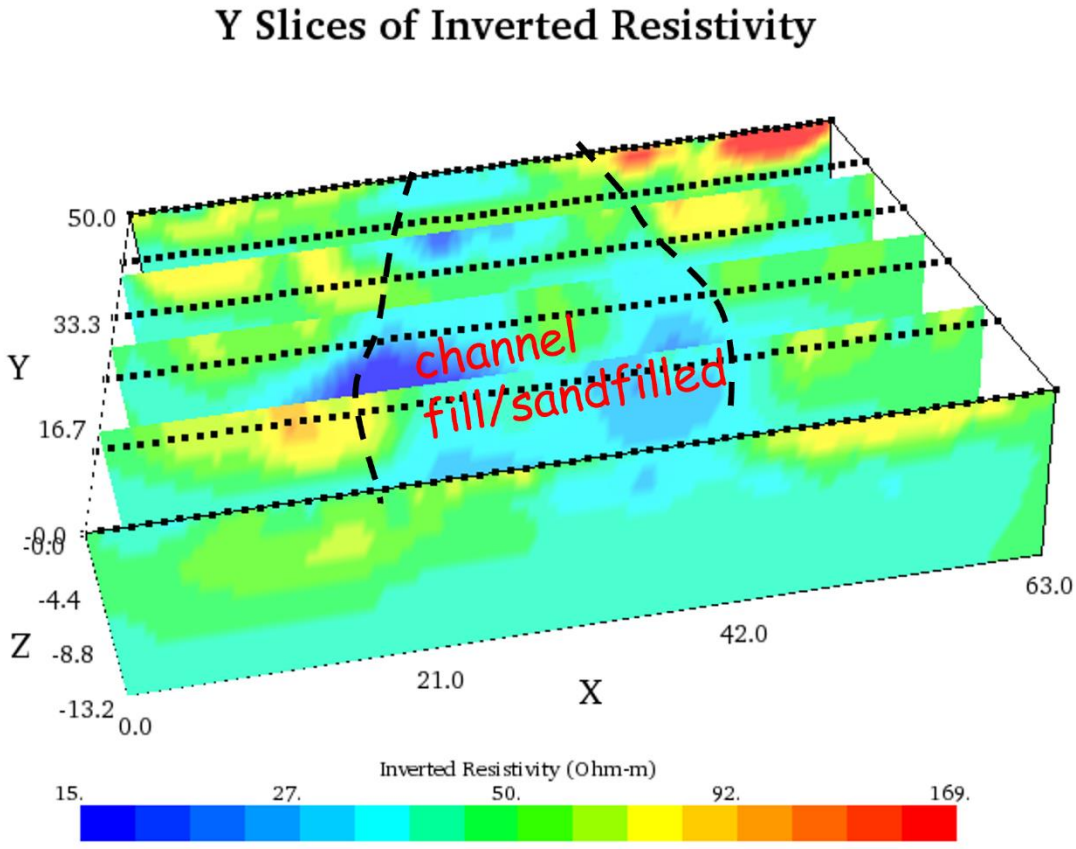

Fig 4.12b Interpreted Y slices of 3D inverted resistivity

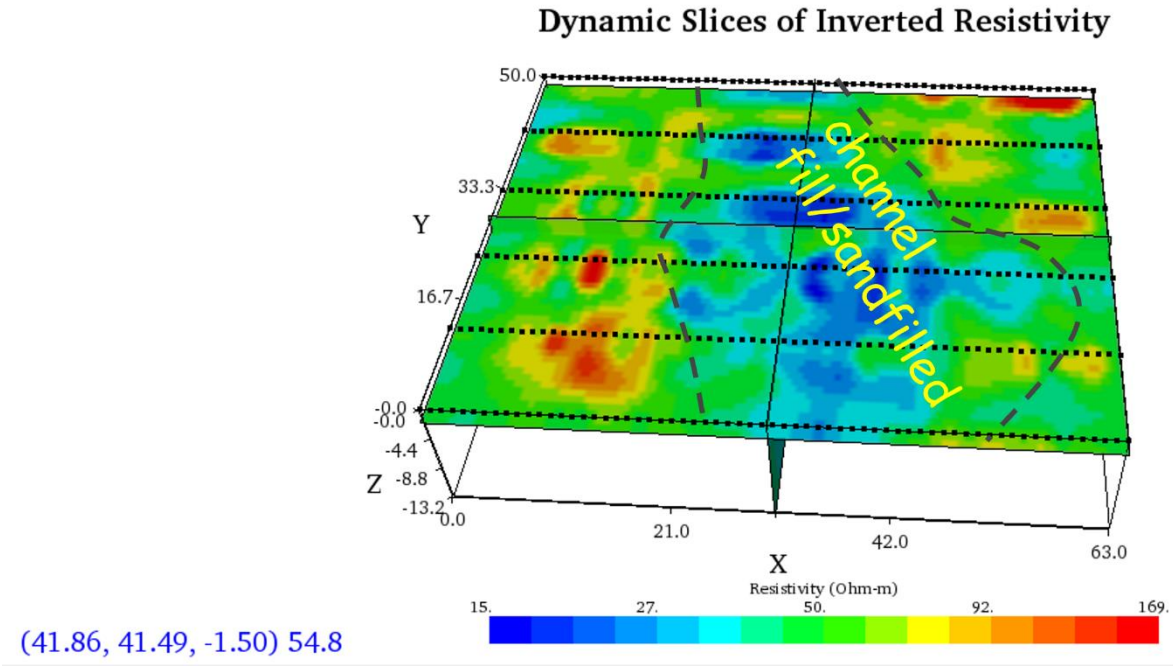

Figure 4.12a. 3D Dynamic Slices of 3D Inverted Resistivity at depth of 1.5m showing the buried/sandfilled river channel

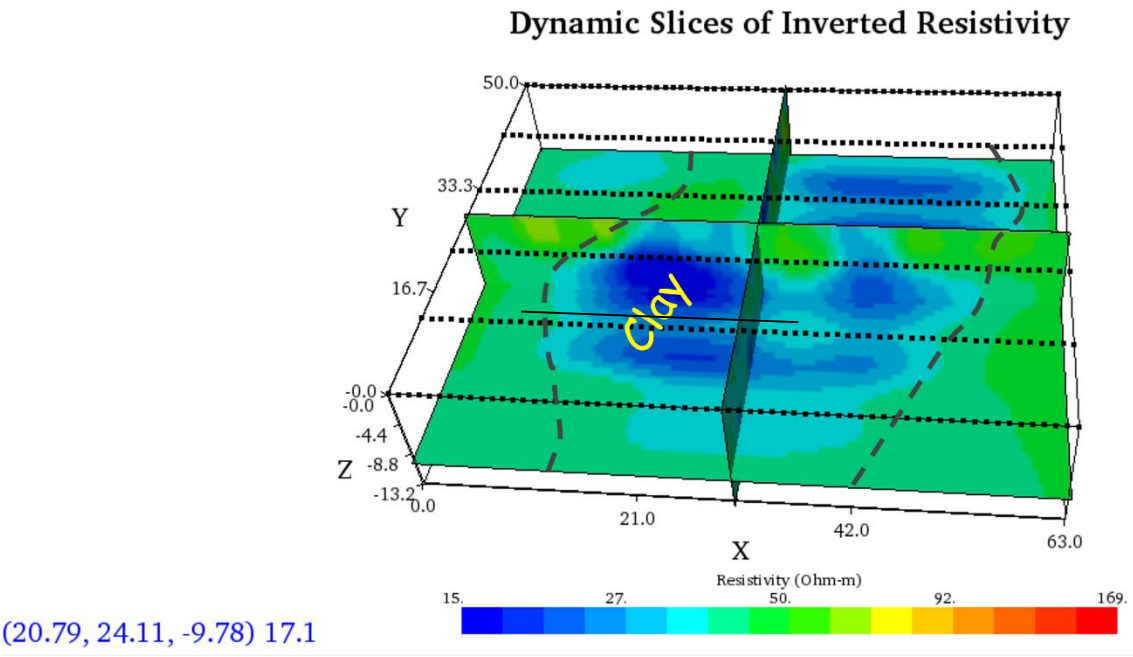

Figure 4.12b 3D Dynamic Slices of 3D Inverted Resistivity Image at depth of 9.78m showing the underlying clay region

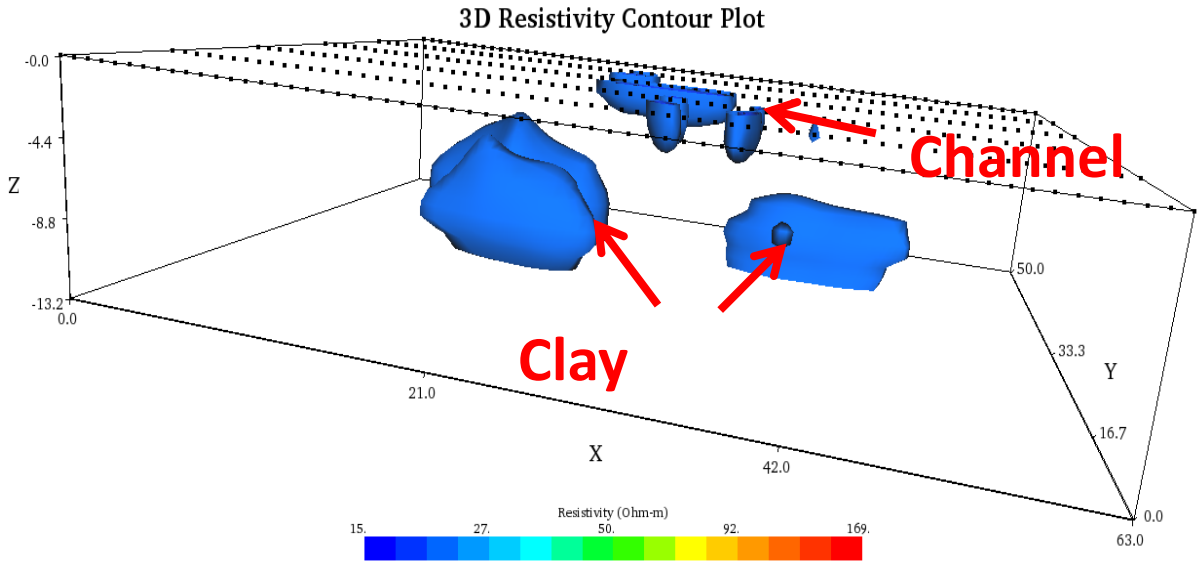

Figure 4.13. Interpreted 3D Iso-Resistivity contour plot

4.2.3 Ground Penetrating Radar

Traverse 1

The interpreted GPR Radargram obtained along traverse 1 with the 160MHz antenna, is presented in Figure 4.14. Two main anomalous plane continuous reflectors can be observed within the depth range of about 2 to 3.5m. Linear continuous anomalies from the plane reflector indicates slight contrast in the homogeneity of the die-electric properties of the study area. The lateral terminations of these reflectors are analogous to an incised channel on a background/country rock. The slight inhomogeneous layers are interpreted to be the sandfilled and channel fill boundaries respectively at respective depth range of about 0.5 to 1m and 1.5 to 3.5m respectively.

Traverse 2

The interpreted GPR Radargram obtained along traverse 2 with the 160MHz antenna, is presented in Figure 4.15. Two main anomalous plane continuous reflectors can be observed within the depth range of about 2 to 3.5m. Linear continuous anomalies from the plane reflector indicates slight contrast in the homogeneity of the die-electric properties of the study area. The lateral terminations of these reflectors are analogous to an incised channel on a background/country rock. The slight inhomogeneous layers are interpreted to be the sandfilled and channel fill boundaries respectively at respective depth range of about 0.2 to 1m and 1 to 3m respectively.

Traverse 3

The interpreted GPR Radargram obtained along traverse 3 with the 160MHz antenna, is presented in Figure 4.16. Two main anomalous plane continuous reflectors can be observed within the depth range of about 2 to 3.5m. Linear continuous anomalies from the plane reflector indicates slight contrast in the homogeneity of the die-electric properties of the study area. The lateral terminations of these reflectors are analogous to an incised channel on a background/country rock. The slight inhomogeneous layers are interpreted to be the sandfilled and channel fill boundaries respectively at respective depth range of about 0.2 to 0.5m and 0.5 to 3m respectively.

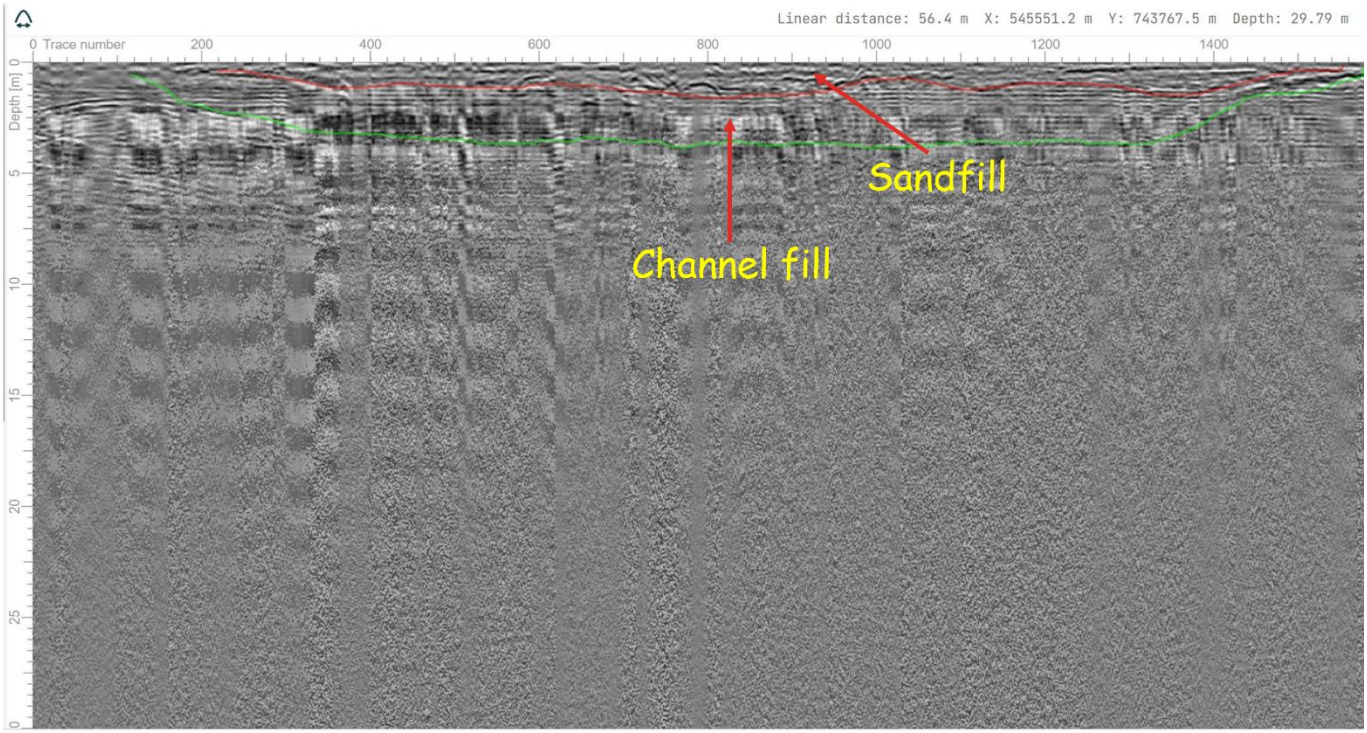

Figure 4.14. Interpreted GPR radargram using the 160MHz antenna along traverse 1

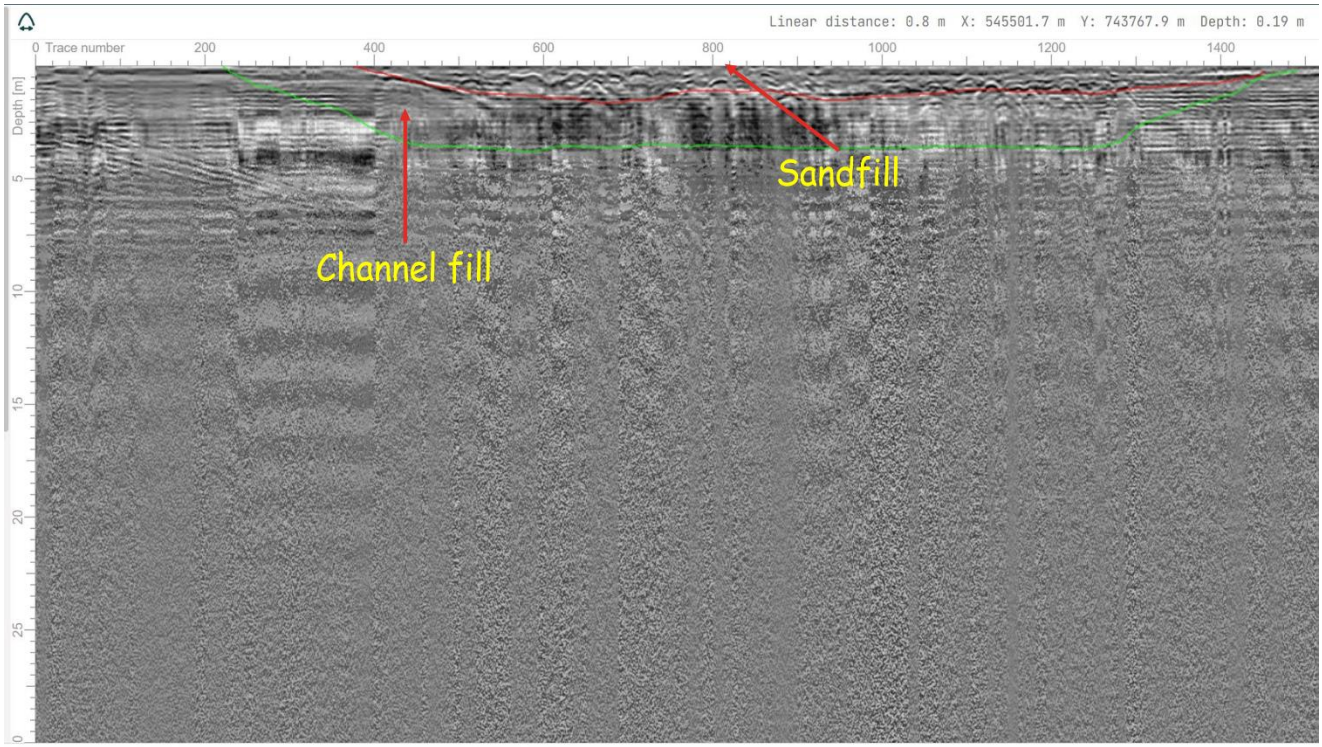

Figure 4.15 Interpreted GPR radargram using the 160MHz antenna along traverse 2

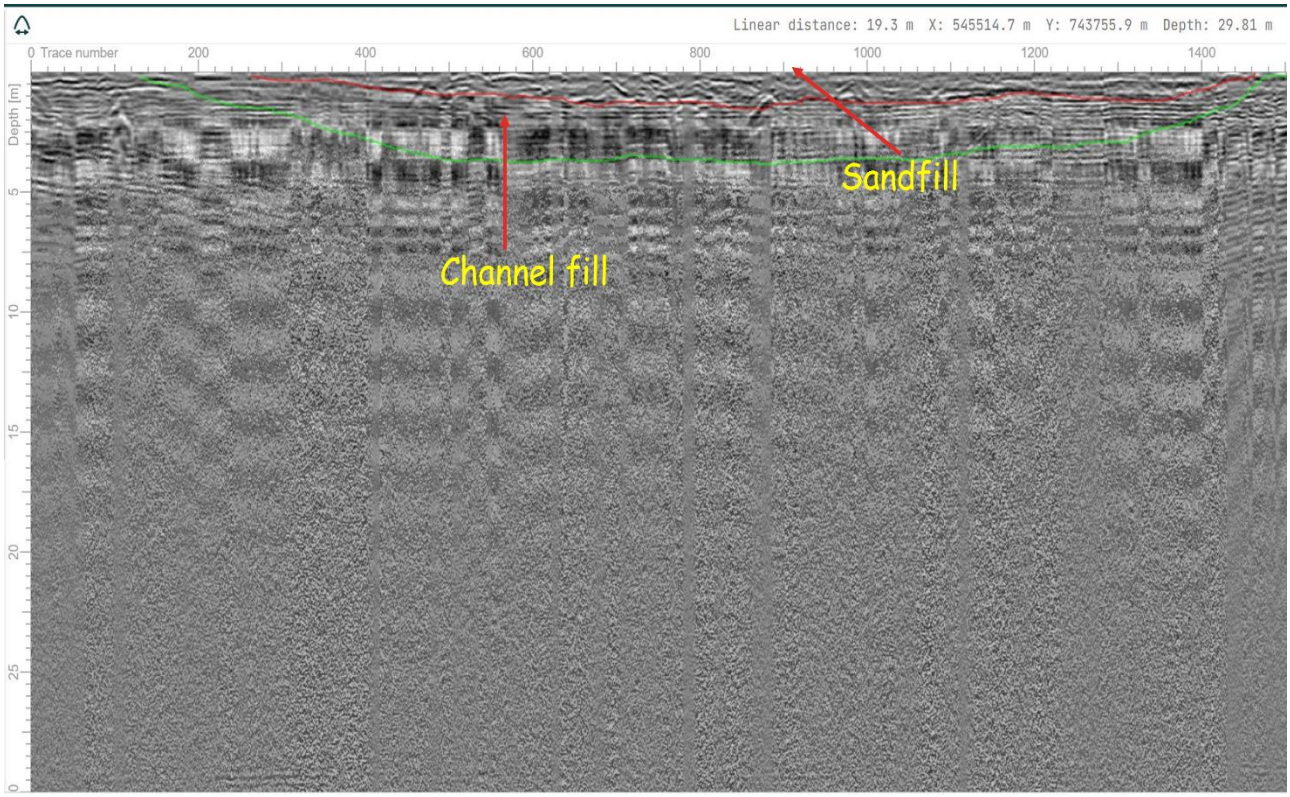

Figure 4.16 Interpreted GPR radargram using the 160MHz antenna along traverse 3

Traverse 4

The interpreted GPR Radargram obtained along traverse 4 with the 160MHz antenna, is presented in Figure 4.17. Two main anomalous plane continuous reflectors can be observed within the depth range of about 2 to 3.5m. Linear continuous anomalies from the plane reflector indicates slight contrast in the homogeneity of the die-electric properties of the study area. The lateral terminations of these reflectors are analogous to an incised channel on a background/country rock. The slight inhomogeneous layers are interpreted to be the sandfilled and channel fill boundaries respectively at respective depth range of about 0.5 to 1m and 1 to 3.5m respectively.

Traverse 5

The interpreted GPR Radargram obtained along traverse 5 with the 160MHz antenna, is presented in Figure 4.18. Two main anomalous plane continuous reflectors can be observed within the depth range of about 2 to 3.5m. Linear continuous anomalies from the plane reflector indicates slight contrast in the homogeneity of the die-electric properties of the study area. The lateral terminations of these reflectors are analogous to an incised channel on a background/country rock. The slight inhomogeneous layers are interpreted to be the sandfilled and channel fill boundaries respectively at respective depth range of about 0.1 to 0.5m and 0.5 to 3m respectively.

Traverse 6

The interpreted GPR Radargram obtained along traverse 6 with the 160MHz antenna, is presented in Figure 4.19. Two main anomalous plane continuous reflectors can be observed within the depth range of about 2 to 3.5m. Linear continuous anomalies from the plane reflector indicates slight contrast in the homogeneity of the die-electric properties of the study area. The lateral terminations of these reflectors are analogous to an incised channel on a background/country rock. The slight inhomogeneous layers are interpreted to be the sandfilled and channel fill boundaries respectively at respective depth range of about 0.2m to 0.5m and 0.5 to 3m respectively.

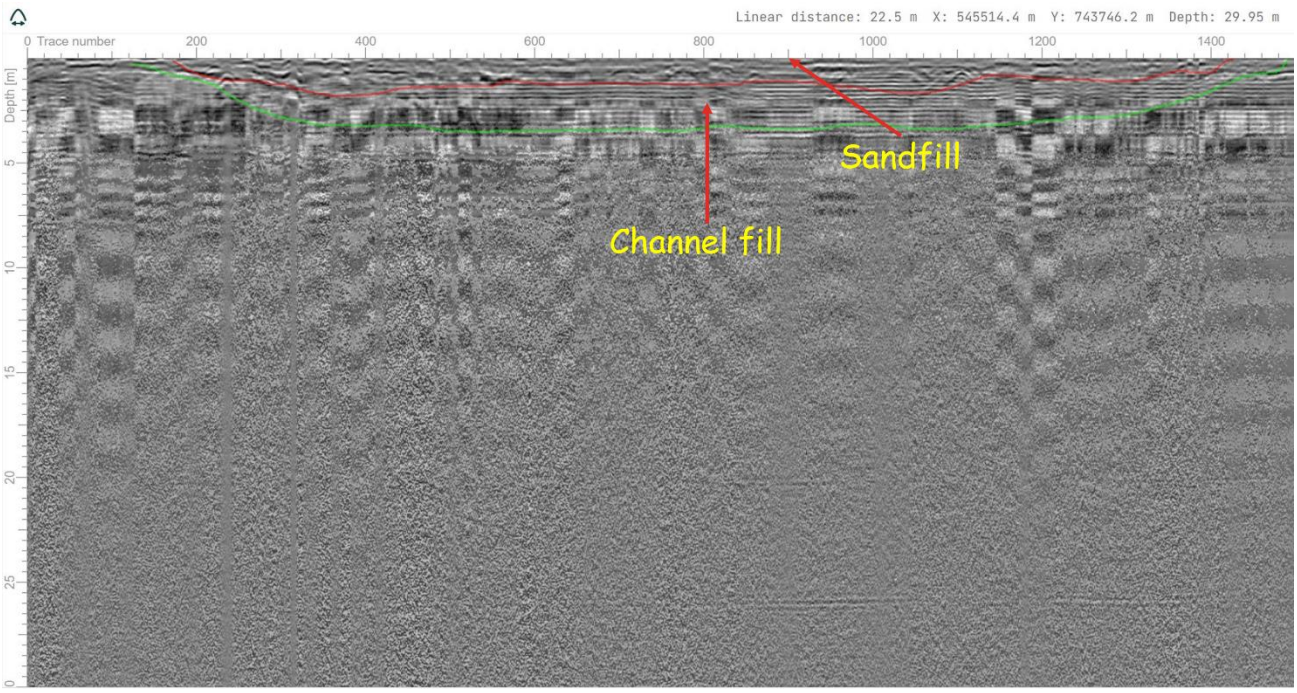

Figure 4.17. Interpreted GPR radargram using the 160MHz antenna along traverse 4

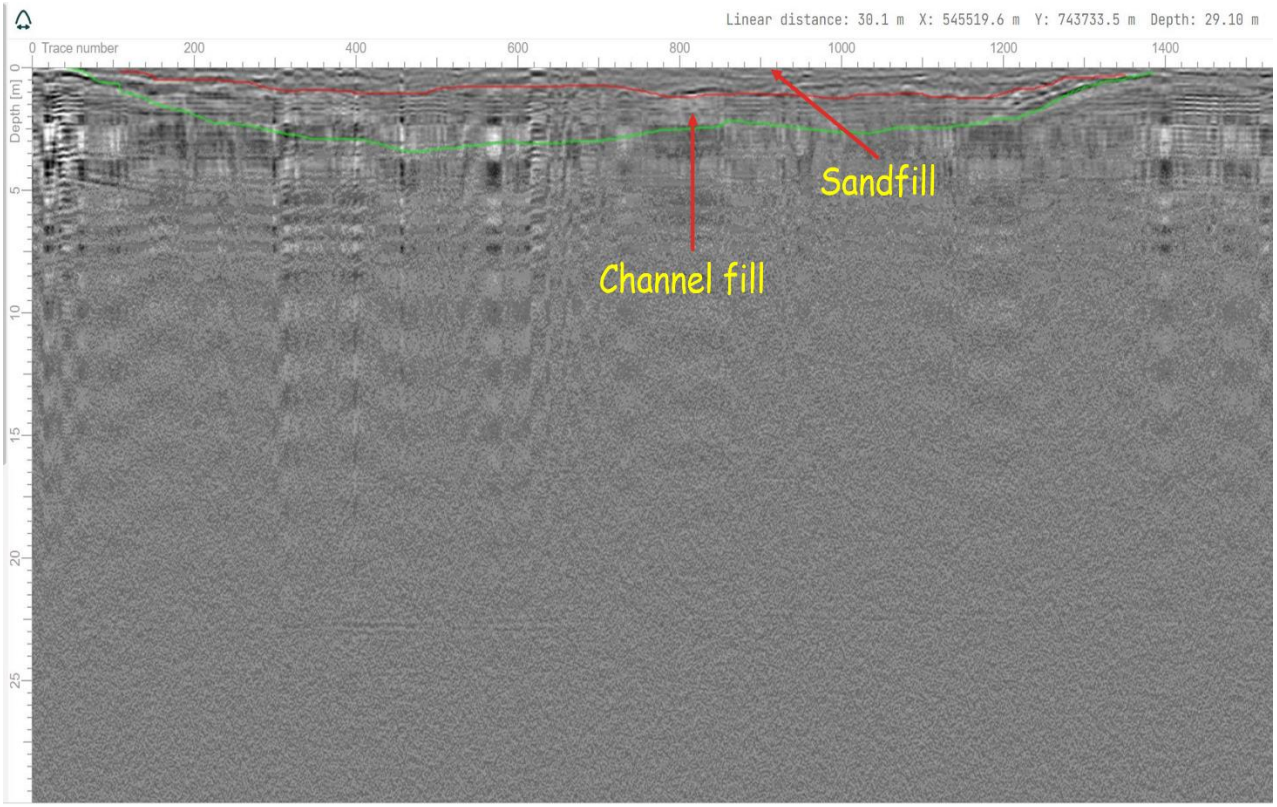

Figure 4.18. Interpreted GPR radargram using the 160MHz antenna along traverse 5

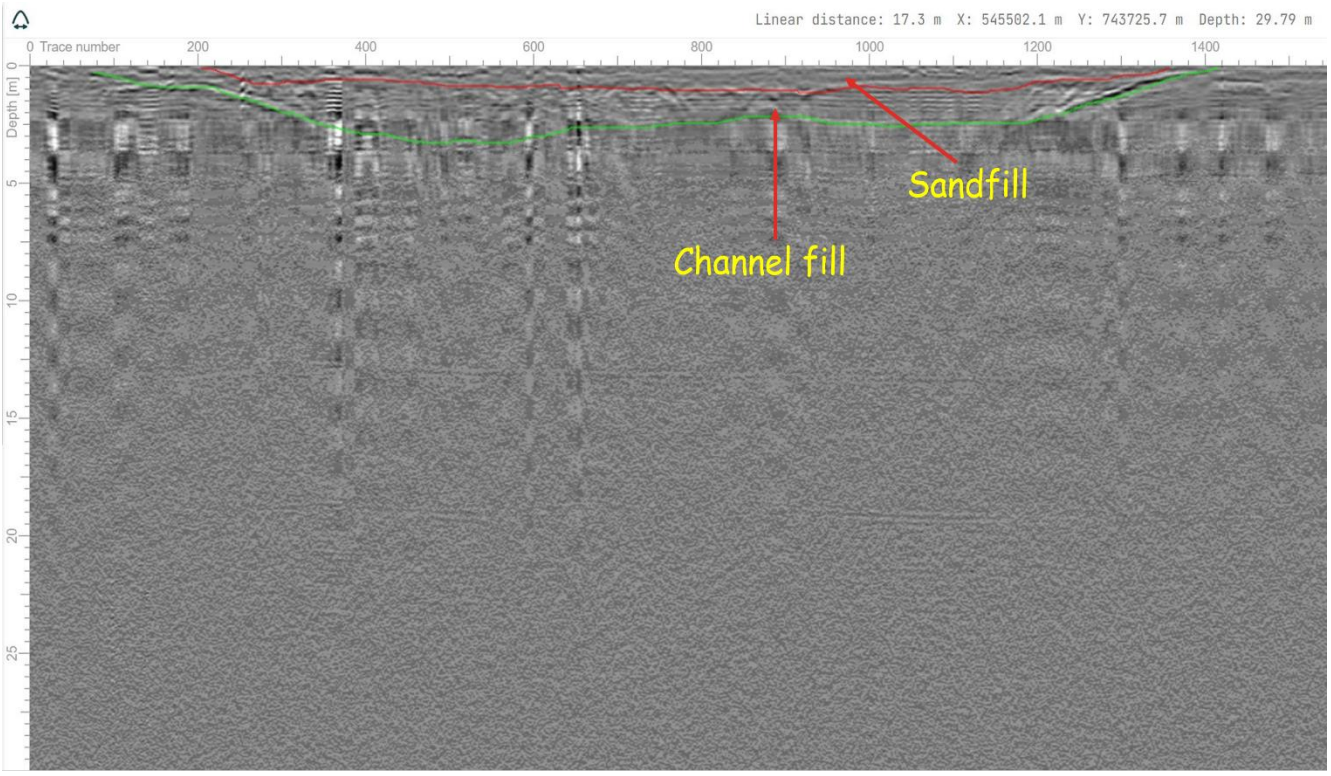

Figure 4.19 Interpreted GPR radargram using the 160MHz antenna along traverse 6

Traverse 7

The interpreted GPR Radargram obtained along traverse 7 with the 160MHz antenna, is presented in Figure 4.20. Two main anomalous plane continuous reflectors can be observed within the depth range of about 2 to 3.5m. Linear continuous anomalies from the plane reflector indicates slight contrast in the homogeneity of the die-electric properties of the study area. The lateral terminations of these reflectors are analogous to an incised channel on a background/country rock. The slight inhomogeneous layers are interpreted to be the sandfilled and channel fill boundaries respectively at respective depth range of about 0.25 to 1m and 1 to 2m respectively.

Traverse 8

The interpreted GPR Radargram obtained along traverse 8 with the 160MHz antenna, is presented in Figure 4.21. Two main anomalous plane continuous reflectors can be observed within the depth range of about 2 to 3.5m. Linear continuous anomalies from the plane reflector indicates slight contrast in the homogeneity of the die-electric properties of the study area. The lateral terminations of these reflectors are analogous to an incised channel on a background/country rock. The slight inhomogeneous layers are interpreted to be the sandfilled and channel fill boundaries respectively at respective depth range of about 0.1 to 1m and 1 to 2m respectively.

Traverse 9

The interpreted GPR Radargram obtained along traverse 9 with the 160MHz antenna, is presented in Figure 4.22. Two main anomalous plane continuous reflectors can be observed within the depth range of about 2 to 3.5m. Linear continuous anomalies from the plane reflector indicates slight contrast in the homogeneity of the die-electric properties of the study area. The lateral terminations of these reflectors are analogous to an incised channel on a background/country rock. The slight inhomogeneous layers are interpreted to be the sandfilled and channel fill boundaries respectively at respective depth range of about 0.1 to 0.5m and 0.5 to 1.5m respectively.

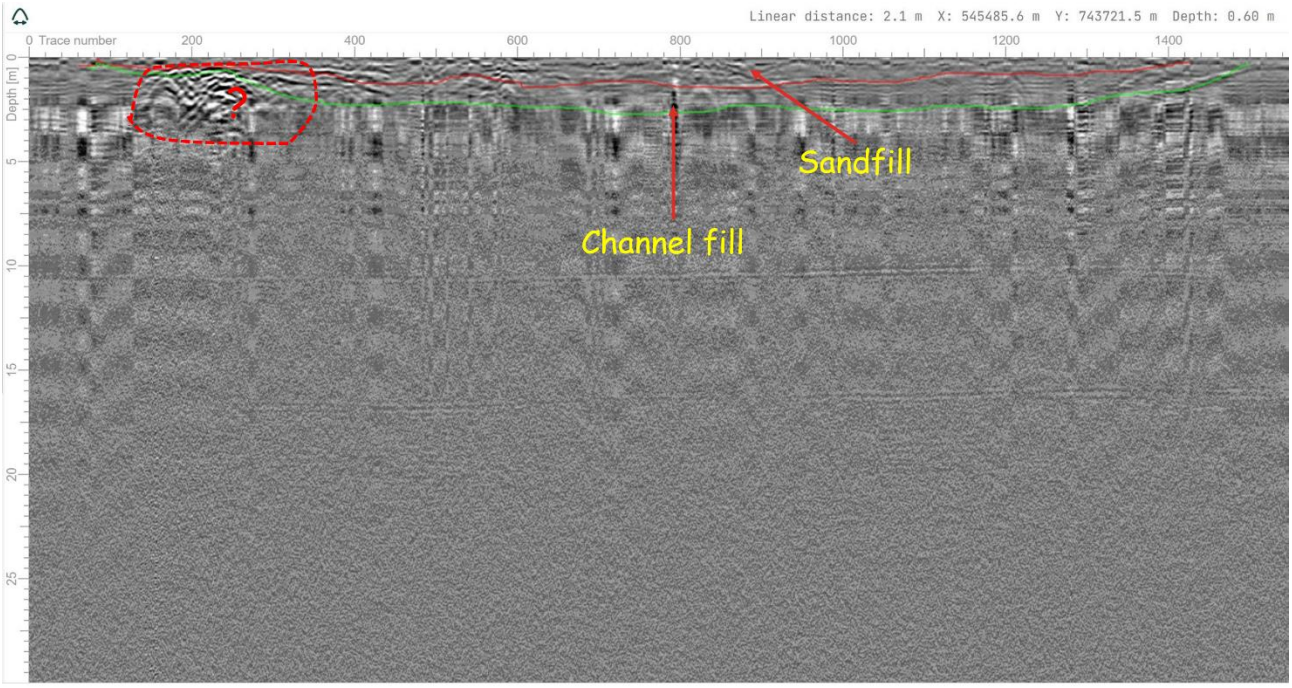

Figure 4.20. Interpreted GPR radargram using the 160MHz antenna along traverse 7

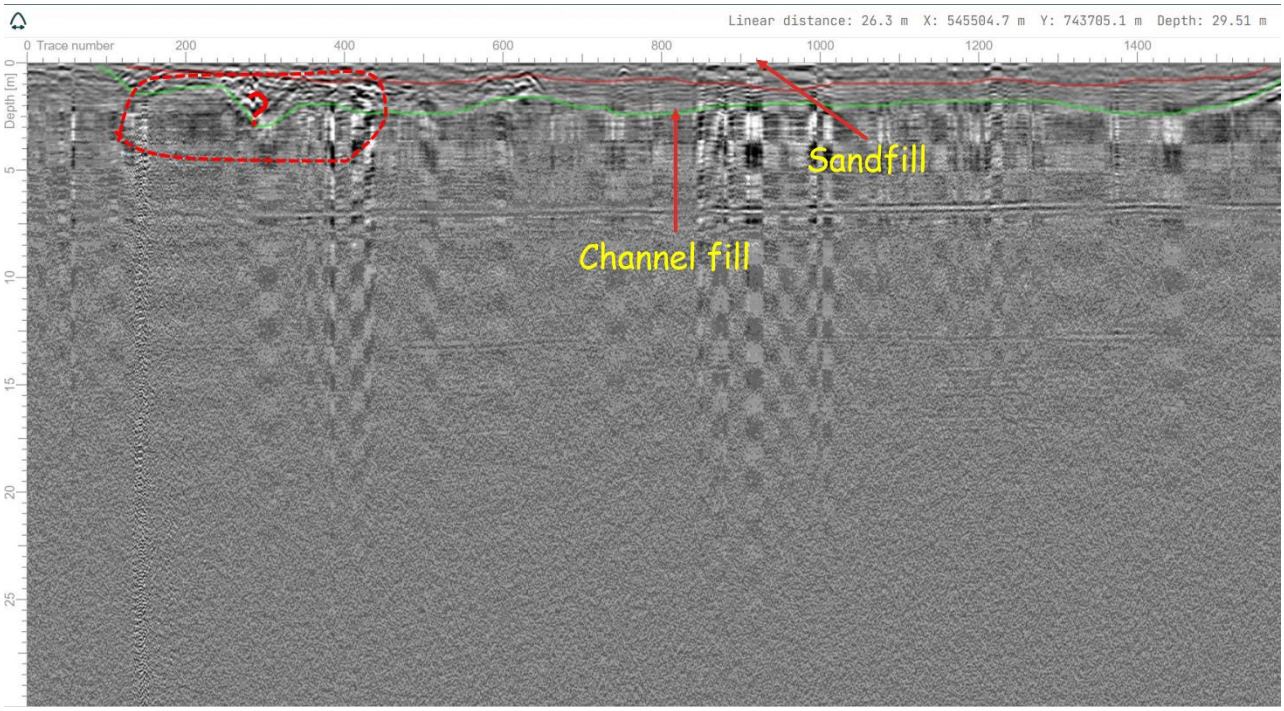

Figure 4.21 Interpreted GPR radargram using the 160MHz antenna along traverse 8

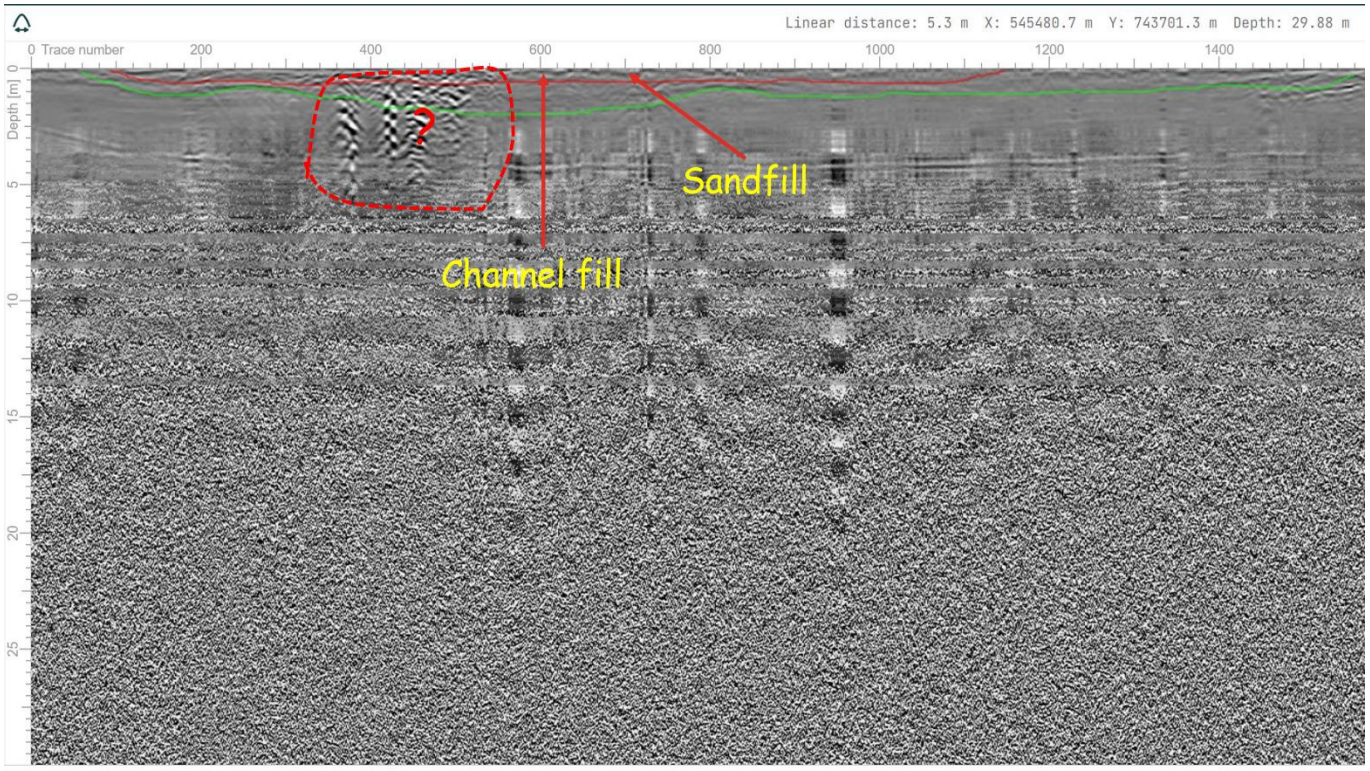

Figure 4.22. Interpreted GPR radargram using the 160MHz antenna along traverse 9

Spatial variation of the thickness map of the sandfilled region

The time map generated from the compiled interpretations of the sandfilled region as mapped on each of the GPR lines is presented as a contour time map in Fig 4.23a. The depth map generated from the time map by using a velocity of 0.1m/ns is presented as a contour depth map in Fig 4.23b. From the depth map, it can be observed that the thickness of the sandfilled region ranges from about 0.4 to 1.4m. The thickness of the sandfill increases northwards as one traverses towards the proximal end of the existing river channel as further shown in the three cross-sectional profiles drawn across the sandfill fill (Figure 4.24).

Figure 4.25 shows the generated 3D depth map of the sandfilled region, the architecture and the configuration are synonymous of the depth of the river channel prior to sandfilling.

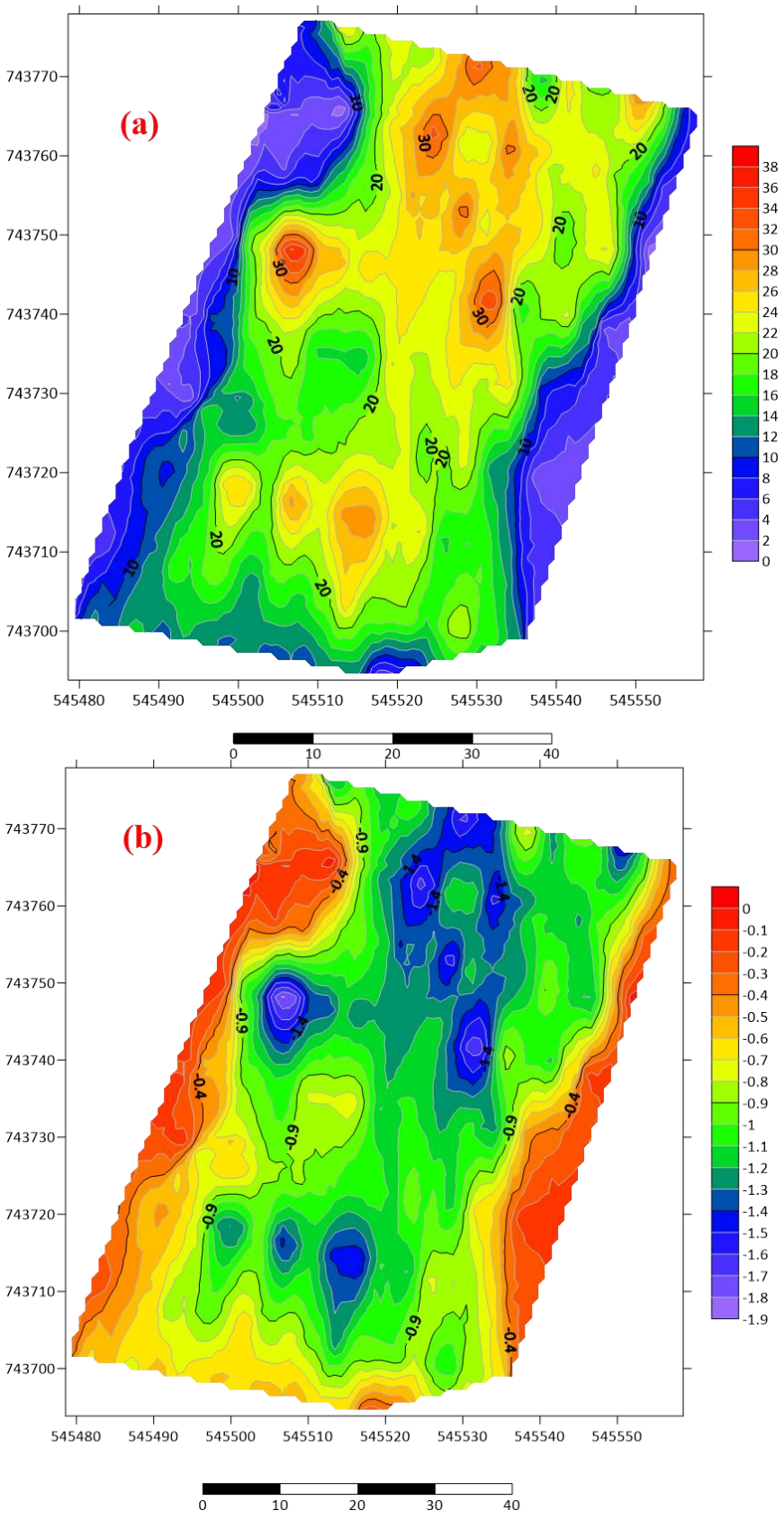

Figure 4.23. (a)Time map and (b) Depth Map of the sandfilled region

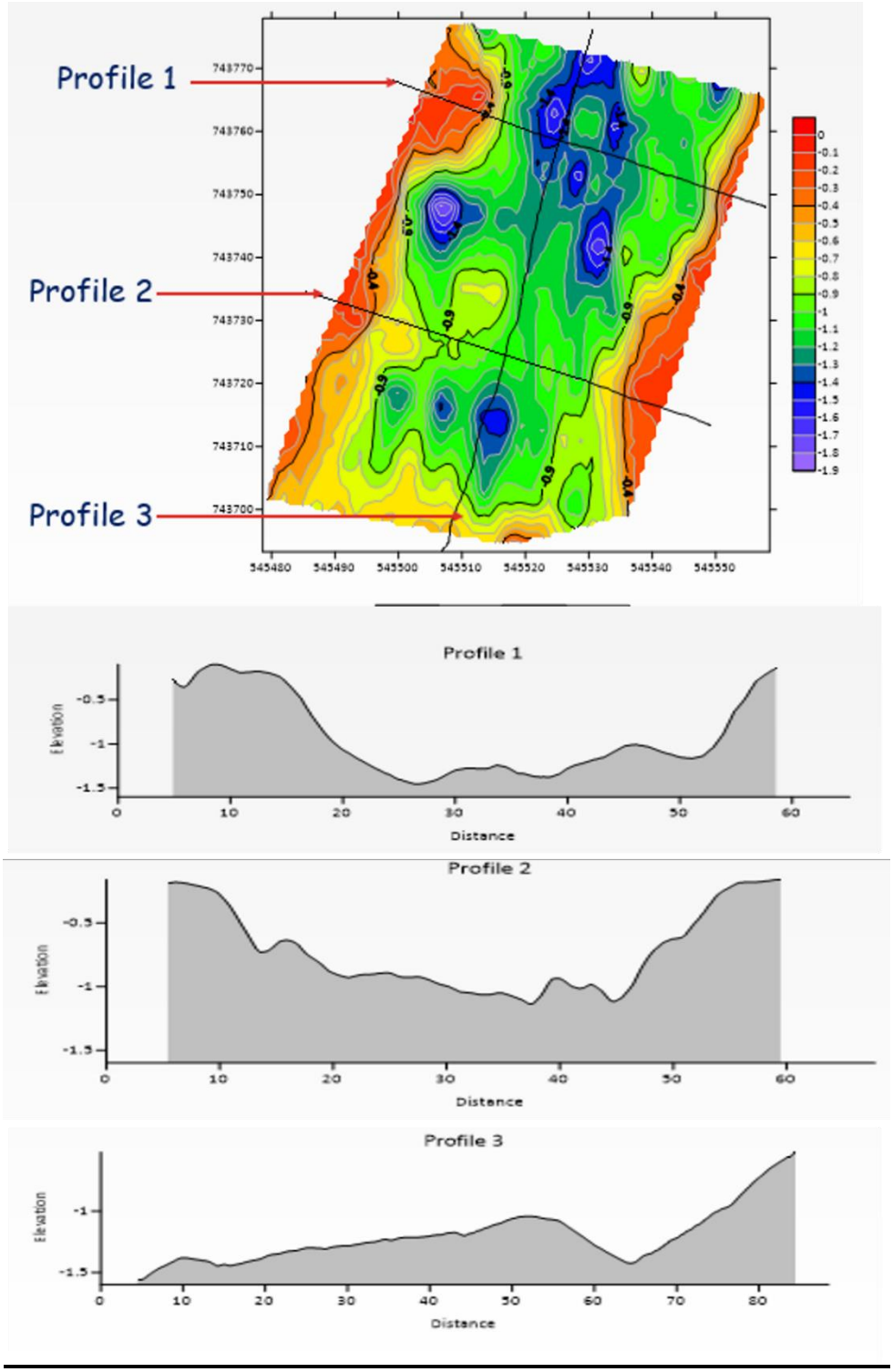

Figure 4.24. Thickness map and cross-sectional profiles of the sandfilled region showing the variation in the thickness of the sandfilled region in the study area

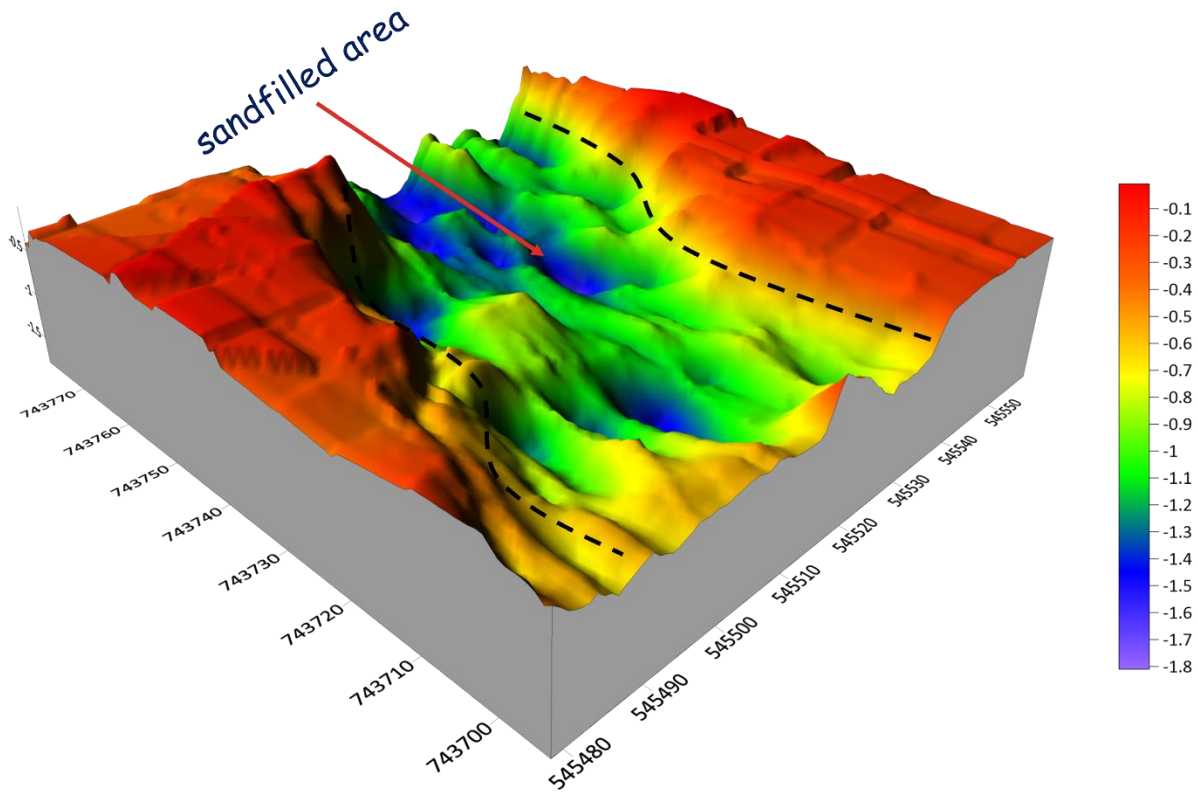

Figure 4.25. Interpreted 3D Depth Map of Sandfilled fill Region

Spatial variation of the depth map of the river channel region

The time map generated from the compiled interpretations of the channel fill region as mapped on each of the GPR lines is presented as a contour time map in Fig 4.26a. The depth map generated from the time map by using a velocity of 0.1m/ns is presented as a contour depth map in Fig 4.26b. From the depth map, it can be observed that the thickness of the channel fill from 1.2 to 3.6m. The thickness of the sandfill increases northwards as one traverses towards the proximal end of the existing river channel as further shown in the three cross-sectional profiles drawn across the depth map of the channel fill (Figure 4.27).

Figure 4.28 shows the generated 3D depth map of the channel fill region, the architecture and the configuration are synonymous of the extent of the country rock incised by the river channel prior to infilling of river sediments.

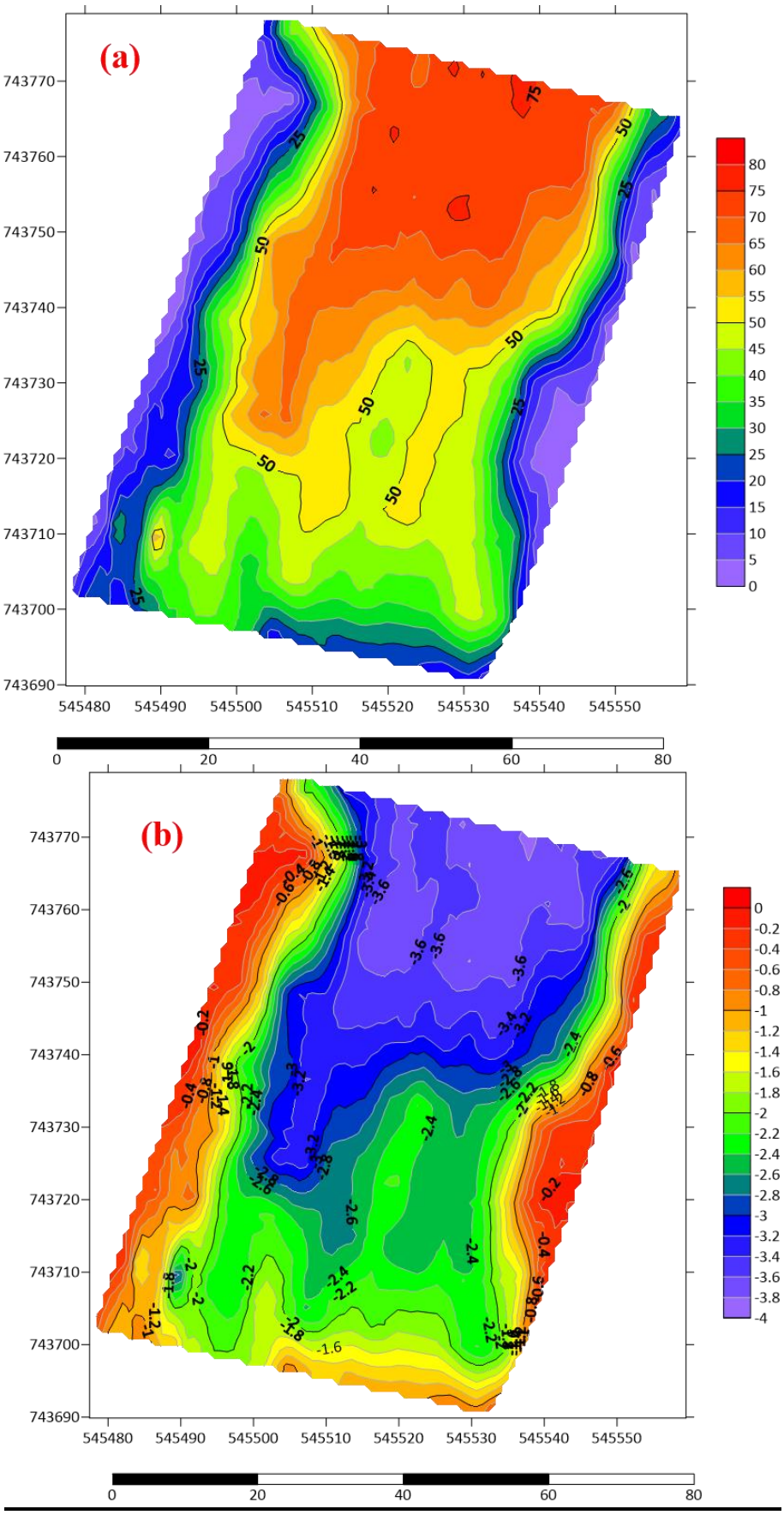

Figure 4.26.(a) Time map and (b) Depth Map of the channel fill region

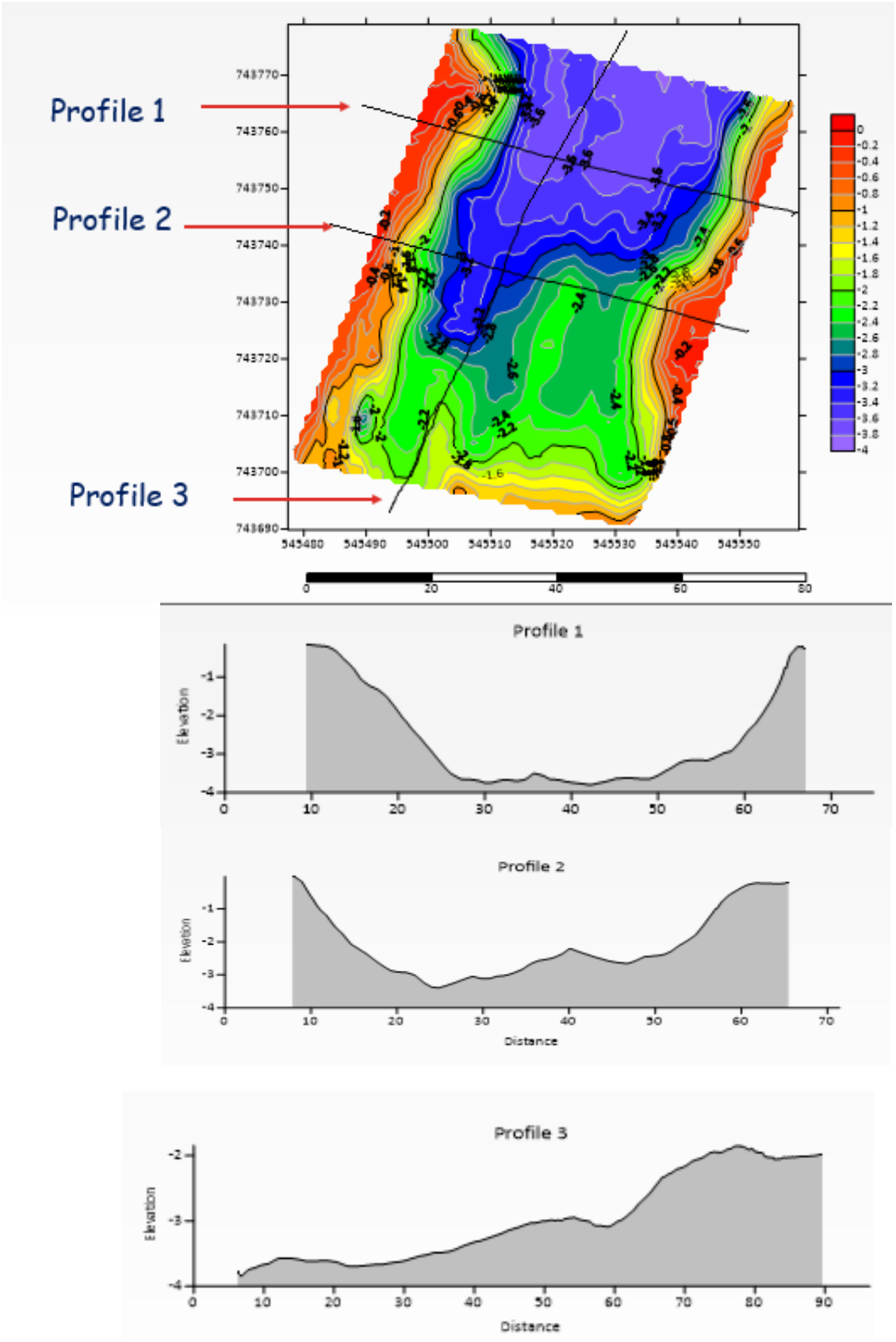

Figure 4.27. Thickness map and cross-sectional profiles of the sandfilled region showing the variation in the thickness of the sandfilled region in the study area

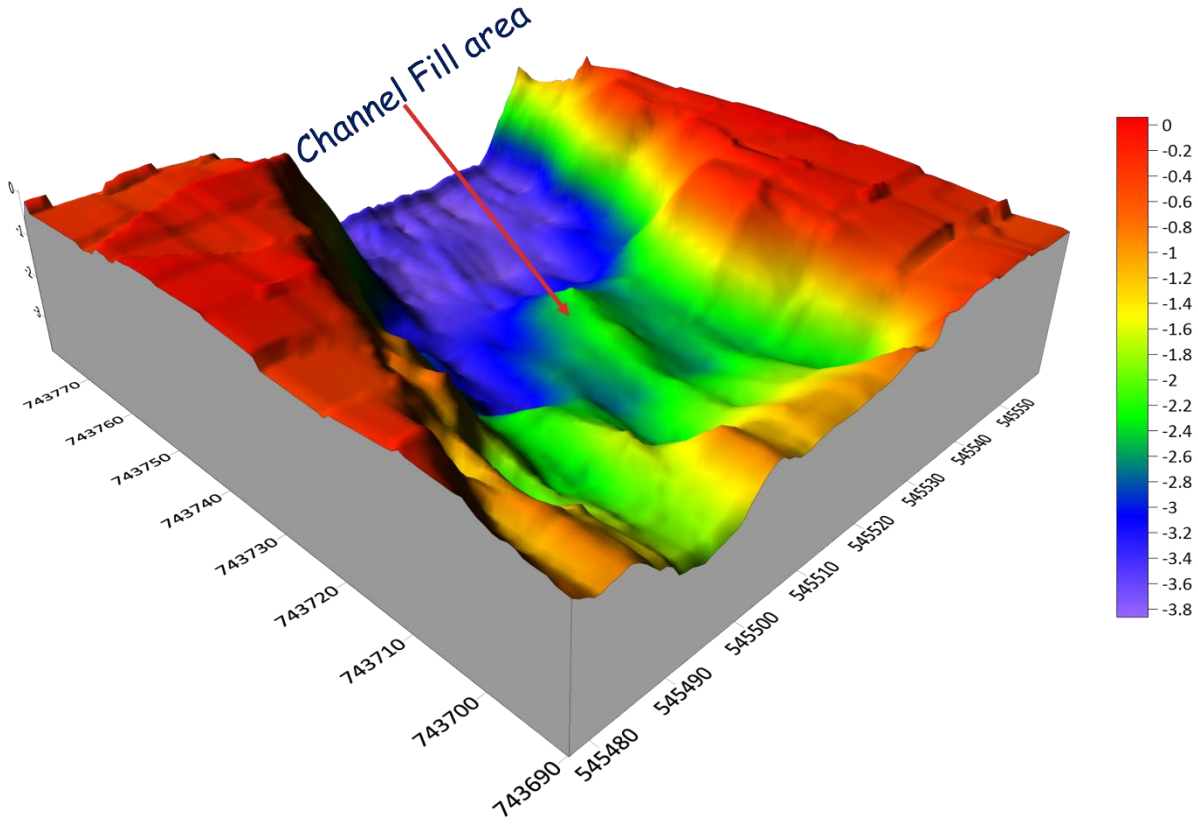

Figure 4.28. Interpreted 3D Depth Map of Channel fill Region

4.2.4 Integration of methods

The results of the electrical resistivity and the GPR methods have been integrated and presented in Figure 4.29 (a to c). The sandfilled/river channel has been delineated as a single geoelectric unit of low resistivity anomalous region at the central part of the 3D inverted resistivity cube (Fig 4.29c). Due to the high vertical and horizontal resolution of the GPR method, the sandfilled and channel fill area has been mapped as different units. From the result presented in Fig 4.29 (a to c), a strong correlation exists for both electrical resistivity and GPR methods as both have delineated the depth and width of the main channel course as 3.6m and about 40m respectively.

The thickness map of the sandfill generated from the GPR interpretation has been overlaid on the historical (Jan, 2015) satellite imagery of the study area prior to sandfilling of the investigated area (Fig 30a). It can be observed that the region identified as the sandfill appropriately aligns with the river channel.

Similarly, the depth map of the channel fill from generated from the GPR interpretation has been overlaid on the historical (Jan, 2015) satellite imagery of the study area prior to sandfilling of the investigated area (Fig 30a). This as shown that the river channel has strongly incised the native rock at the proximal end of the river compared to the distal end of the river. It is possible that the river has been naturally sandfilled due to regrowth or abandonment prior to the anthropogenic sandfilling after 2015. The depth of the channel should be considered for the depth of foundation and foundation type.

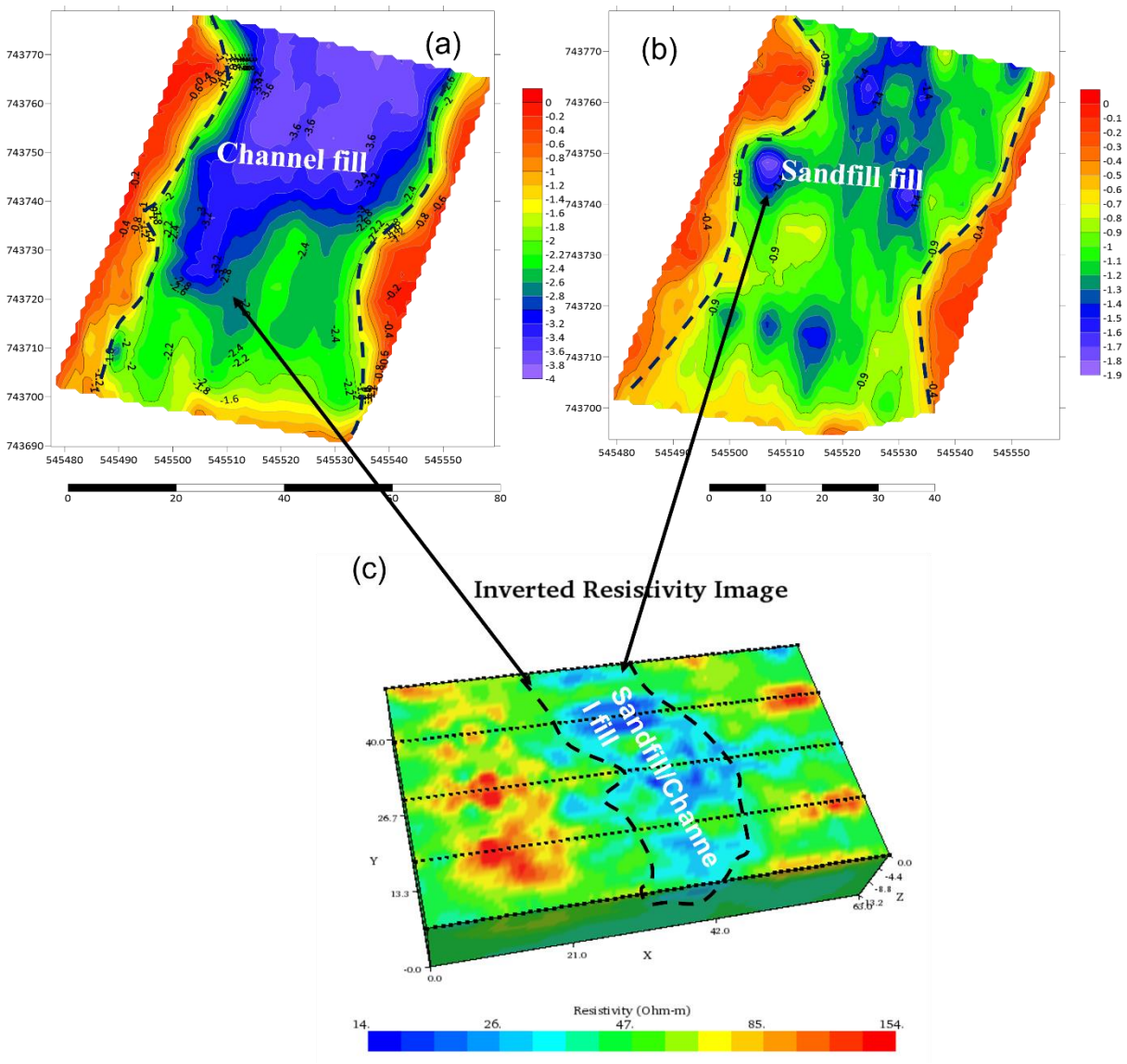

Figure 4.29 (a) GPR radargram showing the Depth-Map of the channel fill region (b) GPR radargram showing the Depth-Map of the sandfill fill region (c) 2D-ERT inverted resistivity image showing the sand/channel fill region

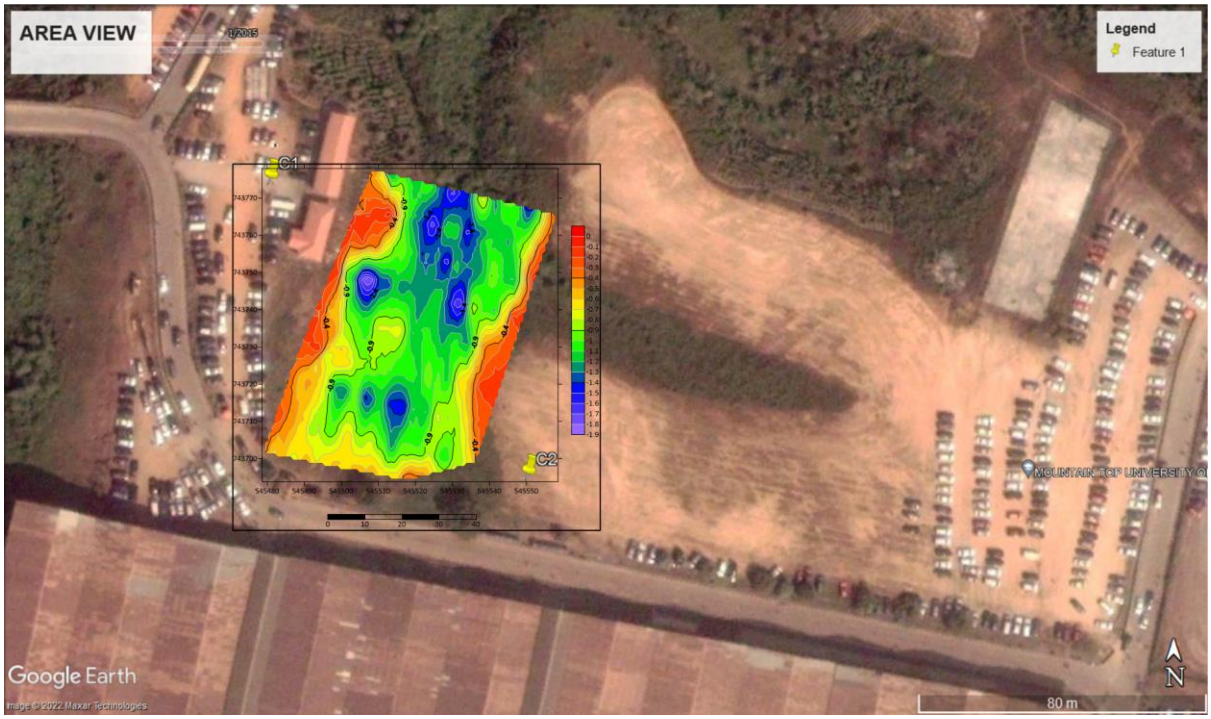

Figure 30 (a) An overlay of the depth map of the sandfilled channel on the historical satellite imagery of 2015

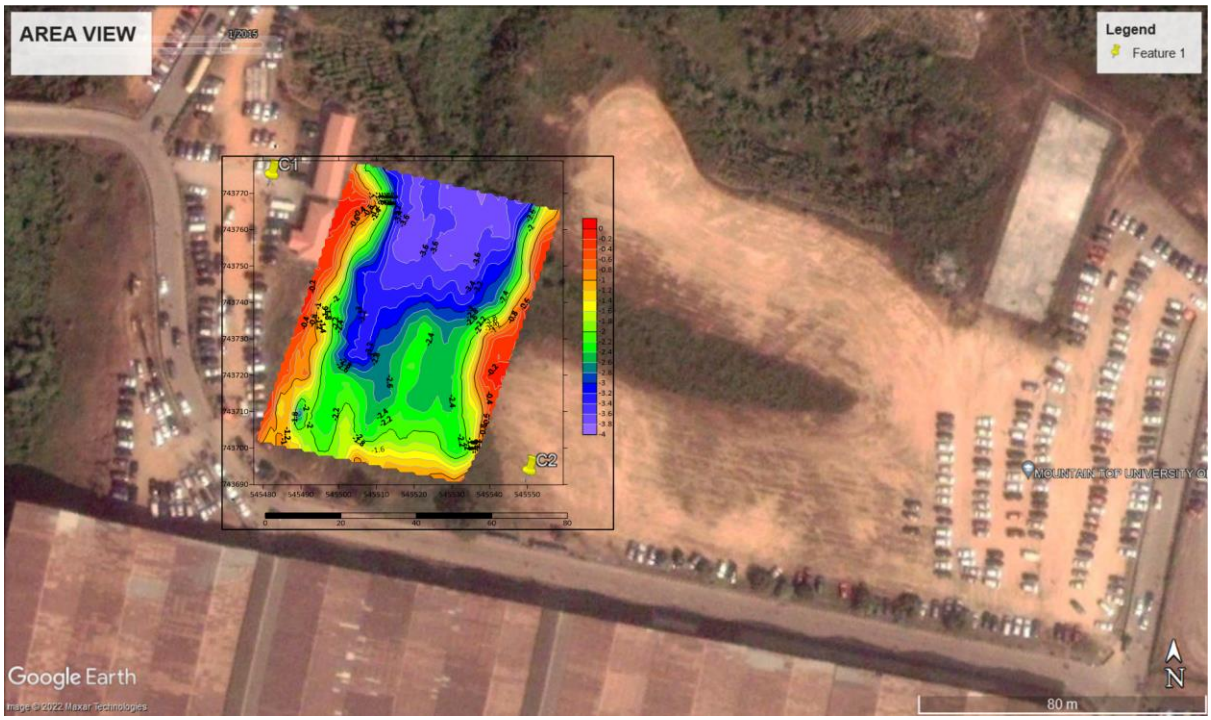

Figure 30 (b) An overlay of the depth map of the river channel on the historical satellite imagery of 2015.

CHAPTER FIVE

CONCLUSION AND RECOMMENDATION

5.1 Conclusion

The integrated geophysical survey involving 2D ERT, and GPR methods have been used to obtain subsurface information about the thickness of the sandfill and depth of the channel fill of parts of a river channel within Mountain Top University.

The results of the nine 2D ERT traverses taken perpendicular to the strike of the buried river channel have characterised the subsurface into two main geoelectric units within the depth of 13.8m. The first region is represented by varying resistivity range of 5 to 1576 Ωm and thickness range of 3 to 8m. At lateral distances of about 16 to 48 m a low resistivity anomaly of 5 to 49 Ωm was observed at a depth range of about 1.5 to 3.8. The configuration of this low resistivity anomaly is analogous to the configuration of an incised channel against the background/country rock. This region is therefore associated to the main course of the sandfill/river channel region. Other regions within the first geoelectric layer are with relatively high electrical resistivity value range of 30 to 1576 Ωm expressive of the native rock (topsoil/lateritic soil) prior to incision by the river channel. The second geoelectric layer is with relatively low resistivity range of 8 to 58 Ωm expressive of sand/clay/sandy clay layer and delineated to an average depth of about 13.8m. The augmented 3D view of the parallel 2D ERT lines have shown that 2D ERT lines proximal to the river channel are infilled with relatively highly conductive materials compared to distal 2D ERT lines. This may indicate varying infill materials (such as peat/clay against sand/clayey sand) or water saturation levels. The possible presence of peat/clay calls for adequate engineering precautions such as pile foundation in the design of the foundation if the region will be considered for future engineering development.
The result of the interpreted 3D inverted resistivity image from the combined parallel 2D lines has provided a 3D view of the subsurface electrical resistivity variation. Low resistivity anomalies can be observed at the central part of the 3D ERT cube which is expressive of the region with the buried/sandfilled river channel. The low resistivity at the central part is analogous to an incised channel fill while the high resistivity at the flanks is analogous to the non-incised country rocks. The 3D inverted resistivity image has provided a robust view of the subsurface through enhanced visualization attainable from the X, Y and Z slices besides the dynamic slices and 3D iso-resistivity surfaces. However, the electrical resistivity method has not provided enough resolution to adequately isolate the sandfilled region from the channel fill region across all the traverses.

The GPR method has provided a high-resolution image of the subsurface and has been able to identify two main anomalous plane continuous reflectors within the depth range of about 2 to 3.5m. The linear continuous anomalies from the plane reflector indicates slight contrast in the homogeneity of the die-electric properties of the study area. The lateral terminations of these reflectors are analogous to an incised channel on a background/country rock. The subtle inhomogeneous layers are interpreted as the sandfilled and channel fill boundaries respectively at respective depth range of about 0.5 to 1.3 m and 1.5 to 3.5m respectively. The depth of the buried channel and the river channel generally reduces at the distal end of the investigated area compared to the proximal end.

The thickness map of the sandfilled region generated from the GPR interpretation have shown the spatial variation of the thickness of the sandfill and depth of the river prior to when it was sandfilled. Likewise, the depth map of the channel fill has shown the spatial variation of the depth to which the river has incised the country rock.

The thickness map of the sandfill and depth map of the channel fill generated from the GPR interpretation has been overlaid on the historical satellite imagery (Jan, 2015) of the study. It can be observed that the region identified as the sandfill/channel fill appropriately aligns with the position of the river channel prior to sandfilling. The depth map overlay has shown that the river channel has strongly incised the native rock at the proximal end of the river compared to the distal end of the river. It is possible that the river has been naturally sandfilled due to regrowth or abandonment prior to the anthropogenic sandfilling after year 2015.

The result of the Electrical resistivity method and GPR has shown consistent correlation in mapping the sandfill/channel river in the investigated area and has delineated the width (28 to 40m) and the depth (2 to 3.5m) of the river channel.

5.2 Recommendations

It is recommended that necessary engineering precautions should be taken in foundation design if the investigated area is to be considered for structural development in the future. Geophysical methods should be integrated with geotechnical methods in subsurface investigation especially in reclaimed and sandfill areas.

Seismic refraction and MASW can be considered to investigate and discriminate the engineering properties of the infill material of the river channel across the investigated area and possible competence as a founding member for foundation of structures.

References

Abayomi, A. O., Michael, A. O., and Moruffdeen, A. A. (2016). Geophysical Investigation of Abandoned Sand-Filled Railway Line: Implication on Adjacent Buildings. *Global Journal of Pure and Applied Sciences Vol. 22, 2016; pp 37 - 41.*

AGI. (n.d.). *1D Geophysical Resistivity Survey: Vertical Electrical Sounding*. Retrieved March 20, 2018, from https://www.agiusa.com/1d-resistivity-survey-vertical-electrical-sounding

Anann, A. P., and Davis, J. L., 1997, *"Ground Penetrating Radar Coming of Age at Last!!", Electrical and Electromagnetic Methods,* Paper 66, p.p. 515–522.

Annan, A.P. (2001) *Ground Penetrating Radar. Workshop Notes, September 2001*, 192.

Archie, G.E. (1942). The Electrical Resistivity Log as an Aid in Determining Some Reservoir Characteristics. *Transactions of the AIME, 146, 54-62.*

Ayolabi E.A, Folorunso, A.F, Eleyinmi A.F, and Anuyah E.O (2009). Applications of 1D and 2D Electrical Resistivity methods to map aquifers in a complex geologic terrain of Four – Square Camp, Ajebo, Southwestern Nigeria. *The Pacific Journal of Science and Technology, 10 (2) pp 657 - 666.*

Aziz, B. Q. (n.d.). *Survey design and procedure*. Lecture. Retrieved March 20, 2018, from https://www.slideshare.net/King1106/lecture-13electrical-method-field-procedure

Barué, G., 2008, "Microwave Engineering: Land & Space Radiocommunications", *John Wiley & Sons, Inc.*

Billman, H. G. 1976. Offshore stratigraphy and paleontology of the Dahomey Embayment. Proceedings of the 7th African Micropaleontology Colloquium, lle-Ife.

B.S, Badmus, O.B, Olatinsu (2009), Geophysical Evaluation and chemical analysis of Kaolin clay deposit of Lakiri Village, southwestern, *Nigeria, Int. J. Phys. Sci 4 p592-596*

Charlton, M. B., 2006, "*Principles of ground-penetrating radar for soil moisture assessment", Journal of Hydrology review on 31st May 2006*.

Chanzy, A., Tarussov, A., Judge, A. and Bonn, F., 1996, "Soil water content determination using a digital ground-penetrating radar", *Soil Science Society of America Journal 60, 1318-1326.*

Cook, J. C., 1975, "Radar Transparencies of Maine and Tunnel Rocks*", Geophysics 40 (5), p.p. 865-885. In Reynolds J. M., 1997.*

Daves, B., Derald, G. S., Duane, G. F., Paul, B., and Grant, N. (2002). Electrical resistivity ground imaging (ERGI). A new tool for mapping the lithology and geometry of channel-belts and valley fills. *Sedimentology. Vol. 49 pp 441 – 449.*

Davis, J. L., and Annan, A. P., 1989, "Ground Penetrating Radar for High-Resolution Mapping of Soil and Rock Stratigraphy", *Geophysical Prospecting, Vol. 37, pp. 531-551.*

De Klasz, I. 1977. The West African sedimentary basins. In The Phanerozoic geology of the world. *The Mesozoic 1. (eds Moullade, M. & Nairn, A. E. M.) pp. 371-399 (Elsevier, Amsterdam.)*

Du, S., and Rummel, P., 1994, "Reconnaissance studies of moisture in the subsurface with GPR." In: Proceedings of the Fifth International Conference on Ground Penetrating Radar, *Kitchener, Ontario, 12-16 June 1994, 1241-1248.*

EPA. (2016, May 18). *Resistivity Methods* (Rep.). Retrieved March 20, 2018, from https://archive.epa.gov/esd/archive-geophysics/web/html/resistivity_methods.html

Jones, H.A. and Hockey, R.D. (1964) The Geology of Part of Southwestern Nigeria Geology. *Surv. Nigeria, Bull, 31, 101 p*

Kearey P., Brooks M., Hill I., (2002). "*An Introduction to Geophysical Exploration*", 3rd ed. Blackwell Science, Oxford.

Loke, M. H., Chambers, J. E., & Kuras, O. (2012, September 26). Instrumentation, electrical resistivity. Retrieved March 20, 2018, *from http://www.landviser.net/content/instrumentation-electrical-resistivity-solid-earth-geophysics-encyclopedia*

Lusch, 1999, "Introduction to Environmental Remote sensing" , *Center for remote sensing and GIS Michigan University.*

Marshall, S. (n.d.). *Electrical Methods - Resistivity Surveying*. Appalachian State University. http://www.appstate.edu/~marshallst/GLY3160/lectures/12_Resistivity.pdf

Nimnate P., Thitimakorn T., Choowong M and Hisada K. (2017). Imaging and locating paleo-channels using geophysical data from meandering system of the Mun River, Khorat Plateau, Northeastern Thailand. *De Gruyter, Open Geosciences, Vol 9 pp 675 – 688*

Obare, J. O. (2020). Application of Geophysical methods in foundation investigation for construction purposes at Olkaria (V) Felds, Kenya., *Global Scientific Journals: Vol 8, Issue 3, pp 121 - 147.*

Okosun, E.A. (1990) A Review of the Cretaceous Stratigraphy of the Dahomey Embayment, West Africa. *Cretaceous Research, 11, 17-27.*
http://dx.doi.org/10.1016/S0195-6671(05)80040-0

Omatsola, M.E. and Adegoke, O.S. (1981) Tectonic Evolution and Cretaceous Stratigraphy of the Dahomey Basin. Journal of Mining and Geology, 18, 130-137

Pantelis, S., & Eleni, k. (2016). Envrionmental geophysics: Techniques, advantages and limitations. *ReasearchGate*, 49.

Petters, S.W. (1982). Central West African Cretaceous-Tertiary Benthic Foraminifera and Stratigraphy. *Palaeontographica Abteilung, 179, 1-104*

Pomposiello, C., Dapea, C., Favetto, A., & Boujo, P. (2012). Application of Geophysical Methods to Waste Disposal Studies. *Municipal and Industrial Waste Disposal*. doi:10.5772/29615

Sandberg, S. K., L. D. Slater, and R. Versteeg, 2002, An integrated geophysical investigation of the hydrogeology of an anisotropic unconfined aquifer: *Journal of Hydrology, 267, 227-243.*

S. Qian and D. Chen, "Joint Time-Frequency Analysis," *Prentice Hall PTR, 1996*

Xu B. and Noel M. 1993. On the completeness of data sets with multielectrode systems for electrical resistivity survey. *Geophysical Prospecting41, 791.-801*

Appendix A: Uninterpreted GPR Radargrams

Traverse 1:

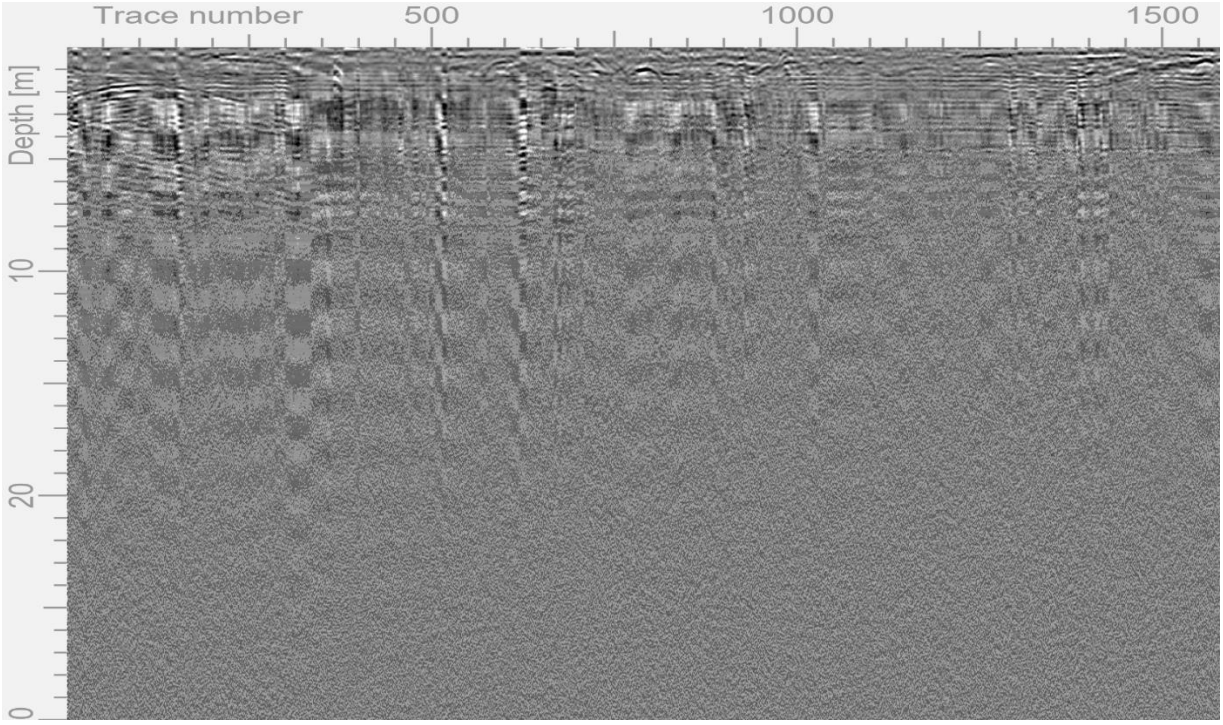

Figure A1 GPR radargram using the 160MHz antenna along traverse 1

Traverse 2

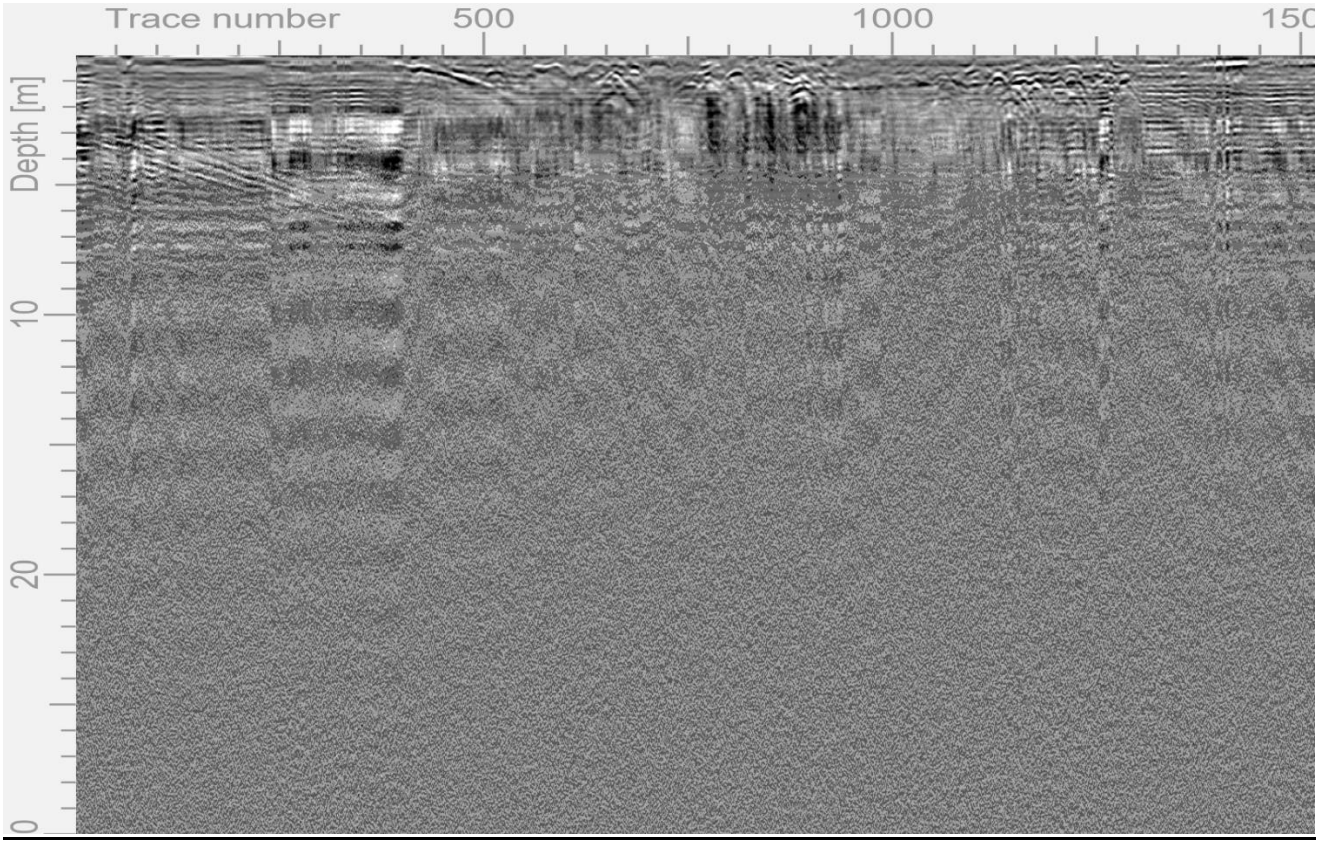

Figure A2. GPR radargram using the 160MHz antenna along traverse 2

Traverse 3

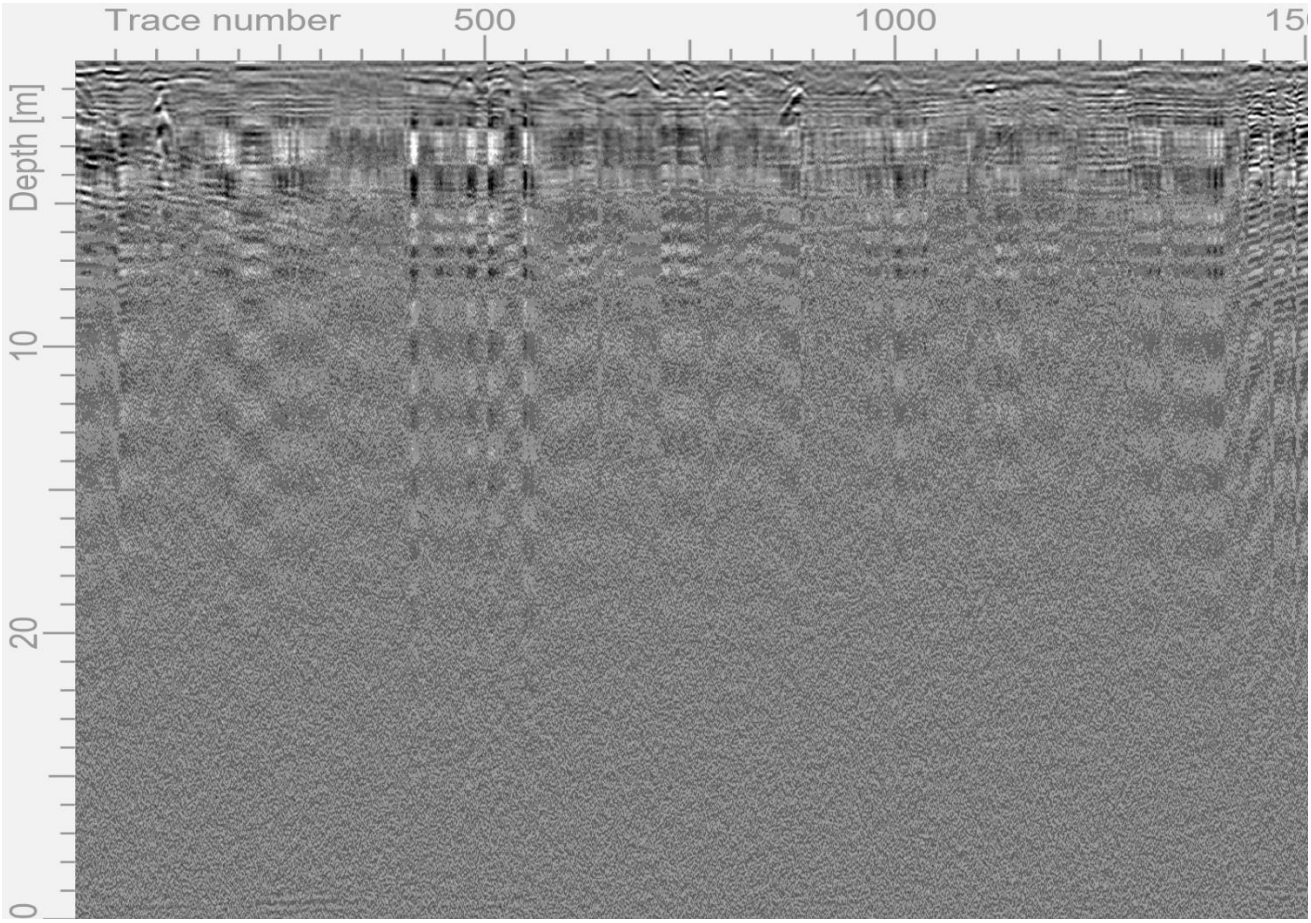

Figure A3. Interpreted GPR radargram using the 160MHz antenna along traverse 3

Traverse 4

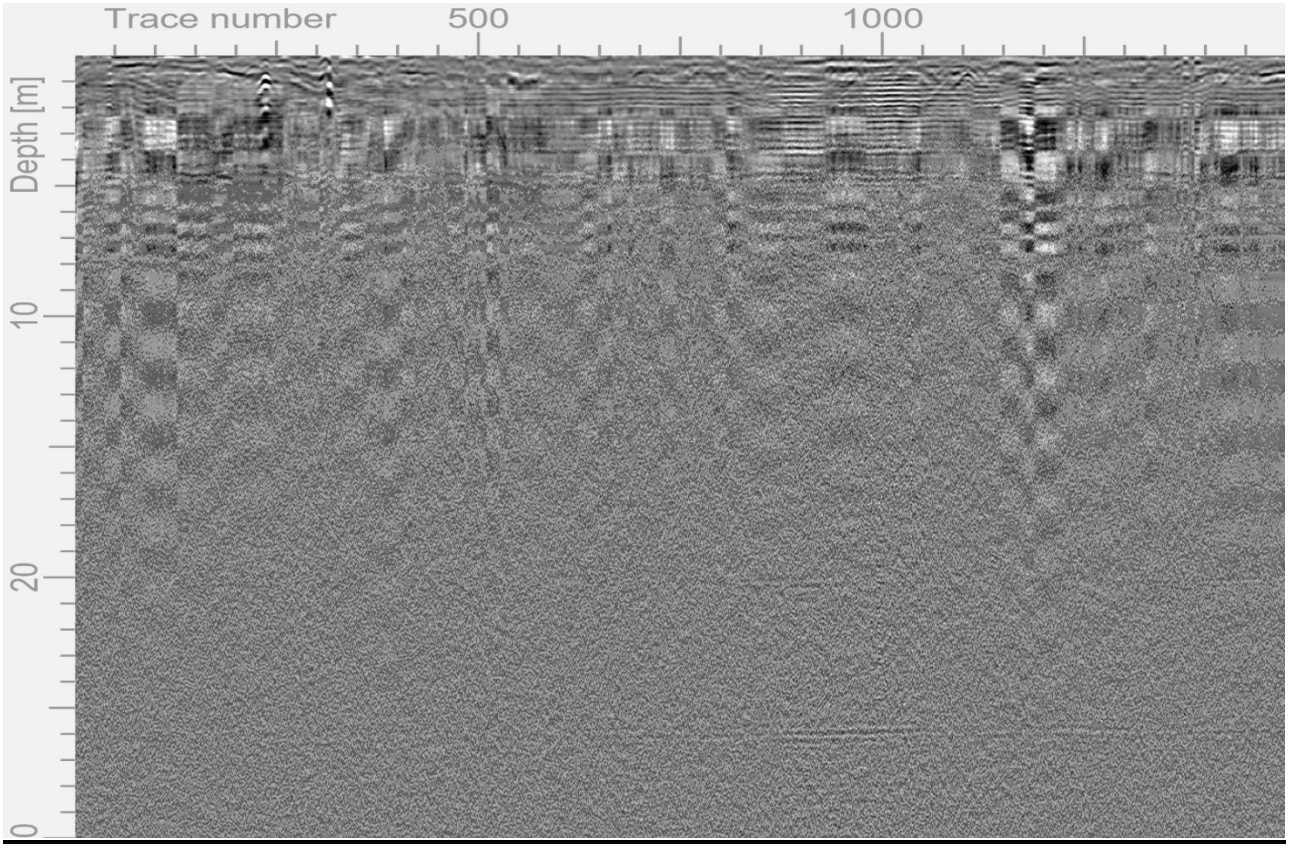

Figure A4. GPR radargram using the 160MHz antenna along traverse 4

Traverse 5

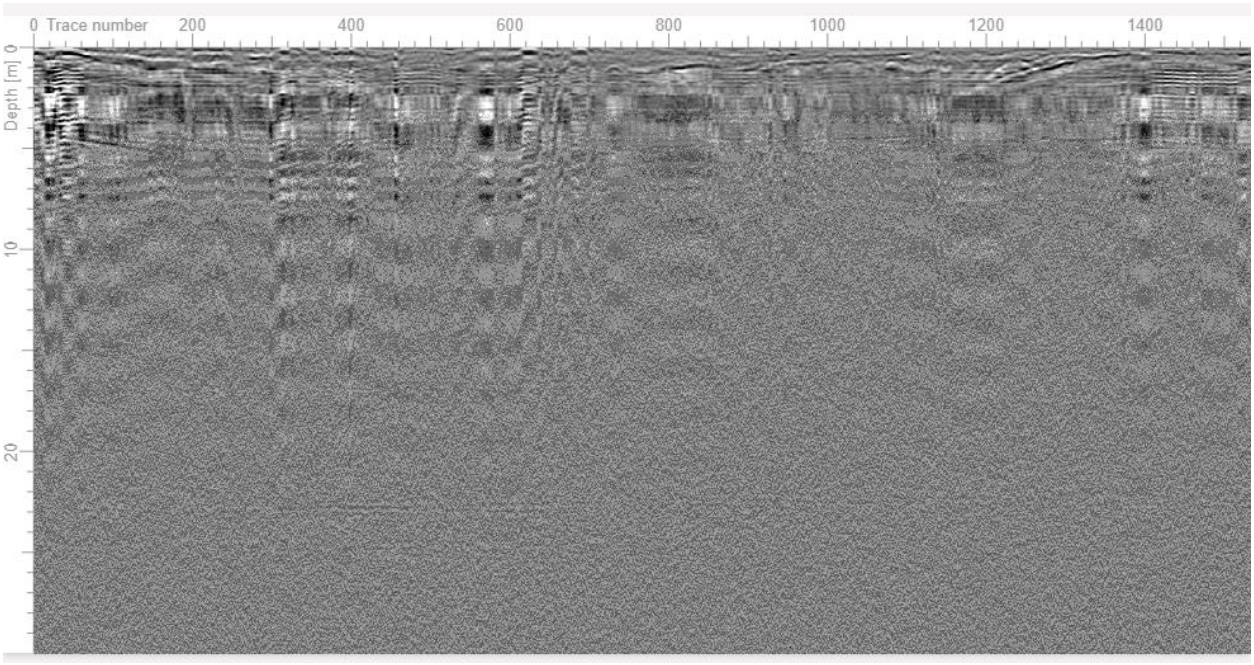

Figure A5. GPR radargram using the 160MHz antenna along traverse 5

Traverse 6

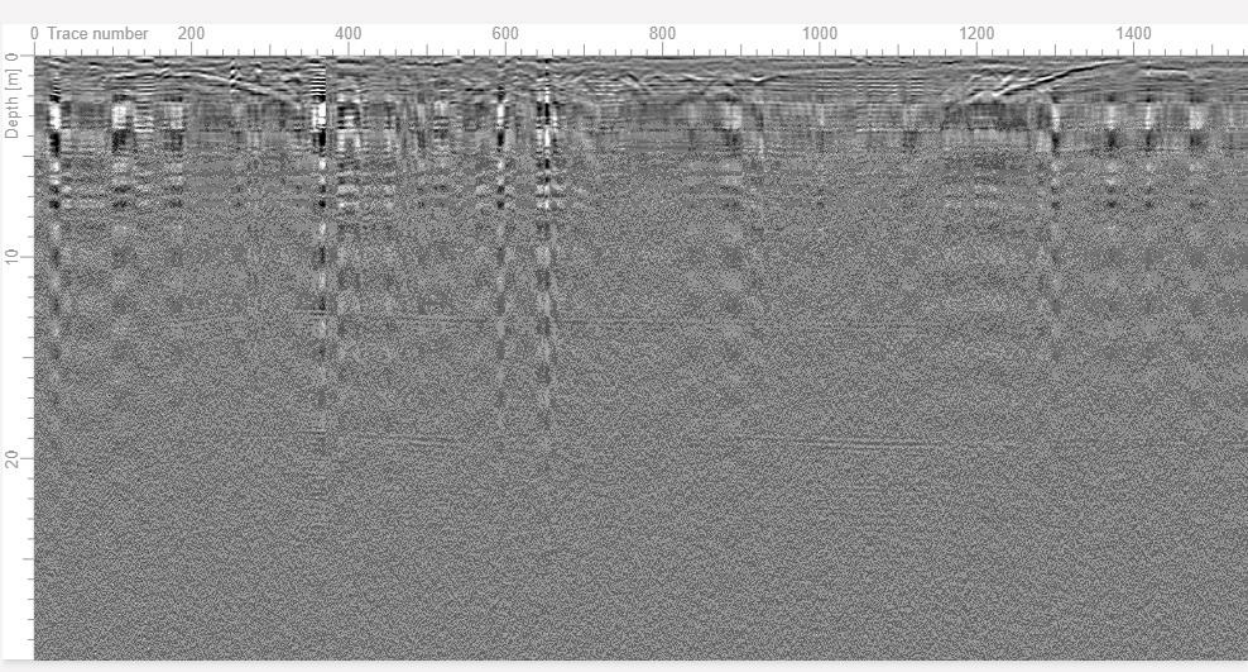

Figure A6. GPR radargram using the 160MHz antenna along traverse 6

Traverse 7

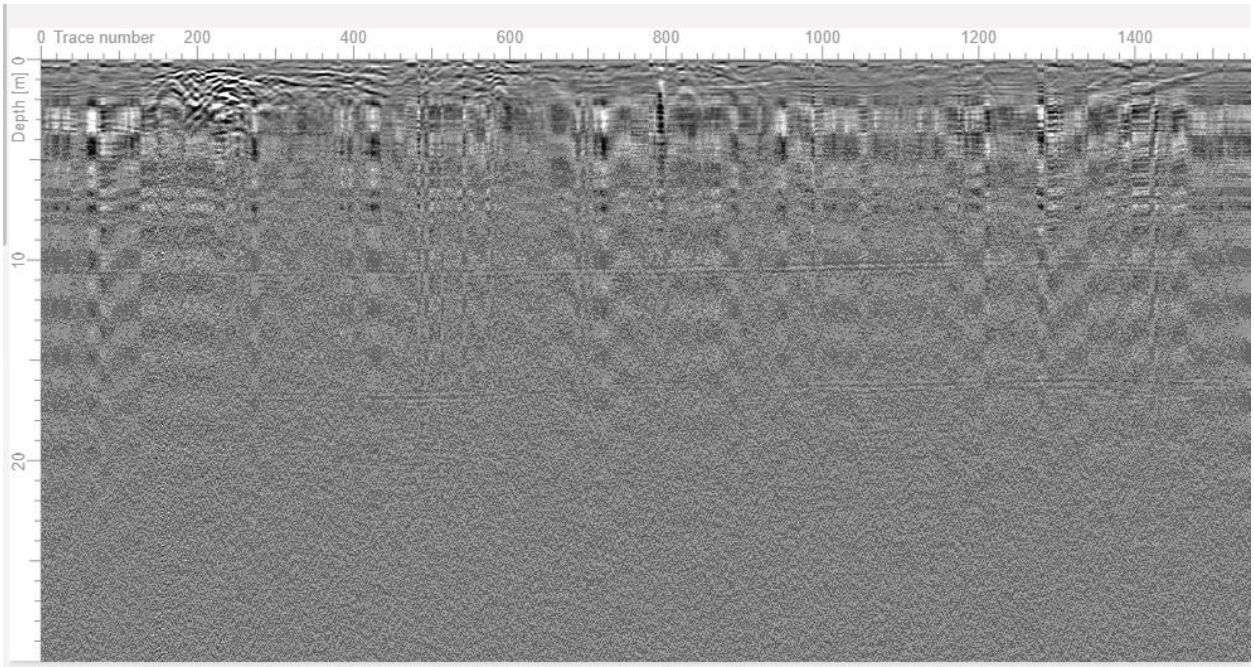

Figure A7. GPR radargram using the 160MHz antenna along traverse 7

Traverse 8

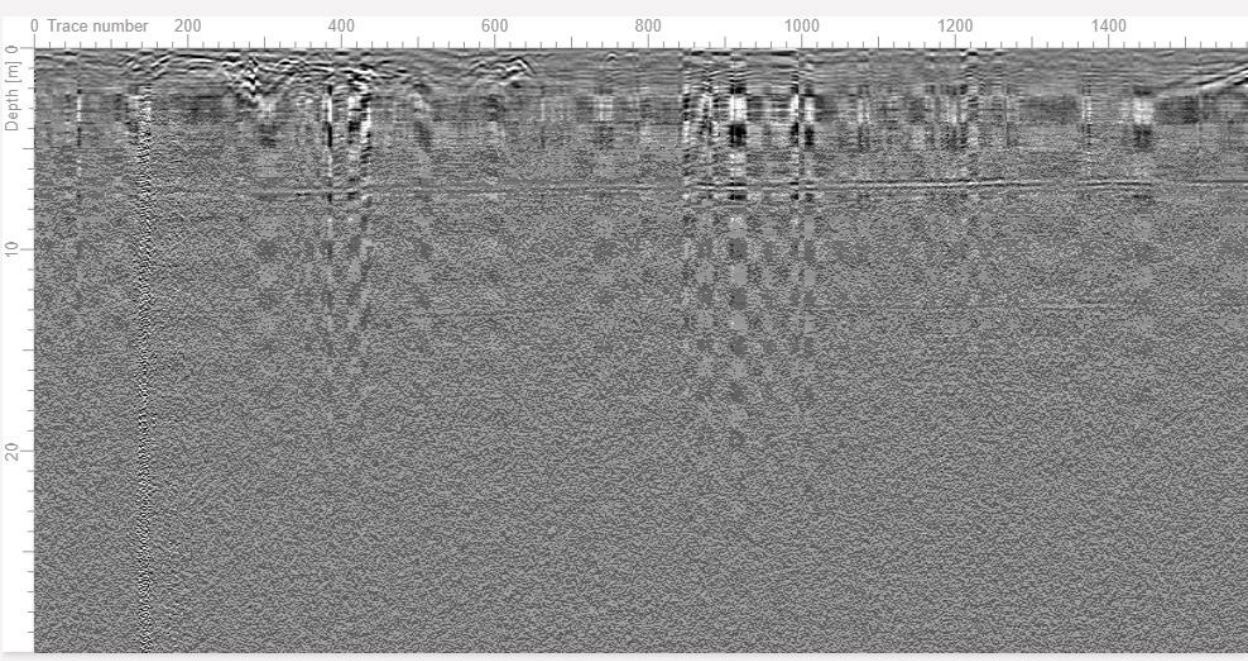

Figure A8. GPR radargram using the 160MHz antenna along traverse 8

Traverse 9

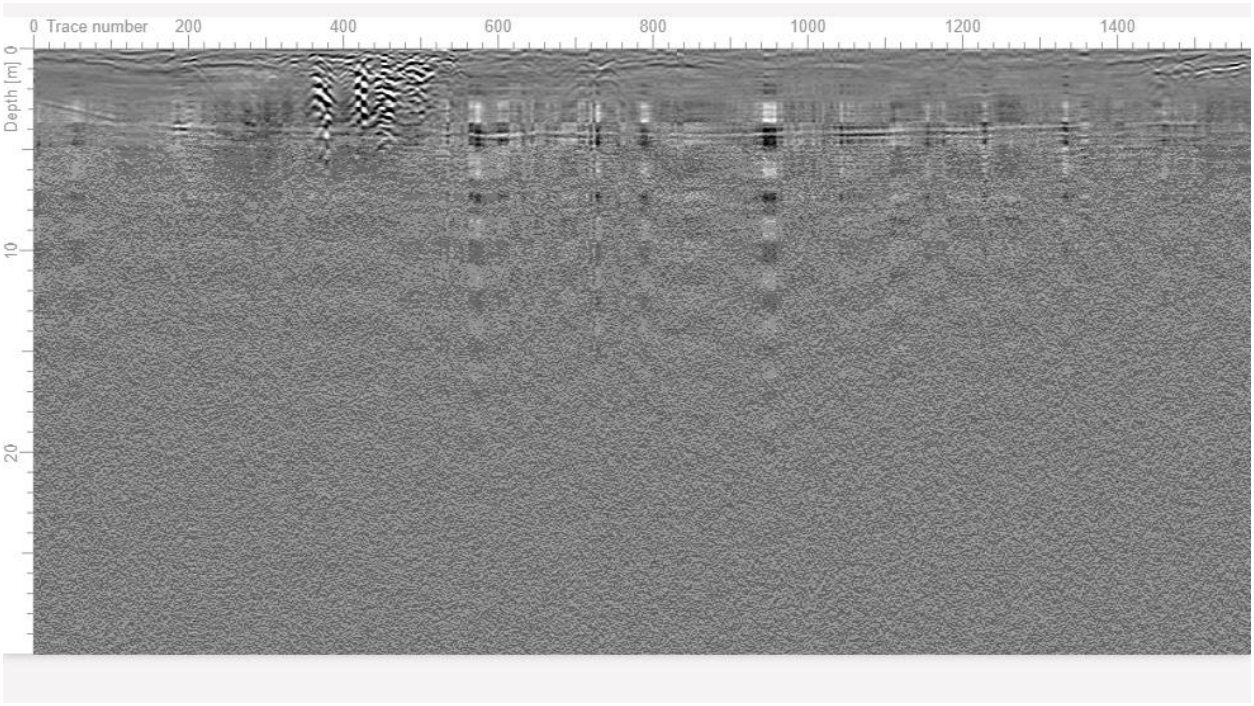

Figure A9. Interpreted GPR radargram using the 160MHz antenna along traverse 9